Fall 12-2020

Synthesis, Characterization, Spectroscopic, and Mesomorphic Studies of New Schiff Base Ligands and Titanium, Cobalt, Nickel and Copper Metal Centers

Raj K. Gurung
Old Dominion University, rguru001@odu.edu

SYNTHESIS, CHARACTERIZATION, SPECTROSCOPIC, AND MESOMORPHIC STUDIES OF NEW SCHIFF BASE LIGANDS AND TITANIUM, COBALT, NICKEL AND COPPER METAL CENTERS

by

Raj Kumar Gurung
M.Sc. May 2009, Tribhuvan University, Nepal
B.Sc. May 2007, Tribhuvan University, Nepal

A Dissertation Submitted to the Faculty of
Old Dominion University in Partial Fulfillment of the
Requirements of the Degree of

DOCTOR OF PHILOSOPHY

CHEMISTRY

OLD DOMINION UNIVERSITY
December 2020

Approved by:

Alvin Holder (Director)

Craig Bayse(Member)

James W. Lee (Member)

John Cooper (Member)

Sandeep Kumar (Member)

ABSTRACT

SYNTHESIS, CHARACTERIZATION, SPECTROSCOPIC, AND MESOMORPHIC STUDIES OF NEW SCHIFF BASE LIGANDS AND TITANIUM, COBALT, NICKEL AND COPPER METAL CENTERS

Raj Kumar Gurung
Old Dominion University, 2020
Director: Dr. Alvin A. Holder

Transition metal complexes with Schiff base ligands offer a wide application in the field of development of catalysis and material. The straightforward synthesis allowed the structural modification and helped to optimize in various application of such complexes. Titanium-containing complexes have been reported to be important for their catalytic and material applications through the coordination of a tetradentate Schiff base ligand, viz. *N*, *N*'-ethylene bis(salicylideneiminate) dianion (salen). Studies reporting the characterization of achiral titanium(IV) salen complexes are scarce due to their intricate nature**.** Such complexes would be comparatively less expensive and easier to prepare synthetically and thus could represent an excellent alternative to the more expensive chiral titanium(IV) complexes. Our research group designed a series of octahedral titanium(IV) Schiff base complexes along with various substituted phenols as ligands, which were assessed for their purity and characterized using various methods and spectroscopic techniques such as elemental analysis, electrochemistry, UV-visible, ^{1}H, ^{13}C, ^{19}F, and ^{49}Ti NMR and FTIR spectroscopies. From the elemental analysis data, the complexes were proposed to have the general structural formula [Ti(salen)OPh-X)$_2$] (where X = F, NO_2 and CH_3). The ^{49}Ti-NMR spectral data showed chemical shifts in the range of +1160 ppm to +1170 ppm, which demonstrated that the magnetic environment showing an

increase in the linewidth with molecular size for the particular titanium(IV) salen complex due to the presence of salen ligand

Another study was focused on the preparation of liquid crystal material using Schiff base ligand and the first-row transition metal ions. To exhibit the liquid crystal property, the design of the ligand plays a vital role. Herein, we used 2,4-dihydroxybenzaldehyde to prepare precursor ligand, at the reactive para-position, the alkoxybenzyl attached to generate precursor aldehyde. O*rtho*-phenylenediamine was used to create novel tetradentate rigid core ligand with flexible alkoxy side chains. These ligands coordinate with Co(II), Ni(II), and Cu(II) metal ions resulting in square planar Schiff base complexes. This thesis is focused on the preparation of stable, pure, and well characterized liquid crystal complexes. Various methods were explored, optimizing the yield and purity. Mesomorphic behavior of the complexes was explored optically, thermally, and by using XRD techniques.

This thesis is dedicated to my mother
Dhan Maya Gurung and father Toran Bahadur Gurung.

ACKNOWLEDGEMENTS

I would first like to thank my advisor Dr. Alvin A. Holder. Thank you for his guidance, patience, and mentorship throughout my doctoral research. I could not have accomplished my Ph.D. journey without his guidance. Additionally, he helped me to improve my grammar and my scientific writing. I also want to thank my dissertation committee members, Dr. Craig Bayse, Dr. John Cooper, Dr. James Lee, and Dr. Sandeep Kumar for their valuable advice and support. I would like to thank our collaborators Dr. Duncan Bruce (University of York, U.K.), Dr. William Jarret (University of Southern Mississippi), Dr. Collin McMillen (Clemson University), and Dr. Riyaz Basha (University of North Texas) for their help and supports. I like to thank Dr. Chee-Hun Kwak and Dr. Mark A.W. Lawrence for their suggestions and support. I would also like to thank Dr. Robert Johnson, Jennifer Vital, Struart Ramsdale and Dr. Valery Kozhenvikov (Northumbria University), for their input in this project prior then me. I also like to thank Dr. Ali Tyemouri and Anuj Thakkar (Civil and Environmental Engineering, Dr. Sandeep Kumar's Lab) for helping me acquiring elemental analysis data.

I would also like to thank my wonderful colleagues in Holder's lab, Michael J. Celestine, Criszcele Tano, Elizabeth Tonsel-White, Khadija Faye, Jennifer Meija, Jaya Chabhra, and Duaa Alajroush for their valuable suggestions and support. I am grateful to my friend whom I met at ODU: Astha Pokhrel, Thu Nguyen, Krishna Raut, Asia Poudel, Gyanendra Kharel, Surya Adhikari, Supreet Khanal, Sujan Manandhar, Kamod Gautam, Bijay Limbu, Depti Dewan, Angela Bhandari and Shankar Karki for their good times, support and suggestions.

I would like to thank the NSF for an NSF CAREER Award (awarded to Dr. Alvin A. Holder), which allowed the successful execution of the completion of this project. I would like to

thank the ODU Chemistry Department faculty and staff for giving me an opportunity to pursue my PhD degree and for the TA support during my time at ODU.

I am very grateful to my amazing friends Suk Gurung and Ram Gurung who always encouraged me to achieve my goals. I also am very grateful to Sapana, Jenis, Mandira, Indira Kumari Ghale and Bal Ghale for their continuous supports and love. I am grateful to my family for their love and support throughout my entire life, and most importantly, I would like to thank my beloved wife Samjhana and my daughter Maya for their unconditional love, care, understanding and support in my life.

NOMENCLATURE

14-TMC	1,4,8,11-Tetramethyl-1,4,8,11-tetraazacyclotetradecane
ap	amidophenolate
bbtmp	2,6-bis(benzimidazol-2′-ylthiomethyl)pyridine
bi	biuret [$H_2NC(O)_2NH$]
BPA-TPA	pentapyridylamine
bpdmpz	bis[(2-pyridylmethyl)-(di(3,5-dimethyl-1H-pyrazolyl)methyl)]amine
C_4mim	1-methyl-3-butylimidazolium
C_n-2,4-sal	4-((3,5-bis(alkoxy)benzyl)oxy)-2-hydroxybenzaldehyde
C_n-2,4-salphen	6,6'-((1E,1'E)-(1,2-phenylenebis(azanylylidene))bis(methanylylidene))bis(3-((3,5-bis(alkoxy)benzyl)oxy)phenol)
CuAAA	copper(I)-catalyzed azide-alkyne cycloaddition
dmgBF_2	difluoroboryldimethylglyoximato
dmpet	2-dimethylphosphino)ethane-1-thiol
(DO)(DOH)pn	N^2,$N^{2'}$-propanediylbis(2,3-butandione 2-imine-3-oxime
DSC	differential scanning Calorimetry
Et_4dien	1,1,7,7-tetraethyldiethyl- enetriamine
LC	Liquid crystal
LCD	Liquid crystal display
NSAIDs	non-steroidal anti-inflammatory drugs

POM	polarized optical microscope
pycd	phenylcyanamide
Salen	*N,N'*-ethylenebis(salicylideneiminate)dianion
SAXS	small-angle X-ray scattering
SmA	smectic A phase
SmC	smectic C phase
tach	cis-1,3,5-triaminocyclohexane
T_c	clearing point temperature
T_m	melting point temperature
tmeda	*N,N,N′,N′*-tetramethylethane-1,2-diamine
TMG	*N, N, N',N'*-tetramethylguonidino
trien	triethylenetetramine
XRD	X-ray diffraction

TABLE OF CONTENTS

Page

LIST OF TABLES

Table Page

LIST OF FIGURES

CHAPTER 1

INTRODUCTION

1.1 General Chemistry of Titanium

Titanium is a group 4 (group IV) element with the symbol Ti. Ti has an atomic number of 22 (electronic configuration = [Ar] $4s^2$ $3d^2$, and an atomic weight of 47.867 g mol^{-1}. It is the ninth most abundant element on Earth. Titanium has two allotropic forms, alpha from and beta form. The alpha form has close packed hexagonal crystal structure, while the beta form has a body-center cubic form, and comparatively, the alpha form is denser than the beta form. Pure titanium metal can exist as a dark gray, shiny metal or as a dark gray powder. Titanium has high melting and boiling points. Titanium is a strong metal like steel but much less dense, highly resistant to corrosion, unaffected by atmospheric air and moisture. Therefore, it is useful in many industrial applications. It is used in aircraft, spacecraft, and missiles because of their low density and ability to withstand extremes of temperature. It is also useful in making alloys, where it is usually added to steel. This enhances the strength and makes it more corrosive resistant. Likewise, the compound of titanium, such as titanium dioxide, is widely used as a white pigment. A table of naturally occurring titanium isotopes and their natural abundances is presented below (Table 1).

This dissertation follows the format of *American Chemical Society*

Table 1. A table of naturally occurring titanium isotopes and their abundances.

Isotope	Atomic mass	Natural abundance (%)
^{46}Ti	45.953	8.25
^{47}Ti	46.952	7.44
^{48}Ti	47.948	73.72
^{49}Ti	48.948	5.41
^{50}Ti	49.945	5.18

Titanium has two low sensitive NMR active nuclei, ^{47}Ti (I = 5/2) and ^{49}Ti (I = 7/2).[1, 2] In comparison, ^{49}Ti is more sensitive than ^{47}Ti and in most frequently used in the analysis. A number of publications are published based on the study of solid-state NMR for the structural characterization of molecular titanium-containing complexes.[2, 3] Due to this nature, the $^{47/49}$Ti NMR spectroscopy is considered as the effective method for probing the electronic environment at the titanium center, and to obtaining the information on geometries of the complexes.[4, 5] Acquisition of titanium NMR spectra is hindered by the low abundance of NMR-active nuclei (^{47}Ti = 7.28 and ^{49}Ti = 5.51%) and low sensitivities. Due to having similar magnetogyric ratios of NMR active nuclei (^{47}Ti = -1.5105 and ^{49}Ti = -1.5109), the resonance of both the nuclei are observed in most of the compound, only separated by approximately -267 ppm [1, 6-8] (Figure 1). In addition, the spectral window for $^{47/49}$Ti NMR spectra is wider, which usually stretches from δ = +1400 ppm to -1400 ppm [4]. ^{49}Ti and ^{47}Ti have the spin quantum number $I > ½$. Due to the quadrupolar nuclei, the quadrupolar line broadening can result over many megahertz [9].

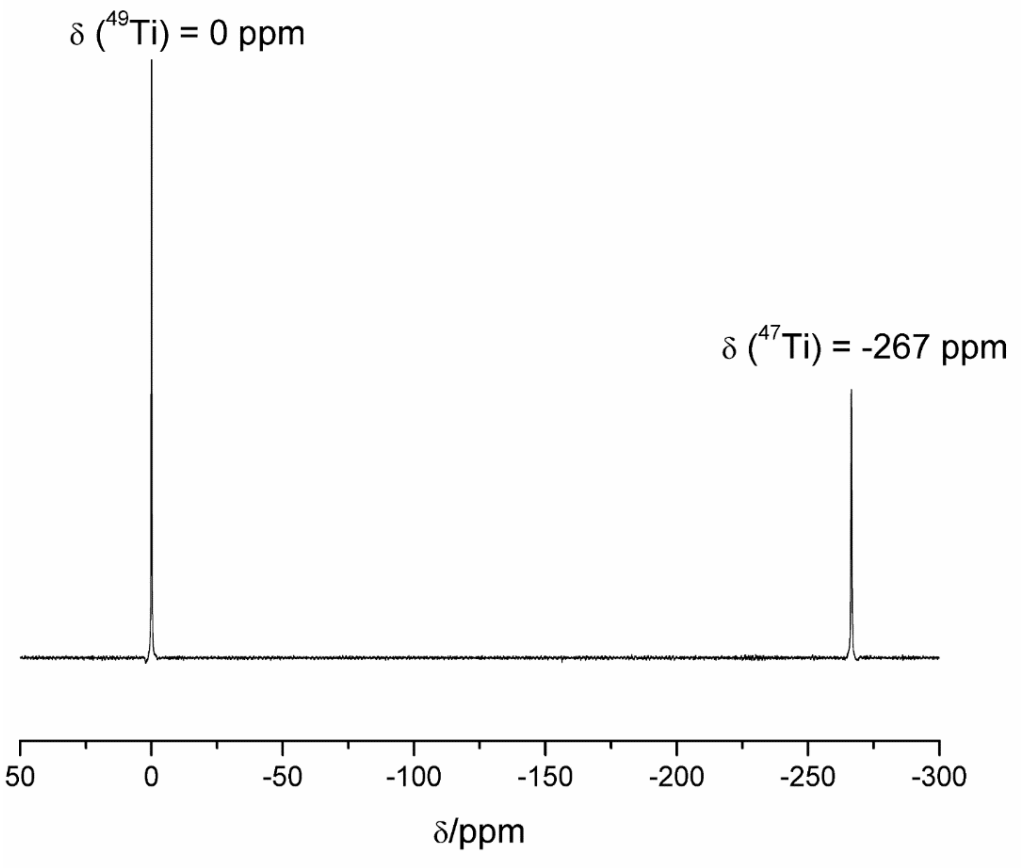

Figure 1. $^{47/49}Ti$ NMR of $TiCl_4$ in $CDCl_3$ shown both nuclei.

The common oxidation states of titanium are +2, +3, and +4. By far, the +4 oxidation state is the most stable and common. Generally, titanium does not react with mineral acids at room temperature, but it can dissolve in hot hydrochloric acid or nitric acid. With aqueous HF, titanium dissolves producing a fluoro complex ($[TiF_6]^{2+}$)along with vigorous hydrogen evolution.[10, 11] Titanium halides such as titanium tetrachloride, is an important binary compound in various inorganic synthesis as starting material. Various oxidation state of titanium with representative examples are shown below in Table 2.

Table 2. Selected titanium species.

Oxidation State	Coordination number	Geometry	Examples
+2	2	Linear	TiH_2, $TiCl_2$
	6	Octahedral	$[TiCl_2(py)_4]$, $[TiCl_2(tmeda^a)_2]$[12]
+3	3	Trigonal	$TiCl_3$, $[Ti(Cp)_2Cl]$
	4	Tetragonal	$[Ti(Cp)_2(dmpet^b)]$
	5	Trigonal bipyramidal	$[TiCl_3(IMes)_2]$ **13**
+4	2	Linear	TiO_2
	4	Tetragonal	$TiCl_4$, $[TiCl_2(Cp)_2]$
	6	Octahedral	$[Ti(salen)Cl_2]$

Note

[a] *tmeda = N,N,N',N'-tetramethylethane-1,2-diamine*

[b] *dmpet = 2-dimethylphosphino)ethane-1-thiol*

1.1.1 Chemistry of Titanium(II)

Titanium(II), $[Ar]3d^2$, is a relatively uncommon oxidation state for a group 4 metal.[12] Compounds of divalent titanium that are sparsely known. Titanium(II) are mostly confined to solid-state compounds such as oxide, hydride, and halides. Low oxidation state titanium complexes are known for their potential use as a catalyst and reagents for organic synthesis. The well-known compounds are titanium(II) halides and titanium(II) oxide. The titanium(II) lacks the aqueous chemistry as they are easily oxidized by water and the only form a short-lived species.[10] Although Koelle *et al.* have described the preparation of the aqueous solution of titanium(II) in the presence of a strong reducing agent.[11] These groups have prepared $[Ti(H_2O)_6]^{2+}$ species by dissolving $TiCl_3$ in aqueous HF, which disproportionate to produce Ti^{II}/Ti^{IV} species as given in equation 1. Excess of fluoride and $[TiF_6]^{2-}$ were removed using Ba^{2+} or Ca^{2+} ions, leaving behind Ti^{2+} aqua species, which was confirmed by absorption spectroscopy.[11]

$$Ti^{3+} + 6F^- \rightarrow [TiF_6]^{2-} + Ti^{2+} \qquad 1$$

Among few titanium(II) complexes, *trans*-[$TiCl_2(tmeda)_2$] (where, tmeda = *N,N,N′,N′*-tetramethylethane-1,2-diamine) and [$TiCl_2(py)_4$] (where, py = pyridine) were synthesized and well characterized and reported.[12, 14] These divalent titanium(II) complexes were obtained by the reduction of the tetravalent or trivalent titanium by reaction with potassium graphite in THF.[14, 15] In another study, Jilles *et al.* prepared Ti(II) species by the reduction of $TiCl_3(THF)_3$ using an excess of lithium in the presence of tmeda. This results in the formation of a mixed valent $Ti^{II/}Ti^{III}$ species which, on reacting with excess lithium, produce Ti^{2+} species (Scheme 1).[14]

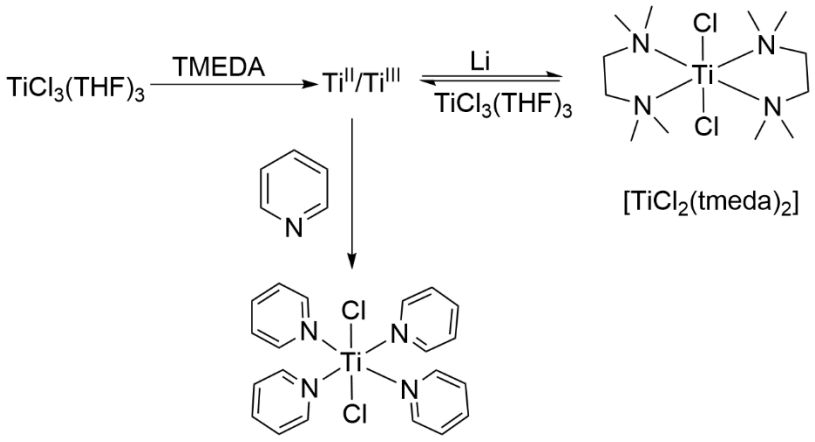

Scheme 1. Synthesis of titanium(II) complexes with octahedral geometries. [14, 15]

1.1.2 Chemistry of Titanium(III)

Titanium(III) complexes usually have octahedral coordination. One of the important binary compounds of +3 oxidation state of titanium is $TiCl_3$. The trichloride is readily oxidized by air and can react to give various other complexes. When heated above 500 °C, they can disproportionate to form oxidized as well as a reduced product.[10] Titanium(III) has an excellent reducing capability due to which it is important in organic syntheses.[16, 17]. For example, aqueous $TiCl_3$ solution can reduce nitro arenes into amino arenes or rapid reduction of quinones into hydroquinones.[18] Large *et al*. also demonstrated the reducing activity of titanium(III), where they

reduced azobenzene to hydrazines.[19] Likewise, another important application of titanium(III) compounds in organic synthesis is the conversion of the nitro group into carbonyl groups. In this reaction, $TiCl_3$ can reduce the N-O bond, and due to the strong affinity of titanium towards the oxygen group, ultimately after hydrolysis, the complete conversion to the carbonyl group.[17] Ti^{3+} have only one electron on its d-orbital and exhibit paramagnetic properties. Due to the paramagnetic nature, electron paramagnetic resonance (ESR) has been widely employed in its characterization to study its geometry and electronic features. $[Ti(H_2O)_6]^{3+}$ is one of the good example to explain ligand field theory on splitting degenerate d-orbitals. $[Ti(H_2O)_6]^{3+}$, when studied using absorption spectroscopy, it exhibits a broad band at 500 nm with a shoulder at 550 nm. During the process, the excited state splits into two different levels, i.e., $^2A_{1g}$ and $^2B_{1g}$ levels. The band around 550 nm corresponds to the transition to $^2A_{1g}$ label while the shoulder is due to the transition to $^2B_{1g}$ level.[20, 21] Titanium(III) complexes with various geometries are shown in below (Figure 2).

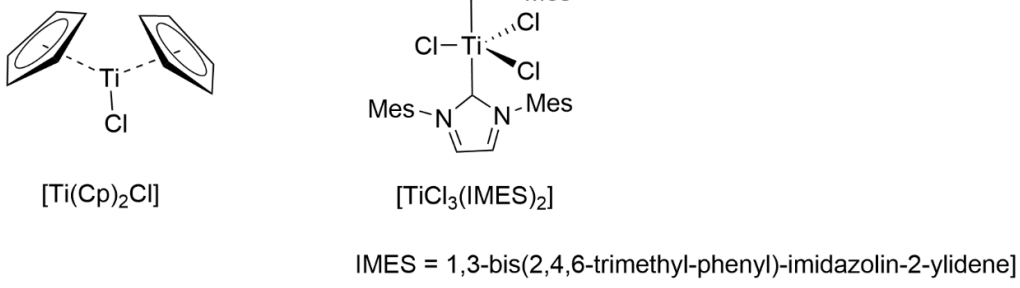

$[Ti(Cp)_2Cl]$ $[TiCl_3(IMES)_2]$

IMES = 1,3-bis(2,4,6-trimethyl-phenyl)-imidazolin-2-ylidene]

Figure 2. Structures of some titanium(III) complexes. [13, 22]

1.1.3 Chemistry of Titanium(IV)

Titanium(IV) complexes generally have octahedral or tetrahedral geometry (Figure 3). $TiCl_4$ is an important binary compound of the titanium +4 oxidation state, which is used in

various applications like smokescreen as it produces heavy white smoke. Titanium tetrachloride is very useful in various organic reactions as a catalyst.[10] Likewise, titanium dioxide, which can be prepared by the hydrolysis of $TiCl_4$, is used as a white pigment due to which it is considered an important compound of titanium.[10] At room temperature, TiO_2 can exists in three different phases: rulite, anatase, and brookite.[23] Beside, a color pigment, TiO_2 is used in photocatalyst and for the removal of the organic pollutant from wastewater.[23]

$$TiCl_4 + 2H_2O \rightarrow TiO_2\ (s, \text{rutile}) + 4HCl\ (aq.) \qquad 2$$

Goa *et al.* [24] utilized the various nitrogen heterocyclic ligands such as piperazine, aminopyrazine, etc. to promote the cluster formation of the titanium-oxo unit, which have potential application in hydrogen evolution reaction.[24] Tetradentate Schiff base salen ligands can react readily with titanium tetrachloride producing an octahedral complexes.[25, 26] These complexes are used in various organic synthesis as a catalyst and also studied for their anticancer properties [25,26-28], and also to produce as new functional materials.[29-31]

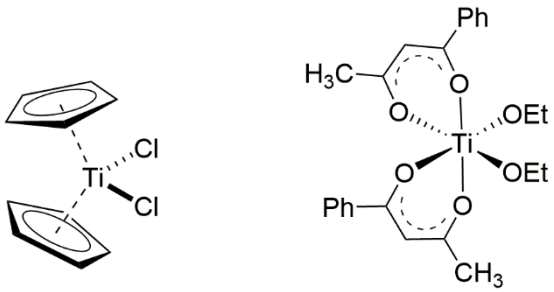

Figure 3. Titanium(IV) complexes with various geometries.

1.2 General chemistry of Cobalt

Cobalt is a group 9 metal that has the symbol Co, an atomic number of 27 (electronic configuration = [Ar] $4s^2\ 3d^7$), an atomic weight of 59.93 g mol^{-1}, and one naturally occurring isotope. Cobalt base pigment is essential for dying glass, ceramic, and enamels. Cobalt is used in

magnet steel and to prepare stainless steel. Cobalt can form numerous alloys with iron, nickel, etc. The magnetic property of cobalt is enhanced when they are alloyed with iron and nickel. Finely divided cobalt is pyrophoric, but the lump meta is stable in air at ordinary temperatures. At 300 °C, it oxidized to cobalt oxide.

Cobalt has a range of various oxidation state ranging from -1 to +4, and the most commonly occurring oxidation state are +2 and +3. The most studied cobalt species are Co^{2+} and Co^{3+} species. Cobalt with lower oxidation states are unstable, and they can be stabilized in organometallic species by π-acceptor ligands. The porphyrin derivatives, macrocyclic complexes, imine/oxime derivatives of cobalt are widely studied for a long period of time due to their importance in various catalytic reactions.[32] For example, complexes like $[Co(dmgBF_2)_2(H_2O)_2]$ (where, $dmgBF_2$ = difluoroboryldimethylglyoximato), $[Co(bis(iminopyridine)]^{2+}$, etc. have shown promising catalytic activity in proton reduction to produce hydrogen. [32, 33] Cobalt with various oxidation state and their representative examples are shown below (Table 3).

Table 3. Selected species of cobalt.

Oxidation State	Coordination number	Geometry	examples
+1	4	Tetrahedral	$[CoBr(PR_3)]$
	5	Trigonal bipyramidal Square pyramidal	$[Co(CO)_3(PR_3)_2]^+$
	6	Octahedral	$[Co(dmgBF_2)_2(H_2O)(py)]$[33]
+2	4	Square planar	$[Co(salen)]$[34], $[Co(dmgBF_2)_2(CH_3OH)]$[35]
	5	Trigonal bipyramidal Square pyramidal	$[Co(Et_2dien)]$[36] $[Co(14\text{-}TMC^a)Cl](BF_4)$[37] $[Co(bpdmpz^b)Cl]ClO_4$ [38]
	6	Octahedral	$[Co(NCS)_6](C_4mim^c)$[39]
	7	Trigonal prismatic	$[Co(BPA\text{-}TPA^d)](BF_4)_2$ [40]
+3	4	Square planar	$[Co(ap^{iPr})^e_2]\bullet 2CH_3CN$[41]
	5	Square pyramidal	$[R(Co(salph)]$[42]
	6	Octahedral	$[CoF_6]^{3-}$

Note:
[a]14-TMC = 1,4,8,11-Tetramethyl-1,4,8,11-tetraazacyclotetradecane
[b]bpdmpz = bis[(2-pyridylmethyl)-(di(3,5-dimethyl-1H-pyrazolyl)methyl)]amine
[c]C_4mim = 1-methyl-3-butylimidazolium
[d]BPA-TPA = Pentapyridylamine
[e]ap = amidophenolate

1.2.1 Chemistry of Cobalt(I)

The isolation of transition metal complexes in a low oxidation state is important in a diverse field, from small molecule activation to catalysis. Low-coordinated cobalt(I) complexes are highly reactive and have found a variety of applications in synthesis, catalysis, and small-molecule activation.[43, 44] Hicks *et.al.*[43] had synthesized a series of low-coordinated, high-spin benzene capped cobalt(I) complexes $[LCo(\eta^6\text{-}C_6H_6)]$ (where L = $N(C_6H_2(C(H)Ph_2)_2Me$-2,6,4)$(SiPh_3)$ (figure 4a). The benzene capped cobalt(I) can readily lose its benzene ligand in solution to give the dimer.[43] The presence of bulky ligand is effective at stabilizing the cobalt(I) complex. Likewise, Dugan *et al.* .[45] prepared bulky β-diketiminate cobalt(I) complex, which is

capable of cleaving the C-F bond in fluorobenzene (Figure 4). [45] Cobalt complexes are considered as important catalysts for hydrogen production. Holder *et al*. has studied electrochemically and spectroscopically the nature of $[Co(dmgBF_2)_2]^-$ complex as a potential catalyst for the production of hydrogen.[33] They reported that the reduction of the cobalt(I) species was influence by ligands present on the axial position. In their study, it was found the Co(I) species has a higher affinity for the pyridine when compared to the Co(II) species; due to this nature, the reduction of the Co(I) to Co(0) was suppressed. The most plausible route in the catalytic evolution of hydrogen involves the formation of a Co(I) species from either Co(III) or Co(II) precursor.[33, 46]

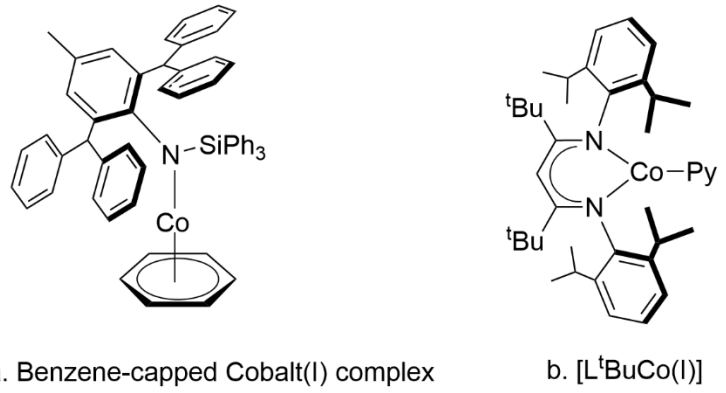

a. Benzene-capped Cobalt(I) complex b. [L^{t}BuCo(I)]

Figure 4. Cobalt(I) complexes with various bulky ligands. [43, 45]

1.2.2 Chemistry of Cobalt(II)

There are numerous Co(II0 complexes that have octahedral or tetrahedral geometries. Only a few five coordinated and square planar complexes are known. Cobalt(II) can form a binary compound with all the four halides, namely CoF_2, $CoCl_2$, $CoBr_2$, and CoI_2. The dark pink cobalt(II) chloride hexahydrate is commercially available and is a common starting material in cobalt(II) chemistry. With some quadridentate tripod ligands and tridentate ligands, cobalt(II)

can form five-coordinate complexes, $[Co(Et_4dien)Cl_2]$ (where Et_4dien = 1,1,7,7-tetraethyldiethyl-enetriamine) along with trigonal bipyramidal or square pyramidal geometries.[36]

Nockemann *et al.* utilized isothiocyanate ligands to prepare paramagnetic cobalt complex, i.e., $(Co(NSC)_4]^{2-}$, which can function as a temperature-dependent switch.[39] When the complex is dissolved in ionic liquid-like (1-ethyl-3-methylimidazolium)thiocyanate, at the different condition of temperature, the complex change its geometry to function as a reversible switch. The coordination of complex from a tetrahedral environment at ambient temperature change to octahedral coordination at a temperature below 230 K (**Figure 5**).[39] They observed and characterized the change in coordination by the change in color from blue (tetrahedral) to red (octahedral) and utilizing the UV-visible spectroscopy.[39]

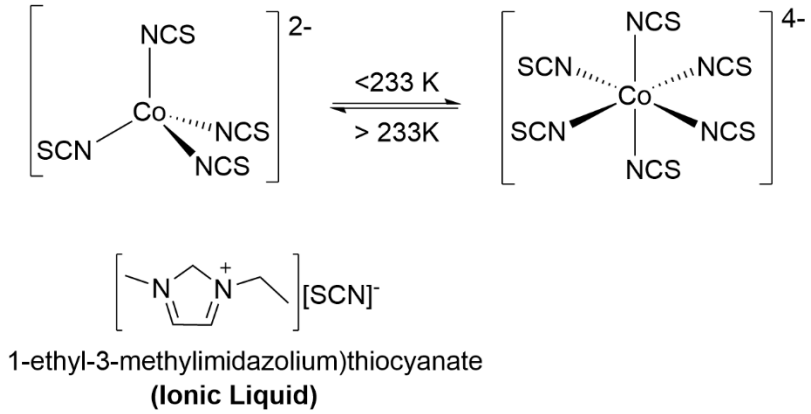

Figure 5. Cobalt(II) complexes with various geometries behaving as a thermochromic switch.

1.2.3 Chemistry of Cobalt(III)

Alfred Werner, in 1913, won The Nobel Prize in chemistry for his contribution to solving the fundamental coordination chemistry of the cobalt complexes. Alfred Werner unravels the previous mysteries of the compounds formed between d-block metal ions and species such as water (H_2O), ammonia (NH_3), and halide ions. A famous problem that led to Werner's theory of

coordination concerns the fact that $CoCl_3$ forms a series of complexes with NH_3 as a ligand, and the formulae are as follows.

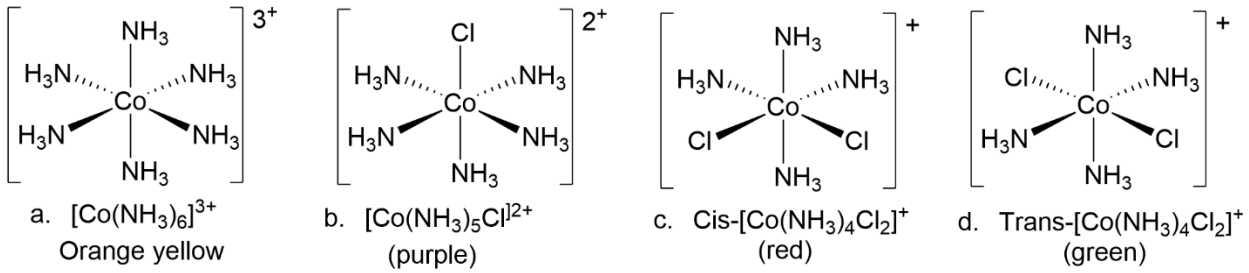

Figure 6. Werner cobalt(III) complexes.

Werner found that the addition of $AgNO_3$ precipitates different amounts of AgCl per equivalent of the cobalt(III) complex.[47] Thus one equivalent of $CoCl_3 \cdot 6NH_3$ reacts with an excess of $AgNO_3$ to precipitate three equivalents of AgCl. Similarly, two equivalents of $CoCl_3 \cdot 5NH_3$ reacts with an excess of $AgNO_3$ to precipitate two equivalents of AgCl, and three equivalents of $CoCl_3 \cdot 4NH_3$ reacts with an excess of $AgNO_3$ to precipitate one equivalent of AgCl.

$$[Co(NH_3)_6]Cl_3 + \text{excess } Ag^+ \rightarrow 3\ AgCl\ (ppt) \quad (3)$$

$$[Co(NH_3)_5Cl]Cl_2 + \text{excess } Ag^+ \rightarrow 2\ AgCl\ (ppt) \quad (4)$$

$$[Co(NH_3)_4Cl_2]Cl + \text{excess } Ag^+ \rightarrow 1\ AgCl\ (ppt) \quad (5)$$

The complexes of cobalt(III) are usually low-spin and are kinetically inert. Only a few binary compounds of cobalt(III) are known, and a limited number of cobalt(III) complexes are commercially available.[47] Cobalt(III) metal ion has a higher affinity for nitrogen donors, and the majority of its complexes contain ammonia, amines, nitro groups, or nitrogen-bonded SCN groups. [10] The majority of cobalt(III) complexes have octahedral geometry and are usually synthesized by oxidation of the corresponding cobalt(II) species.[10] Another interesting complex of cobalt has a cubane structure. Chakrabarty *et al.* have reported the synthesis of cobalt(III)

cubane complex $[Co_4(O_4(O_2CCH_3)_4(py)_4]$ (**Figure 7**) and demonstrated the excellent catalytic properties.[48] It was used for the oxidation of various organic substrates such as alkyl aromatics, alcohols, and terpenoids.[49-51] In one of their study, oxidation of p-xylene under the mild condition of temperature and pressure along with the cubane complex yield 36 % of the conversion to p-toluic acid.[48]

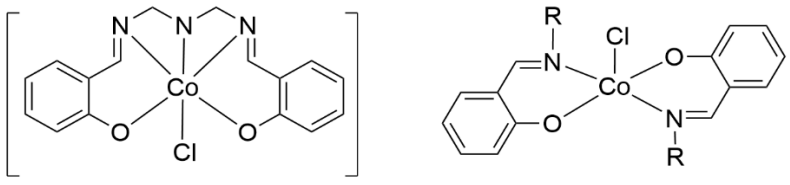

Cobalt(III) Schiff base complexes

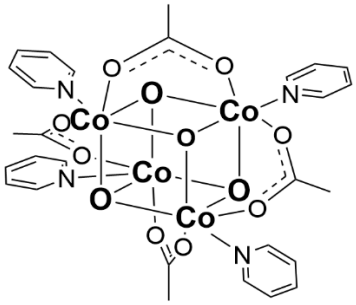

Cobalt(III) cubane cluster

Figure 7. Cobalt(III) complexes with various geometries.[42, 48]

1.3 General chemistry of Nickel

Nickel is a group 10 metal with the symbol Ni and an atomic number of 28 (electronic configuration = [Ar] $4s^2$ $3d^8$, an atomic weight of 58.693 g mol^{-1}, and five naturally occurring isotope. Nickel has high electrical and thermal conductivities and has a higher melting point. The reactivity of the nickel and the cobalt are very similar. It reacts with dilute mineral acids but is resistant to aqueous alkalis. Nickel can react with oxygen at high temperatures to form its oxides. Nickel(II) oxide is a green solid which is also formed when hydroxide, carbonate, or nitrate is heated.[10]

The most common oxidation states of nickel are +2 and +3 states. The complexes of nickel with oxidation numbers 0 and +1 are less meaningful importance, while the complexes with higher oxidation states, i.e., +3 and +4, occur in very few compounds, and the chemistry of such complexes are still not poorly understood.[10] Nickel complexes with various geometries have been reported. The maximum coordination of nickel(II) species is six, and it generally prefers the octahedral geometry. Octahedral nickel(II) complexes have a magnetic moment ranging from 2.9 to 3.4 BM. Likewise, square pyramidal or tetrahedral nickel complexes are paramagnetic. While comparing, the occurrence of tetrahedrally coordinated nickel complexes is sparse. A large number of nickel complexes have square planar geometry. The planar complex of nickel(II) are mostly diamagnetic.[10]

Table 4. Selected species of nickel.

Oxidation State	Coordination number	Geometry	examples
+1	4	Square planer	$[Ni(diene)](ClO_4)_2$ [52]
	5	-	$[Ni(psnet)]BF_4$[53]
	6	Octahedral	$[Ni_2(CN)_6]^{4-}$ [54]
+2	4	Square planar Tetrahedral	$[Ni(porphyrin)]$[55] $[((C_6H_5)_3(PO))_2NiCl_2]$[56]
	5	Trigonal bipyramidal	$[Ni(tpy)(CF_3)]$[57]
	6	Octahedral	$[Ni(H_2O)_6]^{2+}$
+3	4	Square planar	$[Ni(CN)_4]^{2-}$
	5	Trigonal bipyramidal	$[NiBr_3(PEt)_2]$[58]
	6	Octahedral	$[NiF_6]^{3-}$

1.3.1 Chemistry of Nickel(I)

Nickel complexes with oxidation state +1 are very scarce. The dark red cyano complex, $K_4[Ni_2CN_6]$, was synthesized and characterized approximately a century ago.[54, 59] Nickel(I)

complexes are useful as a catalyst and in a biological system. Nickel is an important component of several enzymes, like NiFe-hydrogenase. Generally, nickel(I) species can be obtained by the reduction of Ni(II) species or by the oxidation of Ni(0) species.[59] The dinuclear $[Ni(CN)_6]^{4-}$ tetraanion (figure 7) contains two planar $Ni(CN)_3$ units connected by a Ni-Ni bond. The Ni-Ni bond length was measured 2.32 Å, which is considered the shortest among such types of complexes.[59] James *et al.* [53] reported the prepared a green-colored $[Ni(psnet)](BF_4)$ (where psnet = bis(5-diphenylphosphino-3-thiapentanyl)amine) (**Figure 8**) complex by the reduction of nickel(II) species with $NaBH_4$. Under appropriate conditions, the $[Ni(psnet)](BF_4)$ reacts with acids in non-aqueous media to give hydrogen.

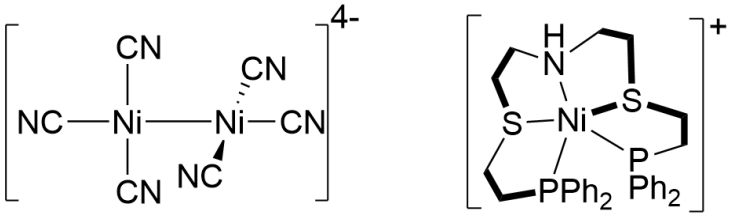

Figure 8. Nickel(I) complexes with various geometries.[54] [53]

1.3.2 Chemistry of Nickel(II)

Nickel(II) and nickel (III) can form a large number of complexes with coordination numbers of 4, 5, and 6. They have been reported to have octahedral, trigonal-bipyramidal, square-pyramidal, tetrahedral and square planar geometries.[10] Octahedral nickel(II) complexes have a magnetic moment ranging from 2.9 to 3.4 BM. Likewise, square pyramidal or tetrahedral nickel complexes are paramagnetic. While comparing, the occurrence of tetrahedrally coordinated nickel complexes is sparse. A large number of nickel complexes have square planar geometry. The planar complex of nickel(II) are mostly diamagnetic.[10] Nickel dimethylglyoxime $[Ni(dmg)_2]$ is an important complex, which has square planar geometry.[60] It was first synthesized

by Chugaev and it is useful in qualitative and quantitative analysis in analytical chemistry.[60] $Ni[P(^tBu)_2(O)NR]_2$ (where R = ^{t}Bu or ^{t}pentyl)being square planar is an exception to this rule as this complex has paramagnetic nature.[61] Ni^{2+} complexes are square planar form, the ligands interact strongly with the metal d_{x2-y2} orbitals, and the resulting σ* orbitals are left unoccupied. While in tetrahedral complexes, the degeneracy of the highest energy d-orbitals leading singly occupying the orbitals.[61] Thus the square planar form is thus favored by stronger bonding whilst tetrahedral or distorted tetrahedral complexes are favored by lower pairing energy. The majority of the complexes with a coordination number of 4 prefer planar geometry. One of the examples of nickel(II) complexes is Schiff base complexes. It has a square planar geometry and mesogenic properties. [62] Likewise, nickel(II) complexes are also studied for their catalytic activities. Nickel-based complexes are reported as an efficient catalyst for the hydrogen evolution reaction.[63] For example, nickel with a stable tetradentate diamine-dioxime ligand, N^2,$N^{2'}$-propanediylbis(2,3-butandione 2-imine-3-oxime ((DO)(DOH)pn), i.e., nickel diimine-dioxime complexes, have are high stability at the acidic condition and demonstrated remarkable electrocatalytic properties (Figure 9).[63]

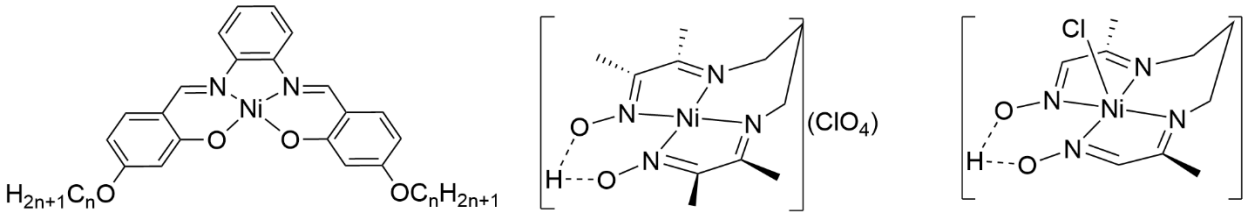

Figure 9. Nickel(II) complexes with various geometries.

1.3.3. Chemistry of Nickel(III)

Nickel(III) complexes have various geometry with coordination numbers four, five, and six. These complexes can behave as a good oxidizing agent but are stabilized by sigma-donor

ligands. Nickel, with the +3 oxidation state have biologically significant.[64] In addition, nickel complexes are widely used in various catalytic reactions.[65, 66] For example, nickel(III) aryl halide $[(^{tBu}N_4)NiArX]^+$ (where X = Br or Cl) are important in cross-coupling and carbon-heteroatom bond formation reaction.[65] In organic chemistry, the formation of C-C and carbon-heteroatom is fundamental in various reactions. Similarly, the synthesis of imido, phosphinidine, and carbene complexes of nickel was reported in the literature.[66] These complexes can undergo group transfer to ethylene, forming the three membered-ring compounds.[66] These complexes are also unique, due to their low coordination.[66-68] The five-coordinated $[NiBr_3(PEt_3)]$ complex is also one of the long-known complexes of Ni(III) oxidation state (Figure 10). Due to its five coordination, the complex has a trigonal bipyramidal geometry. Thus, the complex is paramagnetic and occurs in the low-spin state.

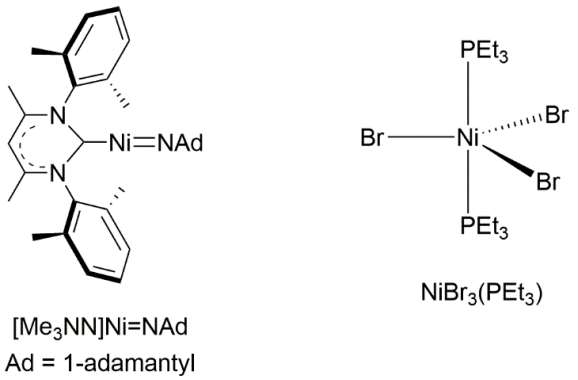

$[Me_3NN]Ni{=}NAd$
Ad = 1-adamantyl

$NiBr_3(PEt_3)$

Figure 10. Nickel(III) complexes with various geometry.

1.4 General chemistry of Copper

Copper is a group 11 metal that has the symbol Cu, an atomic number of 29 (electronic configuration = [Ar] $4s^1\ 3d^{10}$, an atomic weight of 63.546 g mol^{-1} and two naturally occurring isotopes. Copper is the least reactive of the first row metal and is not attacked by non-oxidizing acids in the absence of air but reacts with concentrated H_2SO_4 and HNO_3.

When heated with oxygen, copper reacts to give cupric oxide, or at a higher temperature, it can form cuprous oxide. Copper readily dissolves in nitric acid and sulfuric acid. It is also soluble in ammonia or potassium cyanide solution in the presence of oxygens.[10] Copper commonly have two oxidation state +1 and +2. Complexes with oxidation state +3 and +4 are very rare. Copper is biologically essential, as it serves as a micronutrient necessary for the survival of the cell because it functions as a cofactor of several metalloenzymes. Meanwhile, it is also toxic when present at higher concentrations. The redox activity of the copper makes it potentially toxic because it promotes the formation of reactive oxygen species. Various complexes of copper with different oxidation states are present below (Table 5).

Table 5. Selected species of copper.

Oxidation State	Coordination number	Geometry	Examples
+1	2	Linear	Cu_2O, CuCl
	3	Planar	$[Cu(bbtmp^a)]NO_3$[69]
	4	Tetrahedral	$[Cu(CN)_4]^{3-}$
+2	4	Tetrahedral Square planar	$[Cu(TMG_3tach^b)Cl]^{+}$ [70] $[Cu(ophen(bi^c)_2]^{2-}$ [71]
	5	Square pyramidal	$[Cu(2,3\text{-}Cl_2pcyd^d)(bpy)](PF_6)$[72]
	6	Octahedral	$K_2Pb[CuNO_2)_6]$ $[Cu(trien^e)(diamine]^{2+}$ [73]
+3	4	Square	$[Cu(NH_3)_4]^{2+}$ [74], $[CuCl_4]^{2-}$ [74]
	5	Trigonal bipyramidal	$[Cu(phen)(CF_3)_3]$[74]
	6	Octahedral	K_3CuF_6

Note

[a] *bbtmp = 2,6-bis(benzimidazol-2'-ylthiomethyl)pyridine*
[b] *TMG = N, N, N',N'-tetramethylguonidino and tach = cis-1,3,5-triaminocyclohexane*
[c] *bi = biuret* $[H_2NC(O]_2NH]$
[d] *pycd = phenylcyanamide*
[e] *trien= triethylenetetramine*

1.4.1 Chemistry of Copper(I)

Copper(I) is also known as cuprous. The Cu(I) has a d^{10} configuration, and salts are diamagnetic and colorless. The color results only from the anion or charge-transfer bands. Copper(I) complexes are synthesized by reacting directly with a ligand or by reduction of corresponding Cu^{2+} compound. An inorganic chemist has studied the disproportionation of cuprous compounds into elemental copper and cupric salts, which is important industrially for the preparation of Cu(0) mirrors.[75] Likewise, Cheng *et al.* studied the copper(I) disproportionation where the CuI with β-diketonate enolate or β-keto amide enolate can form Cu^{2+} and Cu species (**Figure 11**).[76] Copper(I) species are important species during the click reactions. Generally, Cu(I) species are generated by the reaction of copper sulfate and sodium ascorbate, which is also known as the Sharpless-Fokin catalyst.[77] Copper(I)-catalyzed azide-alkyne cycloaddition (CuAAA) selectively yields 1,4-disubstituted 1,2,3-triazoles. 1,2,3-triazoles are important molecules used in organic synthesis and drug development. [77-79]

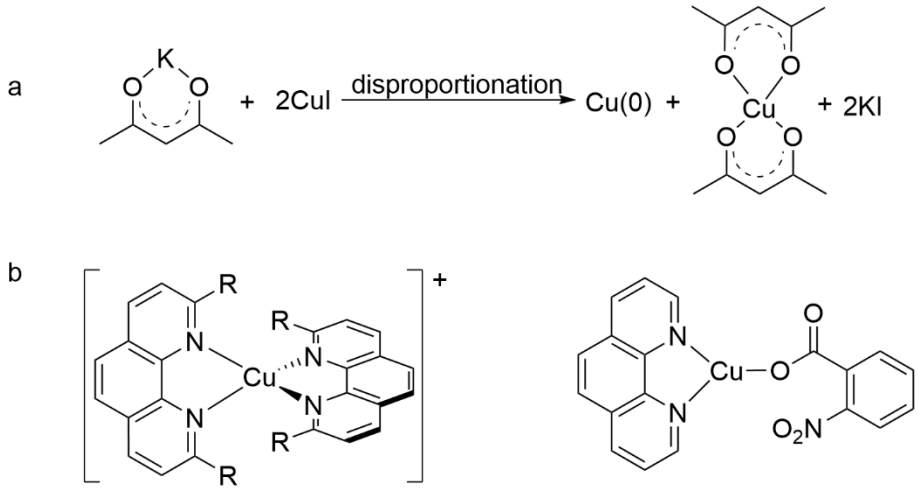

Figure 11. Copper(I) disproportionation reaction (a) and various copper (I) containing complexes(b). [76, 80, 81]

1.4.2 Chemistry of Copper(II)

Copper(II) is also known as cupric. Copper(II) complexes have trigonal-bipyramidal, planar, tetrahedral, and octahedral geometries. Complexes with octahedral and tetrahedral geometries are well known to be a Jahn-Teller active. Due to d^9 configuration, Cu^{2+} complexes are subject to Jahn-Teller distortion if placed in an environment of cubic symmetry. [10 82] The octahedral complex, like CuF_6, undergoes distortion where the axial bond will elongate, and the equatorial bond will be compressed, giving a distorted octahedral geometry.

Copper is a biologically active metal ion with hydrolytic and redox activities.[83] Copper(II) ion can coordinate with various biomolecules with diverse coordination numbers and geometries (**Figure 12**). Thus, copper(II) complexes have been intensely investigated due to their target specific next-generation anticancer and NSAIDs (non-steroidal anti-inflammatory drugs) therapeutics.[84-86] Hussain *et al.* prepared biocompatible Schiff base copper(II) complexes which shown the promising results (**Figure 12**).[86]

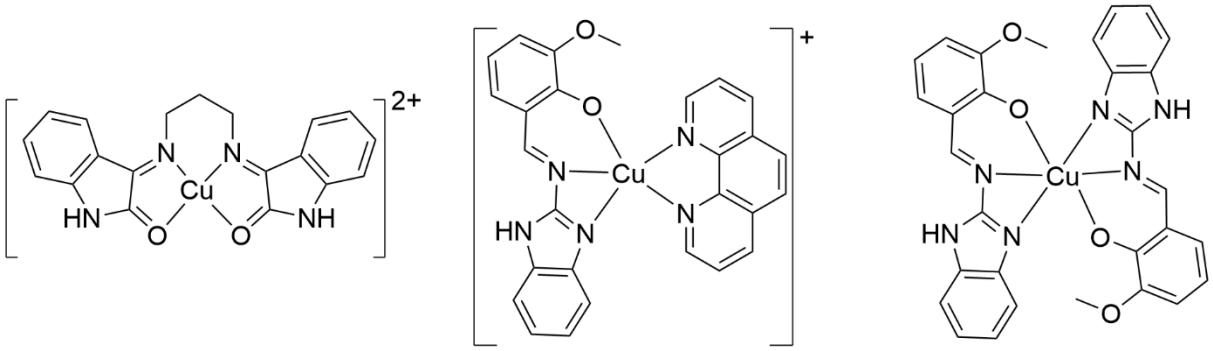

Figure 12. Copper(II) containing complexes.[86, 87]

1.5 Schiff bases

Schiff bases, named after Hugo Schiff (1834-1915), and their transition metal complexes are an important class of inorganic complexes.[88] The first Schiff base ligand was synthesized by the Hugo Schiff, and he was able to observe the azomethine linkage, i.e., RC=N linkage or imine

bond linkage.[89, 90, 91] Generally, the condensation of aldehydes or substituent aldehydes with various amines produce the Schiff bases with high yield.[88 90, 92 93] The formation of a Schiff base from carbonyl groups like aldehydes or ketones is a reversible reaction and can take place under acid or base conditions or upon heating. Schiff bases, which are synthesized using aliphatic aldehydes, are comparatively unstable than the one prepared by using the aromatic aldehydes. They have a moderate electron-donating nature and easily tunable electronic properties. Due to this property, Schiff base ligands are important in various organic and inorganic synthesis (Scheme 2).

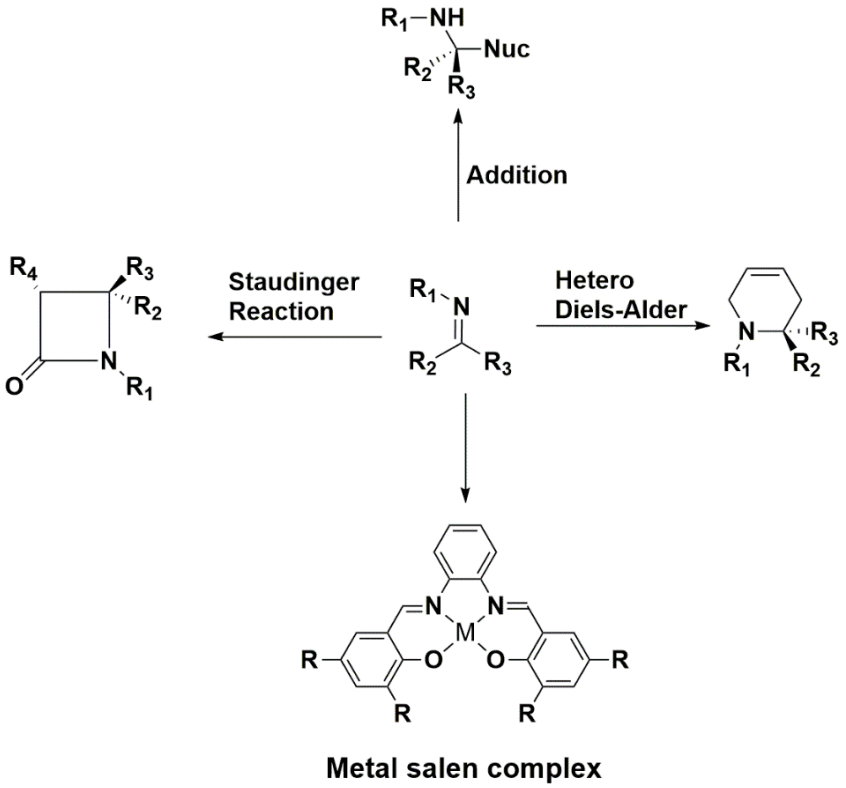

Scheme 2. Various purposes of Schiff base in organic and inorganic synthesis.

Schiff bases are some of the most widely used organic compounds. They are used as pigments and dyes, catalysts, intermediated in organic synthesis, and so on. They also exhibit a wide range of biological activities. Schiff bases have azomethine linkage, which can

accommodate two or more aromatic or heterocyclic scaffolds, which is important for various biological or catalytic applications. Schiff bases behaved as ligands in many inorganic syntheses (**Figure 13**). Depending on the nature of coordination, Schiff base with a variety of denticity can be prepared and can be used to stabilize a wide range of transition metal ion. The Schiff base complexes are intensively investigated as an asymmetric catalyst of olefin epoxidation, oxygenation of an alkene, cyclopropanation sulfide oxidation, the Diels-Alder reaction, C-H activation, and the asymmetric ring opening of an epoxide.[25, 94-97]

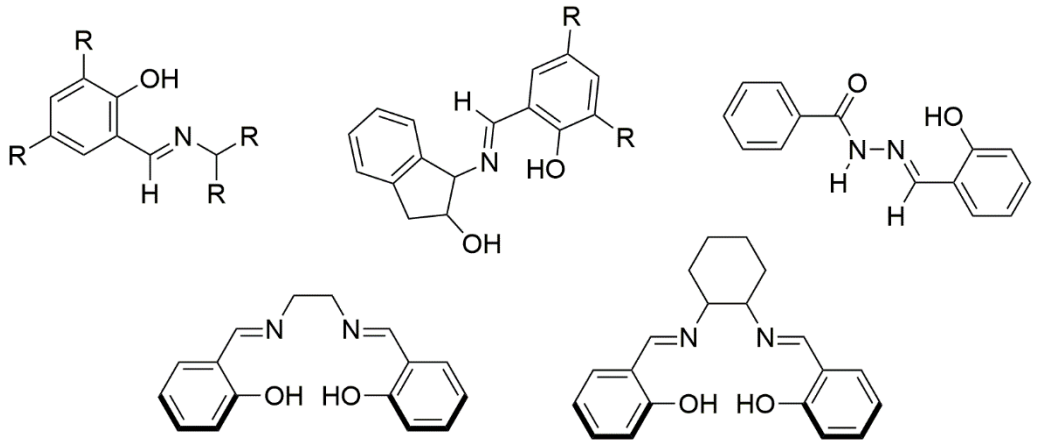

Figure 13. Schiff base ligands with the various mode of denticity.

The *N,N'*-ethylenebis(salicylideneiminate) dianion (salen) is a well-known example of a tetradentate Schiff base ligand. Salen-type ligands are an important type of ligand, which is also known as privileged ligand due to their easily tunable electronic and chelating properties, as well as their conformation properties.[98] These ligands provide rigid and planar coordination with transition metal ions.[99] Thus, they can stabilize the transition metal ions with a variety of oxidation states. Schiff base complexes such as [Fe^{III}(salen)Cl] [100], [Cu(salen)] [101], [Mn(salen)] [102], [VO(salen)] [103], [Pt(salphen-Cl_2] [104], [(*N,N'*-Bis(5-triethylammoniummethylsalicylidene)-1,2-ethylenediiminato)nickel(II)]$(ClO_4)_2$ [105], [Rh(*n*-Bu)(Bu_4salophen)] [106] and Ir(III) Schiff base

complexes [107] were synthesized using salen ligands, and they are extensively studied for their reactivity, catalytic purpose, and therapeutic applications. These transition metal complexes can exist in square planar, square pyramidal, and octahedral geometries [100-105, 108, 109].

Ligands such as diaminobis(phenolato) "salan" when coordinated to titanium(IV) metal center to form [Ti(salan)(O^iPr)$_2$] have been found to exhibit anti-tumor efficacy.[26, 110, 111] An analogous ligand within the same family, ethylenebis(salicylideneiminate) dianion "salen," also showed similar cytotoxicity [26, 110, 111]. These complexes exhibited interesting biological properties. Cisplatin is one of the most popular and effective drugs for cancer treatment, but due to its toxic nature and side effects, various inorganic chemotherapeutic drugs such as alkoxotitanium(IV) complex, titanocene, budotitane, etc., have been explored for the treatment of cancer. [112, 113] Titanocene dichloride and budotitane were the first non-platinum-containing drugs to enter clinical trials as a result of their cytotoxic activity and selectivity similar to those of platinum-containing drugs.[114] Titanium(IV) Schiff base salen complexes have been explored for their anti-cancer applications.[110] Facile substitution at the salen scaffold helped to manipulate the reactivity of complexes towards the cytotoxicity properties, inducing cell death. [115] Tzubery *et al.* [26, 110, 111, 114] had prepared various Schiff base salen ligands to coordinate with titanium(IV) metal center (Figure 13), then carried out anti-cancer studies with the resulting complexes. Titanium(IV) Schiff base complexes were reported to exhibit satisfactory anti-tumor efficacy. [26, 110, 111] Thus, titanium(IV) Schiff base complexes (**Figure 14**) can be attractive alternatives to platinum-based anticancer drugs. However, the drawback of these titanium(IV) salen complexes is their ability to undergo rapid hydrolysis by water to form binuclear species, thus affecting the stability of such complexes [116]. The hydrolyzed products can lead to the formation of oxo-

bridged polynuclear species, which ultimately leads to a decrease in the efficacy of the drugs [116, 117].

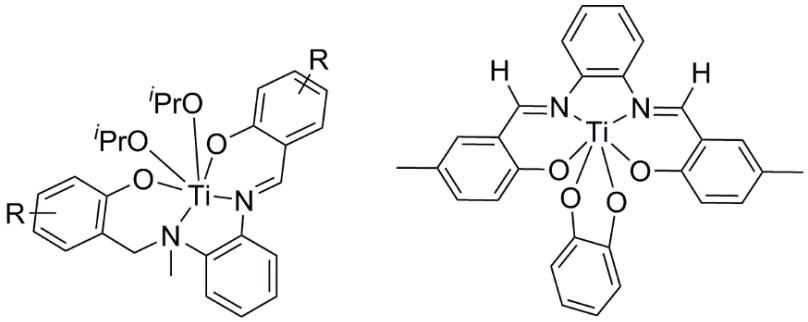

Figure 14. Selected titanium complexes are used in biomedical applications. [26, 110, 111, 114]

Many Schiff bases, which are very important for the preparation of metal complexes, also exhibit catalytic activities in numerous reactions, usually at a higher temperature.[118] Jacobsen Catalyst, which was synthesis during early 1990, is a perfect example of the Schiff base complex used in catalysis. Ever since the pioneering work of Jacobsen and Katsuki, in the enantioselective epoxidation of unfunctionalized olefins, metallosalen complexes have been utilized as efficient catalysts in various organic conversions.[119] Over the past few years, numerous articles had been published on their application in homogenous and heterogeneous catalysis. [120] [121] Chiral Schiff bases and their complexes are one of the most studied chiral catalysts in asymmetric synthesis.

In addition to their biological and catalytic application, Schiff base is also important in material chemistry, as they are used in designing the electronic devices like liquid crystal displays.[122] Metal complexes of Schiff bases derived from salicylaldimine are among the best-known complexes that exhibit liquid crystal properties.[31] These type of compounds continues to be of interest even after over a hundred years of study, as these compounds are used for numerous purpose.[88]

1.6 Concept of Liquid crystals

Liquid crystals exist between the solid phase and the isotropic liquid phase.[123] They are basically molecular materials that combine molecular order and mobility.[124] It is described as a mesophase derived from the Greek word, which means intermediate. It is referred to as the fourth state of the matter.[125, 126] Organic liquid crystal has a long history and is usually referenced to the work of Friedrich Reinitzer[127], who, in 1888, published an article pertaining to the liquid crystal behavior of cholesteryl esters.[128] The cholesteryl benzoate melted to a turbid liquid at 145.5 °C and became clear at 178.8 °C (**Figure 15**), which was referred to as the phenomenon of double melting behavior on increasing the temperature. A German physicist, Otto Lehmann, explained the phenomenon of the double melting point, which refers to an initial as a soft crystal. But later when he observes the presence of opaque phase which exist at different condition having both the properties of liquid and solid, he coined the term liquid crystal. In addition to this, the development of the liquid crystalline material was published in 1922 by Friedel where he classified the various phases of the liquid crystals.[128] The first classification was based on the order and the symmetry of molecular arrangements of the liquid crystalline materials.

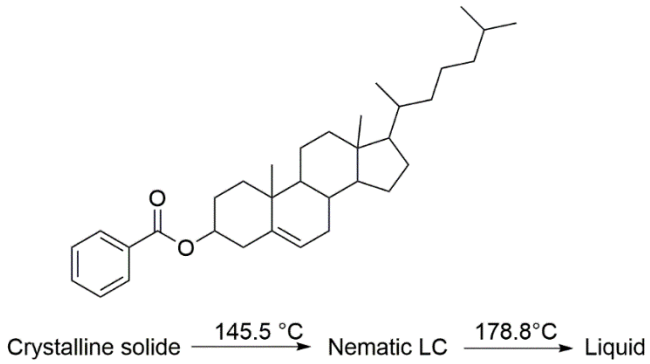

Figure 15. First liquid crystal cholesteryl benzoate compound.

Although there was a significant interest developed on an additional state of matter with no potential application, the future cannot be predicted in this newly discovered state. Indeed, the publication in 1922 by Friedel was a milestone, but due its potential application was not studied in detail until the late 1960s.[129] By the mid-1970s, the liquid crystal has been recognized as a suitable material for the liquid crystal displays due to its unique physical and chemical properties. [130] [131] With the maturation in the field of information technology, liquid crystals are utilized in display technology commercially, manufacturing the liquid crystal display (LCD). LCD is widely used in electronic devices like television, mobile phone display, calculators, etc. Also, liquid crystal materials were used in advancing spectroscopy, imaging, and microscopy techniques. Likewise, liquid crystal technologies are being used as biosensors and biomimicking color-producing substances.[125] [132]

Liquid crystals are broadly classified into two different categories, namely, thermotropic liquid crystal and the lyotropic liquid crystal. Thermotropic liquid crystals change the phase with the temperature (**Figure 16**). At the melting point temperature (T_m), the crystal changes its phase to mesophase, and at a higher temperature, it transforms into the liquid phase, and the temperature at the point is termed a clearing point (T_c). In some cases, it is also termed as enantiotropic due to the formation of the mesophase on both heating and cooling cycles. And these phases are thermodynamically stable.[125] While the lyotropic liquid crystal is solvent dependent and changes their phases with the nature of the solvent.[126] [128] [133] In lyotropic liquid crystals, the appearance of the mesophase is controlled by the concentration of the solvent. [131]

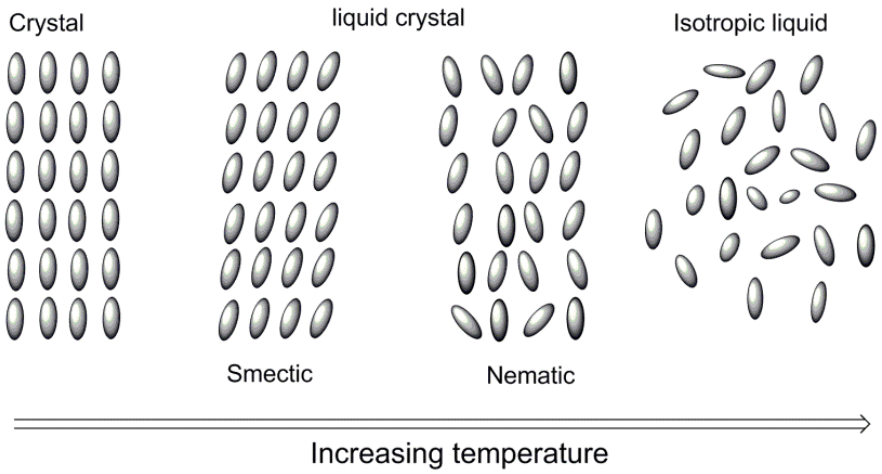

Figure 16. Phase transition of liquid crystal with the increasing temperature.

In the organic mesogens, molecular shape and intermolecular forces play an important role in determining the liquid crystal character of the compound. Similarly, the metal-containing liquid crystals, the structure is very important to determine the mesogenic properties. The presence of metals in liquid crystalline substances induces multiple unique physical properties. The nature of the mesophase also depends on the type of ligands used. Rod-like nematic and smectic shapes are usually found with the long monodentate ligands, while the polydentate ligands are usually responsible for the disk-like discotic liquid crystal. In the rod-like calamitic liquid crystal, the nematic phase is least order while the sematic mesophase is the most order phase.[134]

1.7 Classifications of liquid crystals

Liquid crystal phases are exhibited by certain molecules under a specific set of conditions. Thus, depending upon the conditions that were applied, liquid crystals are organized into two broad categories. If the transition is driven by solvent, then the liquid crystals are termed ‘lyotropic’ while if the transition is achieved by temperature, then those type of liquid

crystals are termed as thermotropic.[128] The classification of the liquid crystal is shown below (**Figure 17**).

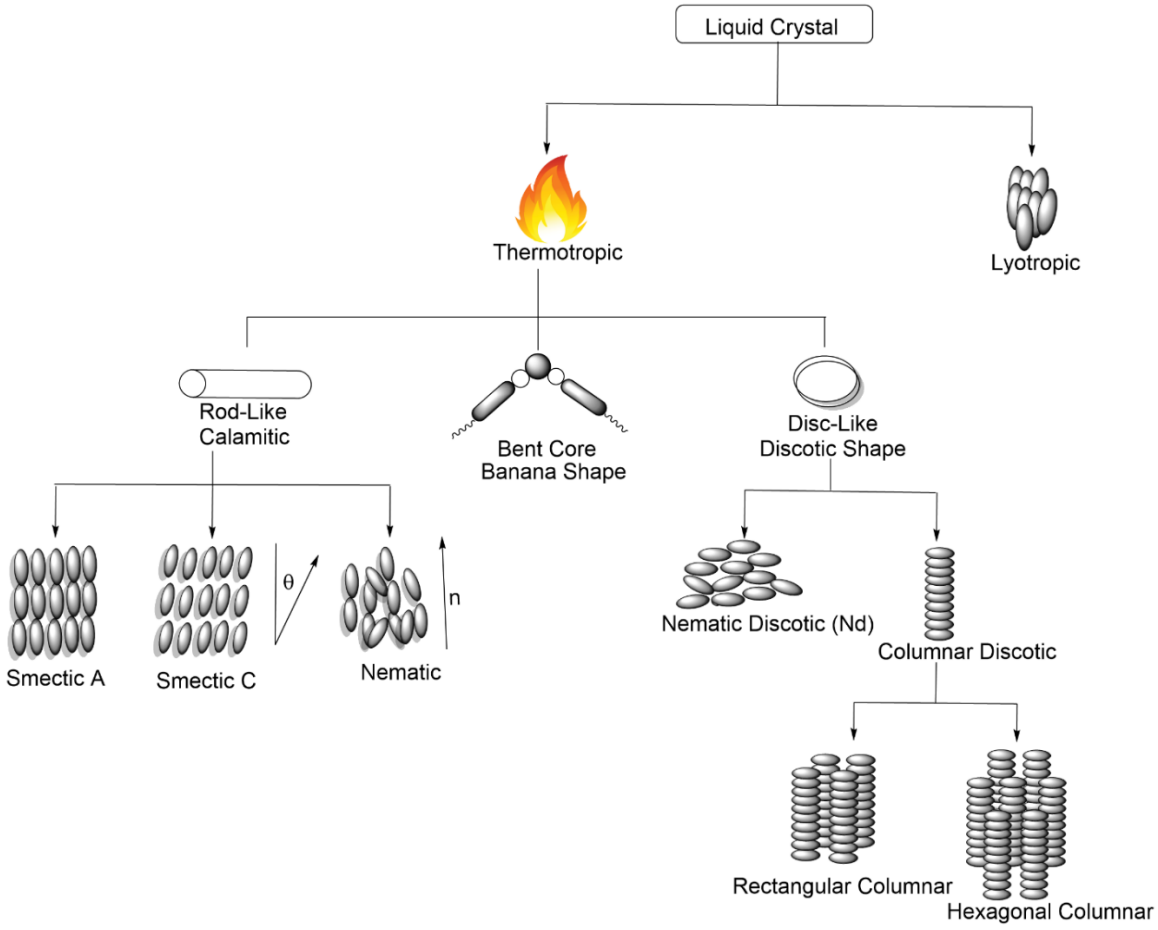

Figure 17. A chart with the classification of liquid crystals.

1.7.1 Lyotropic liquid crystals

The mesomorphic behavior of lyotropic liquid molecules is solvent dependent. Lyotropic liquid crystals are formed by dissolving surfactants in suitable solvents in defined concentration (**Figure 18**).[135] Usually, these types of molecules are amphiphilic in nature. Conventionally, amphiphilic molecules are composed of hydrophilic and hydrophobic groups. The hydrophobic fragments are usually non-polar or weakly polarizable while the hydrophobic parts are polar or charged. [136] [137] Thus, the mesophase of the lyotropic is driven due to balance in hydrophilic and

hydrophobic units. These types of liquid crystals are commonly observed in the biological system. A lipid is an example of biological materials that exhibit lyotropic liquid crystal properties. Soap is one of the well-known examples of lyotropic liquid.[136] The addition of a solvent(e.g., water) will selectively hydrate the hydrophilic portion, preventing hydrophobic regions.[138] Lyotropic mesophases can be considered micelles with ordered molecular arrangement characterized by alternating hydrophobic and hydrophilic regions.[135, 138, 139] When the concentrations are beyond the critical micelle concentration, the micelles will self-organize and form a supramolecular structure.

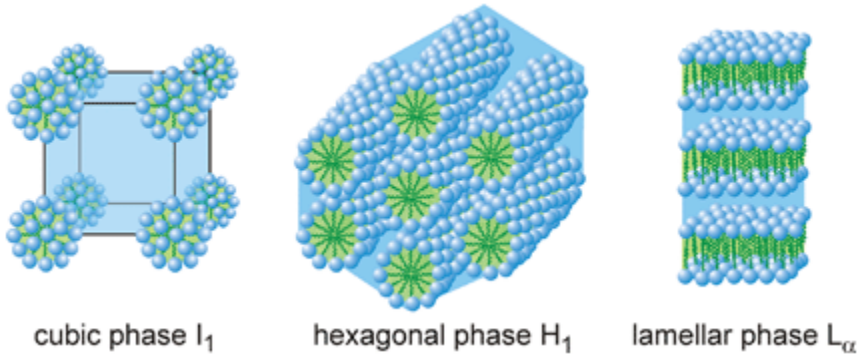

Figure 18. Three different structures of lyotropic liquid crystalline phases. Image from ref.[135] Copyright 2020 New Journal of Chemistry. Reproduced with permission.

1.7.2 Thermotropic liquid crystal

A thermotropic liquid crystal, when heated, passes from the crystalline phase to the liquid crystalline phase, and the temperature at which this phase transition occurs is known as the melting point. By further heating, the liquid crystal transformed into an isotropic liquid. This temperature at which this phase transition occurred is known as the clearing point. The molecule will lose its molecular order. Depending on the nature of the structure feature, thermotropic

liquid crystals are further categorized into calamitic mesogens (rod-like molecules) and discotic mesogen (disc-like molecules).[128, 140 141]

1.7.2.1 Calamitic mesogens

Calamitic systems are the most widely studied thermotropic materials. They have a rod-like molecular arrangement, which comprises of rigid core unit along with the flexible terminal alkyl groups. The core is usually composed of two or more aromatic rings, while the terminal alkyl or alkoxy groups to promote structural anisotropy and helps to lower the melting temperature. [141 30] Calamitic or rod-like molecules display two different types of phases, such as nematic phase and smectic phases.[126] The nematic phase has the least order, and molecules possess only one-dimensional orientational order and no positional order. Due to their various physical properties, nematic molecules have wide application as they can be aligned with electric or magnetic fields. Smectic mesophases have partial translational ordering as they are formed when the rod like molecules organize in layers. Both the phases can exist in a compound as the smectic phases are formed at the lower temperature than the nematic phase.[126]

1.7.1.2 Bent core Liquid crystal

Bent core liquid crystals are another sub-class of thermotropic liquid crystal. This type of liquid crystals attracts attention in the last couple of decades due to their unique shape, unusual symmetry, and packing properties. Bent-core or banana-shaped liquid crystals were first synthesized and investigated by Vorlander et al. in 1932.[142 143] These types of liquid crystal have a bent-shaped core unit resulting in a bent or banana-like shape. A bent-shaped core unit can give rise both calamitic and a number of smectic like phases. Usually, bent-core material possesses a core comprised of five or more aromatic rings, which is responsible for the bent shape.[141] The

bent-core mesogens derived from a 1,3-phenylene core with a group of aromatic rings (**Figure 19**) were found to have numerous phases.[144] This class of material has the ability to form polar order and phase chirality without chiral molecules.[145, 146] Bent core liquid crystal with resorcinol as the central ring and azobenzene with different alkoxy chain introduces large varieties of liquid crystal phases. The addition of halogens helps to exhibit the chirality.[145] Bent-core molecules can generate supramolecular organizations with ferroelectric, antiferroelectric, and various optical properties.[147]

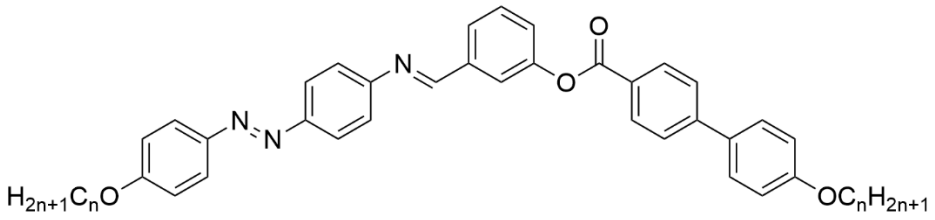

Figure 19. Bent-core or banana shape liquid crystal. [144]

1.7.3 Discotic liquid crystal

Discotic liquid crystal molecules are of a disc like shape.[148] Thermotropic discotic phase was first observed by Chandrashekhar on the hexaester of benzene and published in 1977.[149] [150] [151, 152] Disc like molecules are rather flat and hence possess one, unique short axis.[128] Discotic liquid crystal molecules also generally consist of a rigid central core fused with aromatic rings and peripheral alkyl or alkoxy chains attached to the core.[153] [96] For example, the triphenylenes with typically six or eight long-chain substituents when attached to the core aromatic ring exhibit the discotic mesogen characteristics.[148] [154] [155] [156]

The stacking of the discotic liquid crystals into 1-D columns is the fundamental step in the formation of the columnar molecules. A rigid central core will self-organize into a column in a regular order fashion while the flexible tails are still disordered. The driving force for the

stacking of the molecules arises due to the π-π interactions between the cores.[152, 157] The columns in their ideal condition can have infinite length, and the molecules in a column exhibit only short-range position order.[152] In the columnar phase, the discotic mesogens forms a column, and the columns ordered in a 2-D-lattice with the column axes being parallel to each other.[148] Depending on the nature of the crystal system, a discotic liquid crystal is classified into rectangular columnar (Col_r), hexagonal columnar (Col_h) or oblique columnar phase (Col_{ob}) (**Figure 20**). In the columnar lamellar mesophase, the mesogens are ordered in layers.[152] Cuerva *et al. .*[158] prepared dihalide palladium(II) compounds with pyridyl or isoquinolinylpyraozle ligand, which are lamellar mesophase applicable for the proton conduction.[158] Due to the presence of nanochannels in this type of mesophase, they are applicable for ion transportation, and the fluidic nature of liquid crystal enhances the ion mobilities.[158 159]

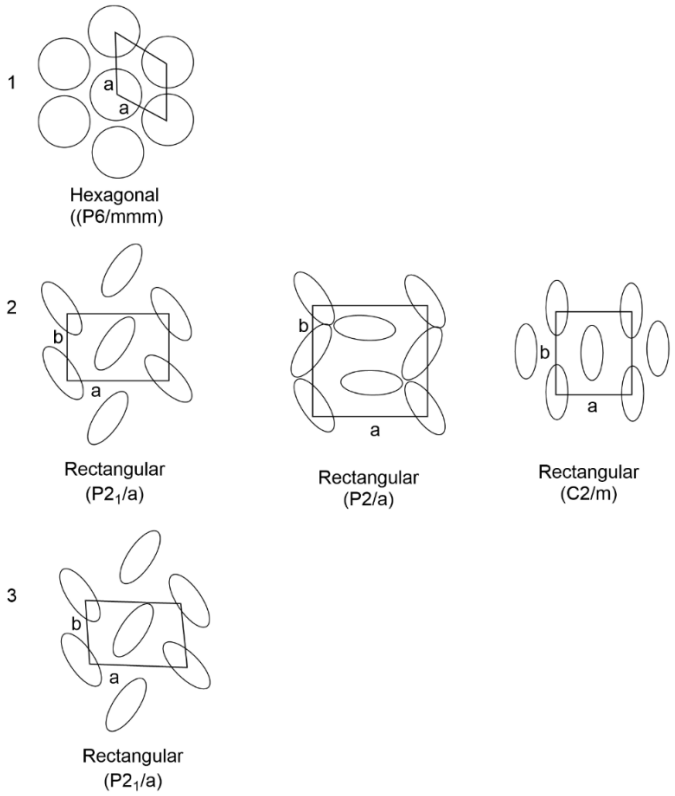

Figure 20. Representation of the lattice of the (1) hexagonal (2) rectangular (3) oblique discotic columnar phase. [128, 152, 160]

1.8 Metallomesogens

Liquid crystals containing metal ions are known as metallomesogens.[134] Such compounds were first made around the early 1900 and were reported in the literature, but the study of metallomesogens significantly increased in the last few decades.[131] Metals can impart useful shapes and properties which are not easily observed in organic liquid crystals. When a metal ion is added to the organic liquid crystal, it may change the polarizability, add, or enhances the electro-optical and magnetic properties.[161] Most of the study of liquid crystal has been originated by utilizing the organic molecules, but when these organic molecules able to coordinate the metal ion from different binding sites, it will act as ligand and stabilized the metal complexes as liquid crystal.[131] The nature of the metal ion helps to exhibit remarkable geometry in the complexes.[31] The appropriate choice of the metal is one of the fundamental steps to determine geometry and characteristics feature in the metallomesogens. A major difference between metallomesogens and most organic mesogens is their greater tendency to exhibit intermolecular dative coordination in the solid state.[162] Thus, mesomorphism has been achieved in nonconventional metal complexes with octahedral, trigonal-bipyramidal, and tetrahedral coordination geometry.[101 163 164] Likewise, the design of the ligand for a metallomesogen involves the consideration of the stability and geometry of the resulting metal complexes.[165]

The rational design of new functional materials opens its broader applications. As much of the space around the metal is occupied by the ligands, the properties of metallomesogens are likely to be dominated by the nature of the ligands. Incorporation of the ligand properties and metal properties will provide the fundamental basis for the preparation of new functional material with wider application.

Solids are anisotropic in nature and possess some degree of positional and orientation order, while the liquid is fluid without the orientation, and they are isotropic in nature.[133] This combination of order and fluidity results in mesophase with anisotropic physical properties, and it is these which have led to their widespread application in low power consumption displays. The ability of metal ions to adopt different coordination geometries allows obtaining a wide variety of mesogenic compounds with structures very different from the classic one in organic derivatives.[166] The metal in such a compound has various roles influencing the geometry of the complex and hence shapes not easily found in organic chemistry, can act as a chromophore, can influence the magnetic behavior, and can be a source of reactivity.[126] It was reported that metallomesogens have importance in electronic devices and display technology. Metal ions play an important role in the resulting mesomorphic properties, and metallomesogens might be obtained by non-mesogenic organic ligands.[167]

Metals like vanadium, iron, nickel, palladium, platinum, iridium, gold, etc. (**Figure 21**) were found to prepare metallomesogens. A large variety of ligands can coordinate with the metal center forming a metallomesogen inducing desired properties. For example, ferroelectric liquid crystal containing iron metal center has applications in the synthesis of a fast switching device, rewritable memories, and optics. [168] Complexes of iridium and platinum have been used in the synthesis of highly efficient luminescence material. [164, 169-172] Likewise, heavy metals into liquid crystalline materials enhance the polarizability of the complex, which are applicable in display devices. [173]

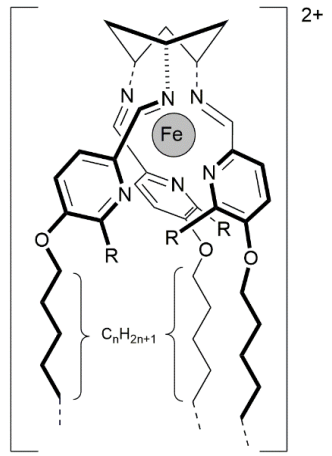

Mononuclear tripodand-base iron(II) metallomesogen

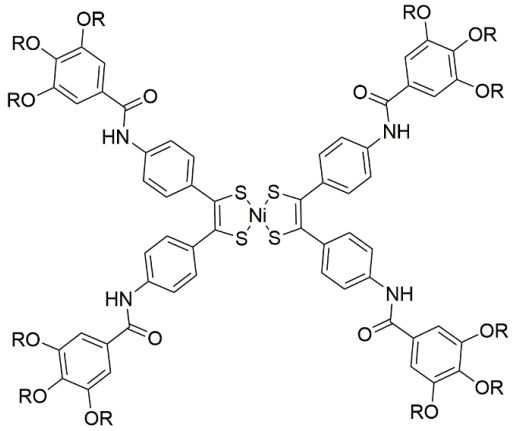

Nickel(II) dithiolene metallomesogen

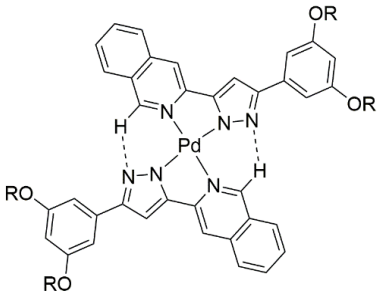

Pd(II) isoquinoline metallomesogen

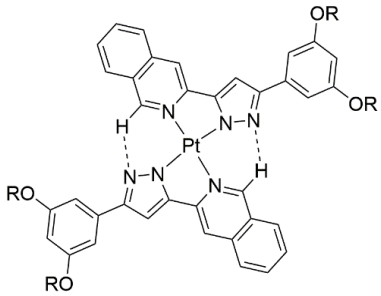

Pt(II) isoquinoline metallomesogen

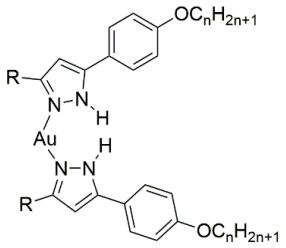

bis(pyrazole gold(I) metallomesogen

Figure 21. Metallomesogens with a selected metal center.

In addition to this, metallomesogens can be prepared using the f-block element. Lanthanidomesogens (**Figure 22**) are a special class of metallomesogens as they contain lanthanide metal ion to form complexes.[174] Due to their predictive electronic, optical, and magnetic metal-centered properties, lanthanidomesogens may have many uses in various optoelectronic

devices, organic light-emitting diodes of a different color, flat and flexible display, luminescent bioprobes hybrid lasers, and many more.[174-176] Lanthanide metallomesogens are known to show narrow emission lines of high color purity characteristics of the metal ion.[177] Due to the magnetic anisotropy, lanthanide complexes are potentially important for the designing of magnetically active liquid crystals.[178] In comparison to the organic diamagnetic liquid crystal, lanthanide-containing liquid crystals can be easily oriented in a weak magnetic field. Maximum magnetic anisotropy was observed in Tb(III), Dy(III), and Tm(III) complexes.[178] Thus, optimizing the various synthetic techniques, various mesogenic Schiff bases, B-diketonate, macrocyclic ligand were used to coordinate with the lanthanides like neodymium, europium, and ytterbium to obtain a lanthanidomesogens. The difficulty of designing the lanthanidomesogens was the bulkiness and large coordination number of lanthanide, which were overcome by decoupling the mesogenic groups and the coordination units via long flexible alkyl spacers and another approach was by increasing the number of long flexible alkyl chains attached to the coordinating units. [174]

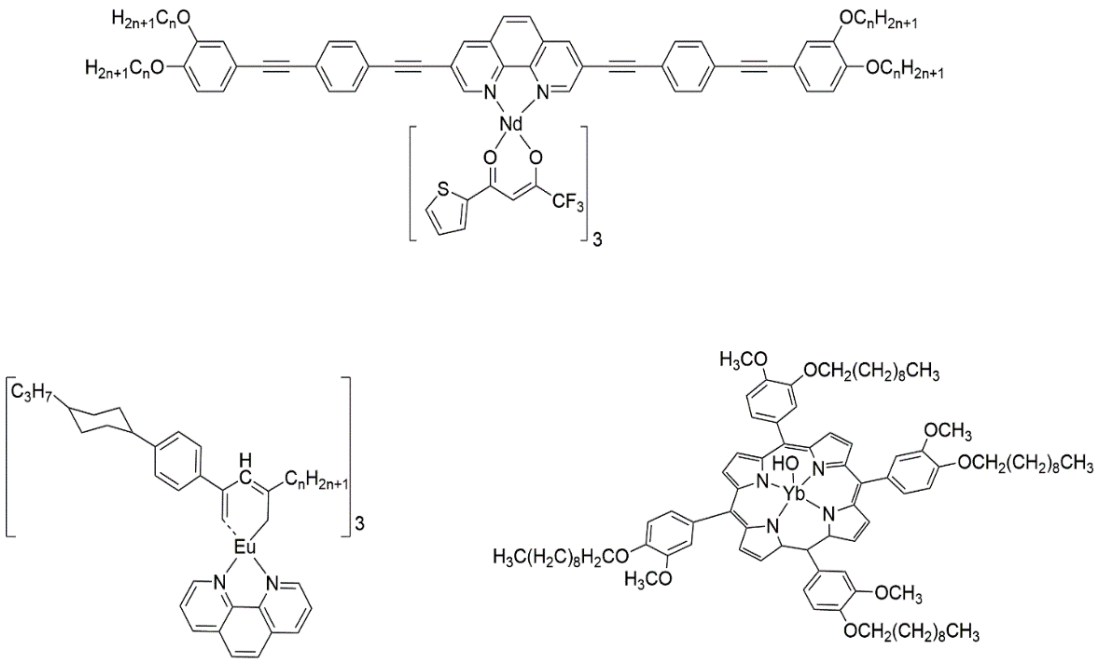

Figure 22. Selected lanthanidomesogens with rare-earth metal centers.

1.8.1 Metallomesogens with Schiff base salen-type ligands

Schiff bases, as mention in an earlier section, are a versatile ligand with various denticity and can stabilize a wide range of metal centers in their various oxidation states. The first row transition metals can form stable metal Schiff base complexes. These type of complexes have widespread application in synthetic, medicinal, optical and electrochemical fields. Metal Schiff base complexes are also extensively studied for the catalytic activities, such as Jacobsen's catalyst.[179] Salen-type ligands, which are derived from salicylaldimine, is an excellent catalyst in organic chemistry. In addition to this, metal complexes of Schiff base derived from salicylaldimine are also known best to exhibit mesogenic properties in metallomesogenic system.[31] The complexes which are derived from salicylaldimine Schiff bases were more likely to have bent-core, rod-like shapes or disc-like shapes. Usually, the Schiff base derived from salicylaldimine has 2 - 4 flexible alkyl/alkoxy side chains. The length of the side chains is adjusted to tune the mesogenic properties of the complex. The bent-core or rod-like shape complexes exhibit the nematic or various smectic phases, while disc like shapes induces the columnar discotic phases. Metal Schiff base complexes can be prepared using various synthetic routes (**Figure 23**). Generally, the monodentate ligands can generate a rod-like structures while the polydentate ligands are responsible for bent-core or disc like liquid crystal molecules.

Ligands based on the π-conjugated salphen framework are studied intensively due to their photophysical and supramolecular properties. The electronic properties and the reactivity of the ligand framework can be easily varied in these systems by careful use of substituent to the overall potential of the resulting salphen ligands. [180] In addition, the phenyl spacer in as salphen ligands increase the rigidity of the ligands making it more planar. Thus, these types of ligands,

when complexes with the metal system suitable for material chemistry like photoresponsive materials, supramolecular assemblies, optical material, and liquid crystalline materials. [180]

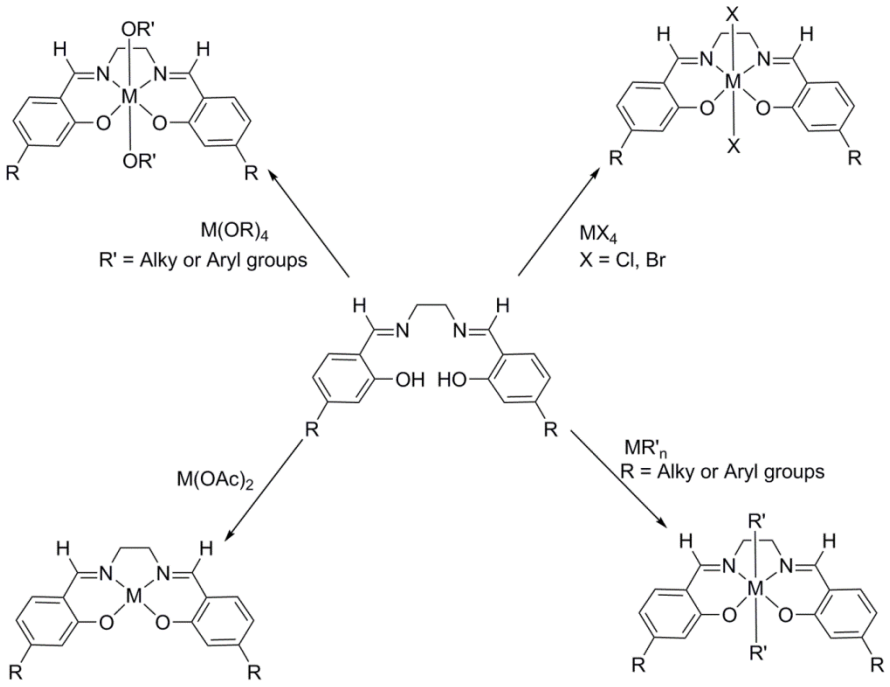

Figure 23. Various route of synthesis of metal Schiff base salen complexes.[181]

Metallomesogens based on salphen ligands have a rigid core favorable for anisotropy. Thus, favoring the supramolecular arrangement favoring mesomorphism. The nature of such material is easily tuned by altering the length of the carbon side chain and the bridging spacer group. Depending upon a metal precursor, the geometry of the metallomesogens can be controlled. Generally, Ni(II), Zn(II), Pd(II), Pt(II) metal center favor the planar geometry, which can be aligned easily along the axis resulting in columnar structures favoring the mesomorphic properties.

1.8.2 Metallomesogens with Co(II), Ni(II) and Cu(II) metal centers

Metallomesogens prepared using cobalt, nickel and copper are of great interest. They can coordinate with various ligands generating unique metallomesogens.[62, 182-187] Metal ions offer unique molecular structures when associated with suitably designed ligands. Hoon Lee *et al.*[186] reported terpyridine with substituted trimethoxypheynyl ligands were used to prepare Co(II) complexes (**Figure 24**) with mesomorphic behavior. These complexes can undergo spin crossover between a high-spin to low-spin altering its magnetic properties, which occurred during the phase transition from crystal to liquid crystal phase. Thus, the spin-crossover mechanism of cobalt(II) terpyridine metallomesogen in this case was phase dependent. Due to this unique property of these complexes, magnetic activity can be controlled. Liquid crystal incorporating paramagnetic metal ions are useful in display and communication technologies.

Similarly, metallomesogens formed by nickel(II) metal center generally have square planar geometry. These complexes are the diamagnetic nature as indicated by its square planar coordination. Giroud and Muller in 1977, first reported the synthesis of mesogenic nickel complex with dithiolenes as a ligand (**Figure 24**).[188] Analogous, mesomorphic nickel(II) complexes were prepared by various groups and their mesomorphic activities were well studied.[184, 189-191] Debnath *et al*.[184] reported the preparation of nickel-bis(dithiolene) metallomesogens. This complex exhibits the mesogenic properties at an ambient temperature. Similarly, nickel(II) complexes of hydrazonic ligands derived from 2,6-disubstituted pyridines and alkyl or aryl hydrazides were synthesized and reported by Battistine *et al*.[182] These complexes are unique as they can occur in monomeric square planar coordination or in dimeric with octahedral coordination. Interestingly, the complex exhibit mesophase and have magnetic properties in its dimeric form. [182]

Metallomesogens based on copper metal centers are studied due to its paramagnetic nature. Mostly the complexes exhibiting liquid crystalline character are of Cu(II) with a square planar coordination with the ligands.[30, 31, 101, 192, 193] For example, metallomesogens with copper(II) β-diketonates have square planar arrangement and are discotic phase in nature (**Figure 24**).

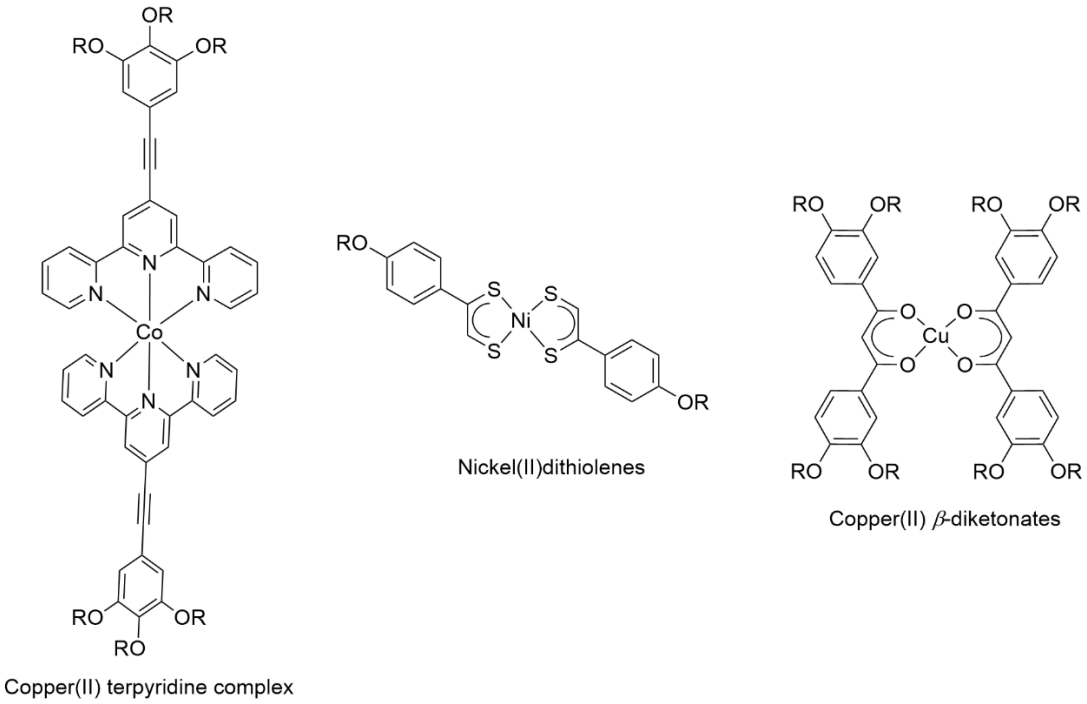

Figure 24. Selected metallomesogen complexes of cobalt(II), nickel(II) and copper(II) metal centers.

1.9 Characterization of Liquid Crystals

Liquid crystal materials are mostly characterized by three main techniques: polarize optical microscope (POM), differential scanning calorimetry, and X-ray diffractometry (XRD). [141] POM helps to reveal the various type of liquid crystal phases depending on the nature of distinct optical texture. However, POM only may not be enough. Therefore, DSC is always employed as a complementary technique to characterize liquid crystals. In addition, XRD is

utilized for the identification and classification of liquid crystal materials. Other techniques like magnetic resonance, neutron scattering, etc. are also useful in characterizing the liquid crystals.[141] However, POM, DSC, and XRD are the most commonly used techniques for the identification and characterization of the liquid crystalline molecules.

1.9.1 Polarized Optical Microscope (POM)

Polarized optical microscopy is an important analytical technique to observe and for the identification of the liquid crystalline material. This type of microscopy follows the principle of the polarization of light. As the natural light is non-polarized light and transmit in all directions. When the light transmitted is restricted to a single plane by filtration of the beam with the polarizer, then the light will propagate in a single plane, which is also termed as plane-polarized light. When two polarizers are crossed, their transmission axes are oriented perpendicular to each other, and light passing through the first polarizer completely vanished or absorbed by the second polarizer or analyzer (**Figure 25**).

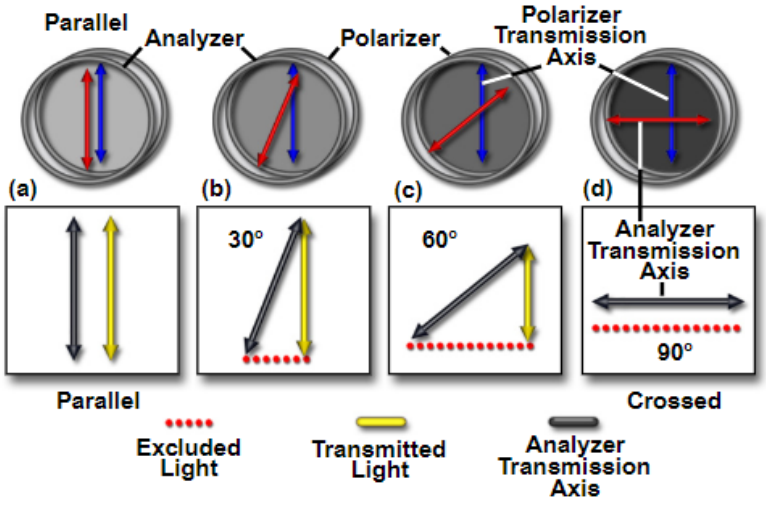

Figure 25. Transmission of polarized light through an analyzer.[194]

Utilizing this basic principle, the polarized optical microscope operates. POM is equipped with a polarizer and an analyzer. The polarizer is placed in the path of transmitting light before the specimen, which behaves as a filter and only allows the plane-polarized light to pass through. The second polarized or analyzer is placed 90° to the first one.Liquid crystalline materials are birefringent or have double refraction, which can be observed under the polarized light due to their optically anisotropic nature. Thus, polarized optical microscopy becomes very useful for identifying and investigating the properties of liquid crystalline materials. When the birefringent sample is placed in between two polarizers, the polarized light enters the sample, and due to their double refraction, the light will be refracted into two different types of rays, first the ordinary ray, while the second one is called an extraordinary ray. The light rays are recombined out of phase after passing through the sample, which creates the contrast after passing through the analyzer with constructive and destructive interference. The schematic diagram of the polarized optical microscope is shown below (**Figure 26**).

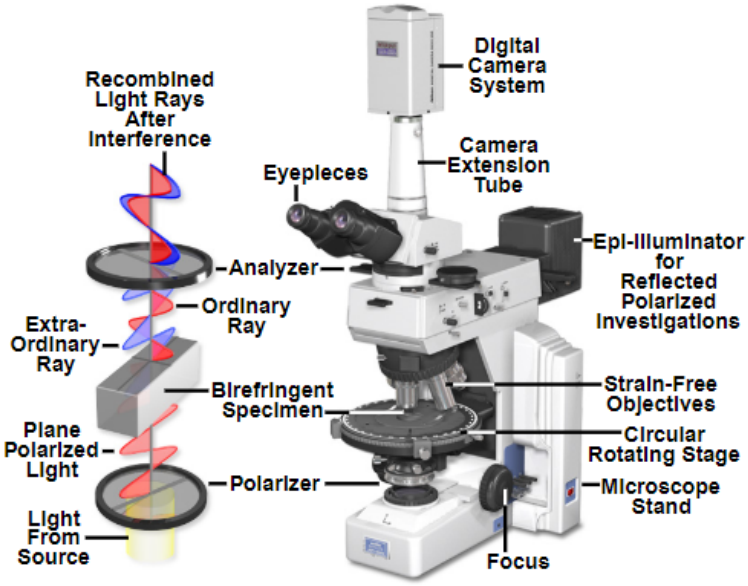

Figure 26. Detailed of polarized optical microscopy (POM).[194]

The experimental setup during the observation of the liquid crystal material requires a POM with certain magnification, with the cross-polarized perpendicular to each other and the temperature-controlled stage. The liquid crystal sample, when sandwiched between a glass slide and coverslip, is placed in between the two polarizers on the heating stage, the linearly plane-polarized light passing from the first polarizer does not vanish completely while passing through the analyzer. Due to this phenomenon, there appears an optical texture that provides information regarding the arrangement of the molecules. Depending on the nature of the various textures observed, the liquid crystal can be categories in various phases. Consequently, when the sample is non-birefringent in nature, the light passing the first polarizer remains unaffected and completely extinguished while passing through the analyzer and thus appears dark without any textures. To observe the texture of the liquid crystal material, it is always advised that the sample is first heated into the isotropic liquid and let it cool, slowing to observe the natural defect textures. This process is very helpful to avoid the paramorphosis from the crystalline state identifying the presence of various defects.[141]

As mention earlier, a liquid crystal, when sandwiched between a glass substrate, can orient either parallel or perpendicular to the glass plane. Due to imperfections and defects in the liquid crystal organization, the microscope preparation will contain a mixture of these orientations. These phenomena will lead to either homeotropic or homogenous orientation of the liquid crystal. Homogeneous orientation is generally due to the planar alignment, while the homeotropic orientation is due to orthogonal alignment.

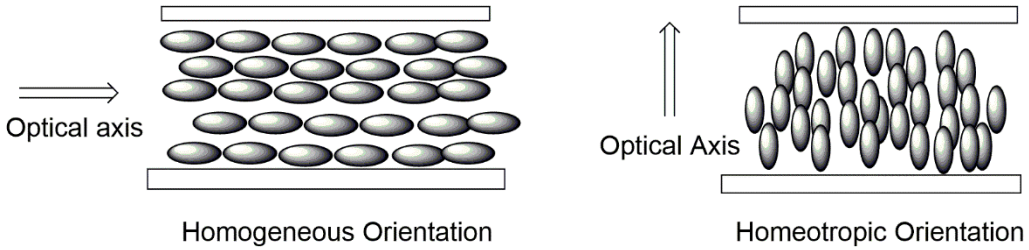

Figure 27. The various orientation of a liquid crystal.

The liquid crystalline samples under investigation, when observed using POM, will appear to have various multi-colored textures (**Figure 28**). The information on different phases of the liquid crystal can be obtained from the polarized optical texture. Schlieren textures can exist in the nematic phase and in some of the smectic phase. In the nematic liquid crystal molecules, the molecules can rotate along the axis. When the director is not parallel to the one of the polarizer, a dark line appears and run along with the sample and join as brushes. Due to this defect present in the liquid crystal, the orientation of the liquid crystal director changes resulting in Schlieren texture. In the smectic phase, when a sample is sandwiched between the glass substrates, the arrangement of different layers become complexed and different layer gets distorted and can slide over one another. Due to this distortion of the smectic phase, they can exhibit the focal conic texture.[195]

Figure 28. Optical textures observed by POM for various liquid crystal materials.[195-197] Reproduced with permission.

1.9.2 Differential Scanning Calorimetry (DSC)

DSC is one of the important techniques for the study of the thermal properties of liquid crystal. It helps to measure the thermal transition of liquid crystal samples as a function of temperature. DSC enables the determination of the melting, mesomorphic, and crystallization temperature of the liquid crystal samples. It measures the thermal transition of materials and monitors the detailed energy absorbed or released by a sample during the transition of the different phases, for example, from the crystalline phase to the liquid crystalline phase. As the sample absorbed the energy, it will result in an endothermic peak, while if the energy is released, then the exothermic peak will be observed. There are two small sample holders in the instrument, one for the sample and another for reference pan (**Figure 29**).

The calorimeter measures the relative uptake or output of heat from a sample with reference to the empty sample holder. Inside the heating chamber, both the sample holders are equipped with a resistance heater and a temperature sensor. Although the furnaces are heated separately, they are connected by two control loops at the current applied to change the temperature at the same rate. This will ensure the rate of heating and cooling remains the same throughout the procedure. Inside the chamber, a nitrogen atmosphere is maintained to prevent the oxidation of the samples at higher temperatures. Usually, the melting point has the largest peak as compare to the mesophase-to-mesophase or mesophase-to-isotropic liquid transition.[141] The change in entropy can be easily calculated by dividing the enthalpy by the temperature and the gas constant, followed by normalization per mole. In the DSC experiment, the difference in the amount of heat required to increase the temperature of a sample and reference is measured as a function of temperature.[198] It measures the amount of heat required to raise the temperature of the sample, then it determines the amount of the heat required to raise the temperature of the reference material. This allows the detection of transitions such as melting, glass transition, and clearing temperature.[199] Thus, when a sample is heated and cooled, the changes in heat capacity are recorded as a function of temperature.[141]

$$\Delta \frac{\mathrm{dH}}{\mathrm{dT}} = \left(\frac{\mathrm{dH}}{\mathrm{dT}}\right) \mathrm{sample} - \left(\frac{\mathrm{dH}}{\mathrm{dT}}\right) \mathrm{ref} \qquad 6$$

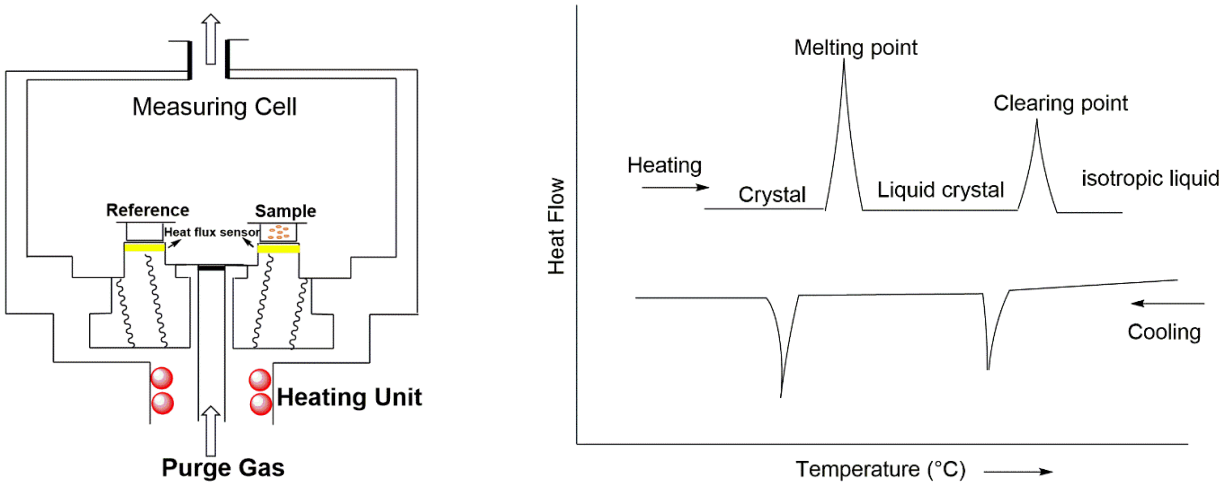

Figure 29. Schematic diagram of DSC (left) and typical DSC thermogram (right) of liquid crystal material.

In all DSC experiments, after the first round of heating and cooling, the second round of heating and cooling is also repeated to ensure reproducibility. In a heat flow DSC, those events which require energy point up and the change in enthalpy is positive, and those type of peak are called the endothermic peaks. In this condition, the instrument will supply more power to the sample to keep the sample and reference furnaces at the same temperature. Likewise, for the exothermic process, the change in enthalpy is negative, and the peak will point downwards. In the DSC thermogram, the first peak, which is usually associated with the melting of the sample, is the largest. The area under the peak usually provides information regarding the change in enthalpy.

1.9.3 X-Ray Diffraction (XRD)

X-ray diffraction is one of the important techniques used to analyze the atomic arrangement of materials. XRD utilizes the well-known Bragg's law for the structural determination of the liquid crystal. It states constructive X-rays reflected by adjacent planes

separated by a distance (d) in a crystal will occur when the path difference, 2d sin θ, between them is an integral multiple of the X-ray wavelength (λ),

$2d \sin \theta = n\lambda$

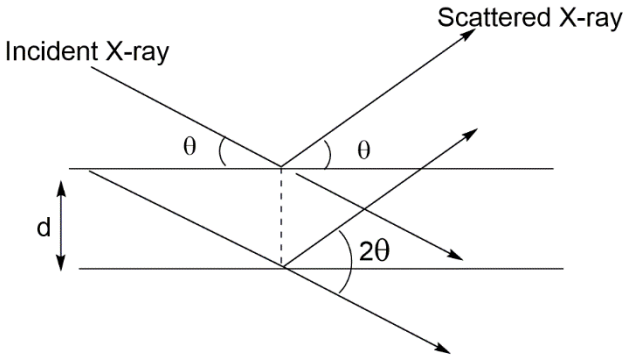

The peaks are observed when the Bragg's law is fulfilled and due to the constructive inference. These positions and the intensity of these peaks provide information on interplanar distances and molecular organization, giving a conclusive characterization of the mesophase.[141] For the hexagonal columnar liquid crystal, the intercolumnar distance (a) can be calculated using the following expression.[31]

$$\frac{a^2}{\left[\frac{4}{3}(h^2+hk+k^2)\right]} = d \qquad 7$$

where h, k, and l are the Miller indices and d, represent the *d*-spacing (Å).

The instrument consists of an X-ray source, a monochromator, a sample chamber, and a detector. Liquid crystals usually exhibit two types of a peak, one intense and sharp peaks in the small-angle region while broad and weak peaks are observed at wide-angle regions. In X-ray diffraction, usually, the identification of liquid crystal with the crystalline solids are distinctive. Due to some degree of order like solid in mesogens, they give rise to larger periodicities, and sharp and intense peaks are observed at smaller angles. Meanwhile, the liquid crystal has fluidity and has some freedom resulting in a wider diffraction peak. This phenomenon results in the

distinctive broad diffuse peak at a large angle. Small-angle X-ray scattering (SAXS) generally refers to where the scattering angle 2θ less than 10°. **Figure 30** is an example of the liquid crystal with the columnar hexagonal phase.[148] The *d*-spacing of the (10) and (11) reflection shows the ratio 1:1/√3. More geometric considerations result in the characteristics ratios of 1:1 ratios of 1:1√3:1//√4:1√7: 1√9: 1√12: 1√13 for the d spacings of the (10), (11), (20), (21), (30), (22), and (31) reflection of a 2-D hexagonal lattice in the small-angle regime.[148]

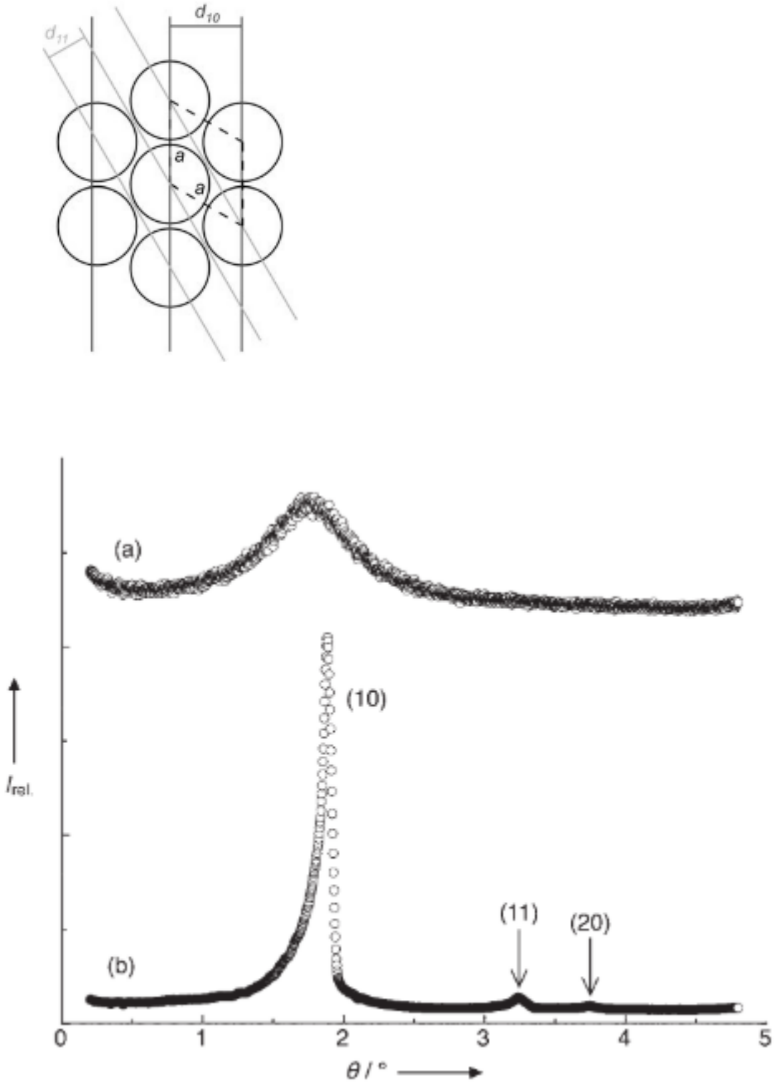

Figure 30. Representative small-angle X-ray scattering of a hexagonal liquid crystal. (a) isotropic melt, (b) Col_h mesophase.[148] Published by Angewandte Chemie. Reproduced with permission.

1.10 Properties of Liquid Crystals

The properties of liquid crystals are due to its birefringence, polarizability, dielectric permittivity, diamagnetism, and viscosity. These properties are described below:

1.10.1 Birefringence

Birefringence is the properties of the liquid crystal or the metallomesogens, which means it possesses two different indices of refraction or double refraction.[200] When a depolarized beam of light is incident through the liquid crystal, the beam is split into two rays taking slightly different paths, and they become linearly polarized, and the two perpendicularly polarized waves propagate at different velocities. This phenomenon happens due to the medium possesses two refractive indices. The birefringence of the liquid crystalline phase is the result of the parallel order of molecules exhibiting a polarizability anisotropy.[201 202] The birefringence of a liquid crystal material at a particular temperature is related to the anisotropy of polarizability, the molar density, and the degree of molecular order.[201]

1.10.2 Magnetism

Most of the liquid crystals are diamagnetic in nature.[203] The magnetic properties can be altered. The values of magnetic susceptibilities are low, but the diamagnetic response of some nematic or smectic liquid crystal can give important information regarding the nature of the liquid crystal. Inorganic liquid crystals, the main contribution of the susceptibility, arises due to aromatic ring incorporated in the liquid crystals. But the paramagnetic liquid crystal can be formed by incorporating various metal centers. As the paramagnetic characteristics originate due to electron-spin bearing metal atom.[201, 203] Thus, metallomesogens with the paramagnetic metal

center can exhibit the magnetic properties which are important in various optic-electric applications.

1.10.3 Dielectric anisotropy

Dielectric properties of the liquid crystalline material are the response of a system to an applied electric field. An electric field affects a liquid crystal by polarizing it. Liquid crystals have anisotropic dielectric properties, which provide structural information regarding the symmetry and orientation of the material. [203] If we consider a nematic phase of the mesogen, the anisometric molecules align along a single direction called the director n. for example is z-axis is parallel to the n, then one parallel to director $\varepsilon_{\parallel} = \varepsilon_{zz}$ while another perpendicular to the director will be $\varepsilon_{\perp} = \frac{1}{2}(\varepsilon_{xx} + \varepsilon_{yy})$. The dielectric anisotropy of the material can be defined as $\Delta\varepsilon = \varepsilon_{\parallel} - \varepsilon_{\perp}$

1.11 Application of Liquid crystal

Liquid crystals are molecular materials that combine molecular order and mobility.[124] This phase is often referred to as a curious phase, and their impact is profound in modern technology.[132] Liquid crystals have found use in numerous applications since its discovery (**Figure 31**).[129] During the 1950s, the liquid crystal materials were used in first cholesteric LC temperature indicators. Liquid crystals were useful in cancer diagnosis or in preparation for the laser devices. In 1965, with the development of liquid crystal displays (LCDs), there was a significant advancement in display technology. Significant breakthroughs in the evolution of liquid crystal technologies occurred in the 1980-1990s.[129] Until now, advance devices like mobile phones, display monitors, TVs, GPS, etc., use liquid crystal material for their manufacturing.[129]

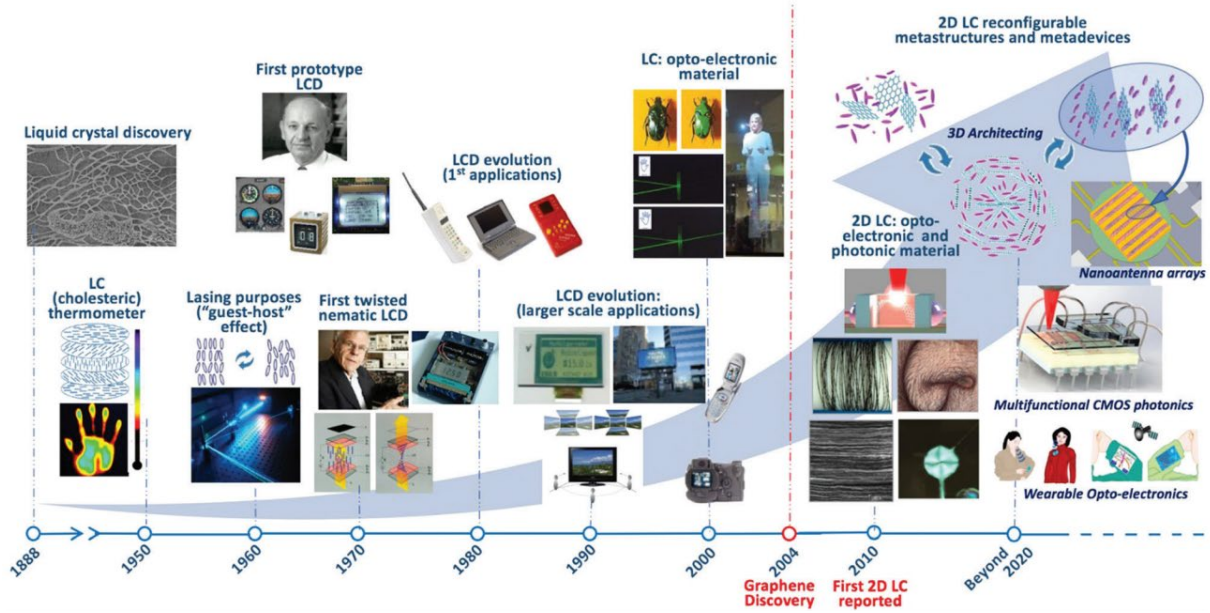

Figure 31. Timeline of the history of liquid crystal phase applications.[129] Published by The Royal Society of Chemistry. Reproduced with permission.

Liquid crystal material in the LC phase has the ability to align the director along an external field. Thus, such materials are applicable to manufacturing in optoelectronic devices. For example, the dispersion of liquid crystalline graphene oxide has been shown to undergo electro-optical switching with low threshold voltage requirements.[129 204]

The rod-like or disc-like liquid crystal can stack together via various intermolecular forces and form a column-like structure. These columns can again self-assemble, forming a rectangular or hexagonal shape. In some cases, they can also result in a helical structure. One of the advantages of such struck is they have void space that can incorporate functional guest molecules through covalent and non-covalent bonding.[124] Another function of such a supramolecular organization in the liquid crystal phase is applicable for the proton conduction. [205, 206]

Liquid crystal materials were found to have an application in the biomedical implications.[132] Scott J. Woltman *et al.*[132] utilized the liquid crystal material for optically probing biological systems. LC was used to synthesize biosensors. As well as the liquid crystal polymers are starting to be used in biomimicking color-producing structures, lenses, and muscle-like actuators.[132] The switchable electro-optic properties of the liquid crystal material make them ideal for the development of biomedical devices. Liquid-crystal tunable filters and spatial light modulators have opened up new pathways for efficient, low-cost optical components and integrated system.[132] An implantable medical device like cardiac pacemakers, cochlear prosthesis devices, and neuroprostheses have integrated liquid crystal polymer (LCP).[207] The biological environment is highly corrosive to many materials and the conductors used to connect the device to other electronic circuits or connectors must be able to withstand immersion of an ionic fluid with as much as a 10 Volt bias across it. [207, 208] Similarly, the liquid crystal with epoxy resin carbon fiber composite material was prepared, which are thermodynamically stable, and this material is vital to the technical field of biomedicine, aerospace, and other sciences. The liquid crystal epoxy resin carbon fiber composite material obtained has shape memory and have a high response rate and the ability to recover when stress.[209]

Introducing chirality was a novel step in the development of new liquid crystalline complexes.[210] Chiral nematic and smectic liquid crystal have captured much attention due to their importance in various fields. Liquid crystals may adopt the various phases like chiral nematic or cholesteric phase if any one component in the complex is chiral.[210] Reactive mesogen (RM) is a polymerizable mesogen or a liquid crystalline compound that is generally found in its monomeric form and can be used to prepare the optical films used in a variety of optical and electro-optical devices. The chiral liquid crystal films synthesized utilizing the reactive mesogens suitable to use

as reflective polarizers or brightness enhancement films. By changing the birefringence or the chirality of the RM material, the optical properties of the chiral liquid crystals can be controlled.[211]

Platinum-based luminescent metallomesogens like bis(3-(3,5-bis(dodecyloxy)phenyl)-(5-pyridin-2-yl)pyrazolate)platinum(II) are used in manufacture organic light-emitting diodes (OLED) devices.[212] The advantage of using platinum-based complexes lies in the geometries of the complex, which is usually square-planar, favoring self-organization due to metal-to-metal interaction, as well as the internal quantum efficiency, are nearly 100% resulting from harvesting both singlet and triplet excitons.[213 214] Cuerva *et al.,*[215] have reported the columnar discotic metallomesogen to have an ability as chemo and thermosensor.[215] Likewise, they also demonstrated the supramolecular organization of the metallomesogen have an ability a proton conductor in the LC phase.[205]

1.12 Preliminary liquid crystal studies with Ti(IV) complexes

The synthesis of discotic hexagonal metallomesogens was initially started in Holder's group in 2007, initiated by Jennifer Vital. Vital used Schiff bases salen and salphen as ligands and titanium(IV) ions to synthesize metallomesogens. Based on the earlier analysis, only C_{18}O-salphen (**Figure 32**) and C_{18}O-salphen Ti(IV) complexes were found to have liquid crystal properties. The liquid crystal properties of synthesized ligands and the complexes were analyzed by using only POM. Vital results indicated that the C_{18}salen ligand has LC properties in a very narrow range of temperature, i.e., 104 °C to 106 °C. In comparison, the complexes exhibit the LC properties in the range of 122 °C to 153 °C. The increase in the thermal stability of the complex is very impressive. Thus, further investigation of such complexes is continued in this project.

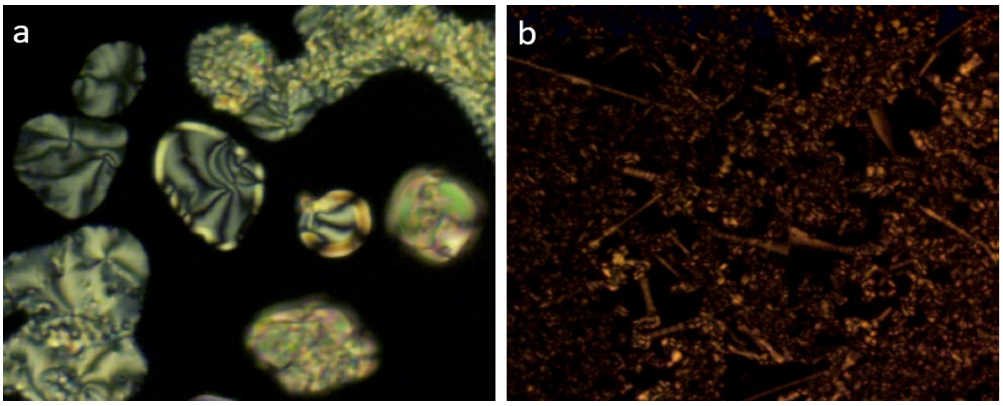

Figure 32. Liquid crystal prepared earlier in Holder's Lab (a) $C_{18}H_{37}O$-salphen, and (b). [Ti($C_{18}H_{37}O$-salphen)]

1.13 Aims of the Project

Liquid crystalline materials are soft matter. Varying degrees of positional order, bond orientational order, and molecular orientational order results in various types of liquid crystal phases such a nematic, smectic and hexagonal phases.[216] Rod-like or disc-like shape molecules can generate a discotic columnar mesogen, which is important in optoelectronic. These types of mesogens are characterized by long-range orientational order in one direction. These types of a molecule can coordinate with various metal centers and exhibit a wide variety of properties. The smart phase transition of the liquid crystal makes them suitable in various applications such as fast switching devices, rewritable memories, non-linear optics, etc.; they are considered important in optoelectronic industries. [217-225] It is now well established that the rod-like or disc-like molecule can generate the discotic liquid crystal, which is applicable in various purposes. Usually, to prepare such liquid crystal, a wide variety of five or six-membered aromatic rings are utilized and are also reported elsewhere. To better understand the fundamental properties and the nature of the metallomesogens, we aimed to synthesize Schiff base salen and salphen-based

metal complexes. Structurally this type of complexes will have a half-disc like a shape. We anticipate this structure of the complexes can form a discotic columnar phase.

From the earlier studies, it was clear that the synthesis of complexes using first row transition metal ions and Schiff bases can produce metallomesogens. Metal ion, when coordinated with the organic liquid crystal, can increase the thermal stability of the complex and enhances the liquid crystal behavior.

Here we first aimed to synthesize a series of titanium(IV) Schiff base complexes. In the first project, we utilized smaller tetradentate Schiff base salen ligand. In this study, the information regarding the mechanism of the synthesis, as well as proper characterization techniques, were developed. We were interested in developing the proper method to obtain the crystals and to solve the crystal structure of the complexes. The ^{49}Ti NMR spectra of the complexes were acquired, which can help to describe the electronic environment around the metal center. This work provided a fundamental understanding of the preparation of the complexes and their various properties.

The second project was the continuation of the earlier work. In this project, the ligands were derived from substituted salicylaldimine. The salen-scaffold were tuned by the addition of the long-tailed hydrocarbon chained with different chain length. For a molecule to behave like a liquid crystal, the molecules are designed where the rigid core molecules are functionalized with one or more flexible hydrocarbon tails. The rigid segment leads to a parallel organization of the liquid crystal material, and the flexible chains provide mobility enhancing the liquid crystalline behavior. A series of ligands (C_nH_{2n+1}-O-salen where n= 16 and 18) were prepared and coordinated with titanium(IV) metal ion prepare resulting in an octahedral geometry. Further, the thermal behavior of the synthesized ligands and the complexes were studied. POM and DSC

were used for the study of the optical and thermal behavior of the synthesized ligands and the complexes.

In conjunction with the second project, the adjustment on the ligand design was made where the core molecules were adjusting, which will directly affect the rigidity of the core. Aromatic amine groups were utilized to adjust the properties of the core unit. The modification of the shape was made to achieve a rod-shape or disc shape molecule, which can exhibit calamitic and discotic liquid crystal phases, respectively. The transition of mesophases from rod-like to disc-like shape was made possible by adjusting the ratio of width-to-length. The ligands synthesized were coordinated with cobalt(II), nickel(II), and copper(II) metal ions resulting in four coordinated metallomesogen complexes. The liquid crystalline properties of the ligands and the complexes were analyzed by POM, DSC, and XRD, where appropriate. The geometrical arrangement of liquid crystal was confirmed by XRD. POM helps to establish the nature of the liquid crystal formed, and DSC was useful in determining the transition temperature during the phase transition.

We have aimed this dissertation will provide a fundamental understanding regarding the ligand design and effect of different geometries on the nature of metallomesogens.

CHAPTER 2
EXPERIMENTAL

Synthesis and Characterization of Transition Schiff Base Salen Complexes

2.1 Materials and Experimental

All reagents were of analytical grade and purchased from Sigma-Aldrich, VWR, and Fisher Scientific.

2.2 Physical measurement

All ^{1}H NMR, ^{19}F NMR, and ^{49}Ti NMR spectra were acquired on a Bruker 400 MHz spectrometer with $CDCl_3$ as a solvent. ^{19}F spectra were referenced to CF_3COOH (δ = -76.55 ppm) as an external standard.[33] ^{49}Ti NMR spectra were acquired (12550 transients were acquired with a saturated solution) at ambient temperature using $CDCl_3$ as the deuterated solvent. All solutions were referenced to $TiCl_4$ (δ = 0.00 ppm) [1] as an external standard. All NMR spectra were processed using ACD/NMR Processor Academic Edition and BRUKER topspin software.

All FTIR spectra were acquired on a Thermo© Nicolet Avatar 370 DTGS (FT IR/ATR IR) spectrophotometer and Bruker Platinum ATR-IR spectrometer. Elemental analysis for carbon, hydrogen, and nitrogen was acquired on a Thermo Scientific FLASH 2000 Organic Elemental analyzer.

Polarising optical microscopy was carried out using an Olympus BX50 polarising microscope equipped with a Linkam scientific LTS350 heating stage, Linkam LNP2 cooling pump, and Linkam TMS92 controller. In addition, polarized optical images were obtained by Briska optical microscope with 10x magnification equipped with two polarizer place 90^{o} to each other. The sample was sandwiched between two glass slides and slowly heated until melt, which was then placed in between the two polarizers of an optical microscope. All the polarized images

were acquired during the cooling cycle. Differential scanning calorimetry was performed on a TA Instruments Q250 DSC equipped with an RCS 90 cooling accessory, and the transition temperatures were determined from the second heating run at a rate of 10 °C min^{-1} by using the Universal Analysis software. Small angle X-ray scattering was recorded using a Bruker D8 Discover equipped with a temperature-controlled, bored graphite rod furnace, custom built at the University of York, England, U.K. Cu-K_α (λ = 0.154056 nm) radiation was used, generated from a 1 μS microfocus source. Diffraction patterns were recorded on a 2048 × 2048 pixel Bruker VANTEC 500 area detector set at a distance of 121 mm from the sample, allowing simultaneous collection of small angle and wide angle scattering data. Samples were measured in 1 mm capillary tubes in a magnetic field of *ca* 1 T.

Structural acquisition by single crystal X-ray diffraction was carried out at 100 K by using a Bruker D8 Venture diffractometer. The data was collected via phi and omega scans using Mo Kα radiation (0.71073 Å) and a Photon 100 detector. Space group determination was carried out with the aid of the XPREP interface of SHELXTL [39]. The structures were solved by intrinsic phasing (SHELXT) and refined by full-matrix least squares techniques on F^2 (SHELXL) [226]. All non-hydrogen atoms were refined anisotropically, and hydrogen atoms were refined in calculated positions using riding models. In the case of complex **3**, the solvent was highly disordered and its electron density was modeled using the PLATON/SQUEEZE program. [227] The crystallographic data has been deposited with the CCDC, deposition numbers 1958627-1958632.

2.3 General synthesis of the ligands using 2-hydroxybenzaldehyde

2.3.1 Synthesis of H_2salen

To a solution of salicylaldehyde (4.5 ml, 41 mmol) in boiling ethanol (50 ml) in a 100 ml round bottom (RB) flask, ethlyenediamine (1.4 ml, 20 mmol) was added. The reaction mixture was thoroughly stirred for 3-4 minutes until flaky yellow crystals were formed. The solution was then cooled in an ice bath with continuous swirling. The crystals were filtered, washed with ethanol, and air-dried. Yield: 93.14%; ^{1}H NMR (400 MHz, $CDCl_3$) δ ppm 3.94 (s, 4 H) 6.83 - 6.91 (m, 2 H) 6.91 - 7.05 (m, 2 H) 7.20 - 7.38 (m, 4 H) 8.36 (s, 2 H) 13.20 (s, 2 H)

2.4 General synthesis of $C_nH_{2n+1}O$-salen type ligand

2.4.1 Synthesis of 2-hydoxy-4-(hexadecyloxy)benzaldehyde ($C_{16}H_{33}O$-sal)

2,4-Dihydroxybenzaldehyde (10 g, 0.07 mol), potassium hydroxide (4.05 g, 0.07 mol), ethanol (200 mL), and 1-bromohexadecane (41.22 g, 0.135 mol) were added to a round bottom flask(500 mL) and refluxed with stirring for 24 hours. After cooling to room temperature, the mixture was added to de-ionized water (75 mL). This mixture was suction-filtered. The solid was collected and allowed to air dry. The solid was added to a 500 mL conical flask; then, methanol was added to ¾ the volume of the flask. This mixture was heated to boiling with stirring (glass rod). As soon as an oily solid was observed at the bottom of the flask, the mixture was quickly filtered hot with a Buchner flask and filter paper. The solid at the bottom of the flask was retained. More methanol was added to the flask and the procedure was repeated. The combined filtrates were cooled. The deposited white precipitant was filtered and retained. Yield = 12.00 g (47 %). FTIR (KBr , ν/cm-^{1}): 2916, 2849(s) (CH) 1678(s) (C=O); ^{1}H NMR ($CDCl_3$)/ δppm 0.89 (t, *J* = 1.00 Hz, 3 H) 1.25 - 1.37 (m, 25 H) 1.45 (d, *J* = 7.92 Hz, 2 H) 1.75 - 1.90 (m, 2 H) 4.01 (t, *J* = 6.60

Hz, 2 H) 6.42 (d, *J* = 2.20 Hz, 1 H) 6.53 (dd, *J* = 8.69, 2.31 Hz, 1 H) 7.42 (d, *J* = 8.80 Hz, 1 H) 9.71 (s, 1 H) 11.48 (s, 1 H)

2.4.2 Synthesis of 2-hydoxy-4-(n-octadecyloxy)benzaldehyde ($C_{18}H_{37}O$-sal)

This preparation was adapted from I. Aiello *et al.*, Eur. *J. Inorg. Chem.* **1999.** 1367-1372. 2,4-dihydroxybenzaldehyde (10 g, 0.07 mol), potassium hydroxide (4.05 g, 0.07 mol), ethanol (200 mL), and 1-bromooctadecane (45 g, 0.135 mol) were added to a round bottom flask (500 mL) and refluxed with stirring for 24 hours. After cooling to room temperature, the mixture was added to de-ionized water (75 mL). This mixture was suction filtered. The solid was collected and allowed to air dry. The solid was added to a 500 mL conical flask: then methanol was added to ¾ the volume of the flask. This mixture was heated to boiling with stirring (glass rod). As soon as an oily solid was observed at the bottom of the flask, the mixture was quickly filtered hot with a Buchner flask and filter paper. The solid at the bottom of the flask was retained. More methanol was added to the flask, and the procedure was repeated. The combined filtrates were cooled. The deposited white precipitant was filtered and retained. Yield = 13.851 g (51%). FTIR (KBr , ν/cm-^{1}): 2916, 2849(s) (CH) 1678(s) (C=O); ^{1}H NMR ($CDCl_3$) δ/ppm: 0.89 (t, *J* = 1.00 Hz, 3 H) 1.30 (d, *J* = 1.00 Hz, 30 H) 1.86 (s, 2 H) 4.01 (s, 2 H) 6.34 - 6.46 (m, 1 H) 6.46 - 6.58 (m, 1 H) 7.42 (d, *J* = 8.80 Hz, 1 H) 9.71 (d, *J*=0.44 Hz, 1 H) 11.47 (s, 1 H)

2.4.3 Synthesis of $C_{16}H_{33}O$-salen

$C_{16}H_{33}O$-sal (3.00 g, 8.18 mmol) was added with ethylenediamine (0.25 g, 273.24 µl, 4.09 mmol) in ethanol (80 mL) and 3 drops of glacial acetic acid were mixed, and the mixture was refluxed overnight for 16 hours with constant stirring in a 100 ml RB flask. The yellow

solution was then cooled to room temperature and finally cooled on an ice bath. The solution was filtered. The precipitate was washed with ethanol and air-dried. Yield = 2.095 g (69 %). FTIR (KBr , ν/cm-^{1}): 2916,2849(s) (CH) 1617(s) (C=N), 1114(s) (Ar-O); ^{1}H NMR (*$CDCl_3$*)/ δppm = 0.88 (t), 1.19 - 1.48 (m), 1.26 (s), 3.84 (s), 3.94 (s), 6.39 (s), 7.07 (s), 8.19 (s), 13.64 (br. s.)

2.4.4 Synthesis of $C_{18}H_{37}O$-salen

$C_{18}H_{37}O$-sal (1.116 g, 2.37 mmol) was added with ethylenediamine (0.0858 g, 1.43 mmol) in ethanol (40 mL), and 3 drops of glacial acetic acid were mixed, and the mixture was refluxed overnight for 16 hours with constant stirring in a 100 ml RB flask. The yellow solution was then cooled to room temperature and finally cooled on an ice bath. The solution was filtered. The precipitate was washed with ethanol and air-dried. Yield = 0.8674 g (91 %). FTIR (KBr , ν/cm-^{1}): 2916, 2849(s) (CH) 1617(s) (C=N), 1114(s) (Ar-O); ^{1}H NMR (400 MHz, $CDCl_3$)/δ ppm 0.89 (s, 6 H) 1.22 - 1.50 (m, 60 H) 1.72 - 1.82 (m, 4 H) 3.85 (s, 4 H) 3.95 (s, 4 H) 6.34 - 6.43 (m, 4 H) 7.03 - 7.11 (m, 2 H) 8.20 (s, 2 H) 16.67 (m, 2 H)

2.4.5 Synthesis of $C_{14}H_{29}O$-2,5-ester-en

3-Formyl-4-hydroxyphenyl-3,4,5-tris(tetradecyloxy)benzoate (1.0092 g, 1.14 mmol) was added to a 250 mL RB flask with a stir bar. Ethyl acetate (50 mL) was then added and the mixture was heated until add solids were dissolved. Ethylenediamine (40.00 uL, 0.59 mmol) was added. The mixture was refluxed for two hours at 110 C. the reaction mixture was then cool to room temperature and further cool down using ice-bath. The solid precipitate were then filtered and washed (ethyl acetate, ethanol and ether). The product was dried over vacuum. Yield = 0.8182g

(80 %). FTIR (ν/cm^{-1}): 1727s (C=O), 1637s (C=N), 1202 (C-O). ^{1}H NMR (*CDCl$_3$*)/ δppm = 0.88 (td, *J* = 6.93, 1.76 Hz), 1.26 (d, *J* = 2.42 Hz), 1.61 (br. s.), 1.70 - 1.88 (m), 3.97 (s), 4.05 (q, *J* = 6.60 Hz), 7.00 (s), 7.11 (s), 7.38 (s), 8.36 (s), 13.36 (m).

2.5 General synthesis of the ligands C$_n$-2,4-salphen ligand

2.5.1 Synthesis of methyl-3,5-bis(dodecyloxy)benzoate

A solution of methyl-3,5-dihydrooxybenzoate (20 g, 130 mmol) K_2CO_3 (32.88 g, 237.9 mmol) and 1-bromododecane (59.29 g, 57.01 mL, 237.9 mmol) were refluxed in 2-butanone (100 mL) for 24 h. After completion of the reaction, the reaction mixture was cooled to room temperature, the mixture was filtered through fine frit and the solvent evaporated under reduced pressure. Yield = 29.12 g (49 %). Calc for $C_{32}H_{56}O_4$; C, 76.14; H, 11.18, Found; C, 76.41; H, 11.35. FTIR (ν/cm^{-1}): 1721s (C=O), 1323s (C-OMe); ^{1}H NMR (*CDCl$_3$*) δ/ppm: 0.84 - 0.94 (m), 1.24 - 1.48 (m), 1.56 (s), 1.73 - 1.91 (m), 3.42 (t, *J* = 6.93 Hz), 3.90 (s), 3.98 (t, *J* = 6.49 Hz), 6.64 (t, *J* = 2.31 Hz), 7.17 (d, *J* = 2.20 Hz); ^{13}C NMR (*CDCl$_3$*) δ/ppm: 14.09 (s), 22.68 (s), 23.12 (s), 26.01 (s), 28.18 (s), 28.77 (s), 29.18 (s), 29.34 (s), 29.36 (s), 29.43 (s), 29.56 (s), 29.62 (s), 29.65 (s), 31.91 (s), 32.86 (s), 34.00 (s), 52.14 (s), 68.34 (s), 106.62 (s), 107.66 (s), 131.83 (s), 160.17 (s), 166.99 (s).

2.5.2 Synthesis of methyl-3,5-bis(octadecyloxy)benzoate

A solution of methyl-3,5-dihydrooxybenzoate (5.0 g, 29.74 mmol), K_2CO_3 (8.22 g, 59.47 mmol) and 1-bromododecane (19.83 g, 59.47 mmol) were refluxed in 2-butanone (100 mL) for 24 h. After completion of the reaction, the reaction mixture was cooled to room temperature, the mixture was filtered through fine frit and the solvent evaporated under reduced pressure. Yield =

10.57 g (53 %). Calc for $C_{44}H_{80}O_4$; C, 78.51; H, 11.98, Found; C, 78.11; H, 11.35. FTIR (ν/cm^{-1}): 1721s (C=O), 1323s (C-OMe); ^{1}H NMR (*CDCl₃*) δ/ppm: 0.84 - 0.94 (m), 1.24 - 1.48 (m), 1.56 (s), 1.73 - 1.91 (m), 3.42 (t, *J* = 6.93 Hz), 3.90 (s), 3.98 (t, *J* = 6.49 Hz), 6.64 (t, *J* = 2.31 Hz), 7.17 (d, *J* = 2.20 Hz); ^{13}C NMR (*CDCl₃*) δ/ppm: 14.09 (s), 22.68 (s), 23.12 (s), 26.01 (s), 28.18 (s), 28.77 (s), 29.18 (s), 29.34 (s), 29.36 (s), 29.43 (s), 29.56 (s), 29.62 (s), 29.65 (s), 31.91 (s), 32.86 (s), 34.00 (s), 52.14 (s), 68.34 (s), 106.62 (s), 107.66 (s), 131.83 (s), 160.17 (s), 166.99 (s).

2.5.3 Synthesis of 3,5-bis(dodecyloxy)phenyl methanol

To a suspension of $LiAlH_4$ (4.70 g, 123.8 mmol) in THF (100 ml) was added dropwise a solution of methyl-3,5-bis(dodecyloxy)benzoate (25.00 g, 49.52 mmol). The mixture was refluxed for 6 hours under argon, quenched with water and acidified with 2M HCl. After being stirred for 10 min, the mixture was extracted with CH_2Cl_2 (6 x 100 ml). The combined organic layer was washed subsequently with brine and water, dried over anhydrous Na_2SO_4 and evaporated to dryness to give a product. Yield = 22.30 g (95 %) Calc. for $C_{31}H_{56}O_3$: C,78.09; H,11.84 , Found: C, 78.33; H 12.01. FTIR (ν/cm^{-1}): 1721s (C=O), 1323s (C-OMe) ^{1}H NMR NMR (*CDCl₃*) δ/ppm : 0.91 (t, *J*=1.00 Hz), 1.22 - 1.52 (m), 1.71 - 1.85 (m), 3.96 (t, *J*=6.49 Hz), 4.64 (s), 6.40 (t, *J*=2.31 Hz), 6.52 (d, *J*=2.20 Hz); ^{13}C NMR NMR (*CDCl₃*) δ/ppm : 22.67 (s), 26.04 (s), 29.26 (s), 29.34 (s), 29.38 (s), 29.58 (s), 29.59 (s), 29.63 (s), 29.66 (s), 31.91 (s), 65.49 (s), 68.08 (s), 100.61 (s), 105.09 (s), 143.18 (s), 160.57 (s)

2.5.4 Synthesis of 3,5-bis(octadecyloxy)phenyl methanol

To a suspension of $LiAlH_4$ (1.41 g, 37.14 mmol) in THF (50 ml) was added dropwise a solution of methyl-3,5-bis(dodecyloxy)benzoate (10.00 g, 14.86 mmol). The mixture was refluxed

for 6 hours under argon, quenched with water and acidified with 2M HCl. After being stirred for 10 min, the mixture was extracted with CH_2Cl_2 (3 x 100 ml). The combined organic layer was washed sebsequentlywith brine and water, dried over anhydrous Na_2SO_4 and evaporated to dryness to give a product. Yield = 8.63 g (90 %) Calc. for $C_{43}H_{80}O_3$: C,80.06; H,12.50 , Found: C, 79.80; H 12.21. FTIR (ν/cm^{-1}): 1721s (C=O), 1323s (C-OMe) ^{1}H NMR NMR (*CDCl₃*) δ/ppm : 0.91 (t, *J*=1.00 Hz), 1.22 - 1.52 (m), 1.71 - 1.85 (m), 3.96 (t, *J*=6.49 Hz), 4.64 (s), 6.40 (t, *J*=2.31 Hz), 6.52 (d, *J*=2.20 Hz); ^{13}C NMR NMR (*CDCl₃*) δ/ppm : 22.67 (s), 26.04 (s), 29.26 (s), 29.34 (s), 29.38 (s), 29.58 (s), 29.59 (s), 29.63 (s), 29.66 (s), 31.91 (s), 65.49 (s), 68.08 (s), 100.61 (s), 105.09 (s), 143.18 (s), 160.57 (s)

2.5.5 Synthesis of 3,5-bis(dodecyloxy)benzylbromide

A solution of 3,5-bis(dodecyloxy)benzyl alcohol (2.01 g, 4.22 mmol), triphenylphosphine (1.35 g , 5.15 mmol), and carbon tetrabromide (3.50 g, 10.56 mmol) in dry CH_2Cl_2 (50 mL) was stirred at room temperature for 4 h under Ar. The solution was washed with aq satd $NaHCO_3$ (2 x 25 mL) and aq satd NaCl (2 x 25 mL), dried over Na_2SO_4 and concentrated in vacuo. The crude product was purified using column chromatography (SiO_2: Hexane:CH_2Cl_2 = 4:1) Yield = 1.69 g (81 %). Calc for $C_{31}H_{55}BrO_2$: C, 68.99; H, 10.27, Found: C, 69.13; H 10.41. FTIR (ν/cm^{-1}): 1721s (C=O), 1323s (C-OMe) ^{1}H NMR (*CDCl₃*)/d ppm: 0.91 (m), 1.22 - 1.51 (m), 1.72 - 1.84 (m), 3.95 (t, *J*=6.60 Hz), 4.43 (s), 6.40 (t, *J*=2.31 Hz), 6.54 (d,*J* =2.20 Hz); ^{13}C NMR (*CDCl₃*) δ/ppm:14.09 (s), 15.48 (s), 22.68 (s), 26.03 (s), 29.23 (s), 29.34 (s), 29.37 (s), 29.56 (s), 29.59 (s), 29.63(s), 29.66 (s), 31.91 (s), 33.76 (s), 61.15 (s), 68.13 (s), 101.48 (s), 107.23 (s), 107.42 (s), 139.52 (s), 160.44 (s), 178.21 (s)

2.5.6 Synthesis of 3,5-bis(octadecyloxy)benzylbromide

A solution of 3,5-bis(dodecyloxy)benzyl alcohol (2.01 g, 4.22 mmol), triphenylphosphine (1.35 g , 5.15 mmol), and carbon tetrabromide (3.50 g, 10.56 mmol) in dry CH_2Cl_2 (50 mL) was stirred at room temperature for 4 h under Ar. The solution was washed with aq satd $NaHCO_3$ (2 x 25 mL) and aq satd NaCl (2 x 25 mL), dried over Na_2SO_4 and concentrated in vacuo. The crude product was purified using column chromatography (SiO_2: Hexane: CH_2Cl_2 = 4:1) Yield = 4.51 g (52 %). Calc for $C_{43}H_{79}BrO_2$: C, 72.95; H, 11.25, Found: C, 72.75; H 11.01. FTIR (ν/cm^{-1}): 1721s (C=O), 1323s (C-OMe) ^{1}H NMR (*CDCl$_3$*)/d ppm: 0.91 (m), 1.22 - 1.51 (m), 1.72 - 1.84 (m), 3.95 (t, *J*=6.60 Hz), 4.43 (s), 6.40 (t, *J*=2.31 Hz), 6.54 (d,*J* =2.20 Hz); ^{13}C NMR (*CDCl$_3$*) δ/ppm:14.09 (s), 15.48 (s), 22.68 (s), 26.03 (s), 29.23 (s), 29.34 (s), 29.37 (s), 29.56 (s), 29.59 (s), 29.63(s), 29.66 (s), 31.91 (s), 33.76 (s), 61.15 (s), 68.13 (s), 101.48 (s), 107.23 (s), 107.42 (s), 139.52 (s), 160.44 (s), 178.21 (s)

2.5.7 Synthesis of C_{12}-2,4-sal ligand

A suspension of 2,4-dihyroxybenzaldehdye (0.346 g, 2.5 mmol), KI (0.076 g, 0.46 mmol) and $NaHCO_3$ (0.272 g, 3.24 mmol) in anhydrous MeCN (60 mL) was stirred at 70 °C for 15 minutes. A warm solution of 3,5-bis(dodecyloxy)benzyl bromide (1.0 g, 0.536 mmol) in dry THF (10 mL) was added slowly and stirred at reflux was continued for 3 days. The precipitate formed was filtered and washed with THF. The combined filtrate were evaporated in vacuum and the residue was purified by gradient column chromatography (SiO_2hexane:ethylacetate = 9:1 and hexane:EtOAc 4:1). Yield = 0.783 g (71%) %, Calc; C, 76.47; H, 10.13; Found: C, 76.69; H, 10.50; ^{1}H NMR ($CDCl_3$)/δ ppm 0.91 (d, *J* = 13.64 Hz, 6 H) 1.31 (m, 32 H) 1.46 (d, *J* = 7.92 Hz,

4 H) 1.79 (m, 4 H) 3.96 (t, *J* = 6.60 Hz, 4 H) 5.05 (s, 2 H) 6.44 (s, 2 H) 6.53 (m, 3 H) 6.63 (m, 1 H) 7.45 (d, *J*=8.58 Hz, 1 H) 9.74 (s, 1 H) 11.47 (s, 1 H)

Literature[228] :

^{1}H NMR ($CDCl_3$, 500 MHz): δ/ppm 0.88 (t, 6H, *J* = 7.0 Hz). 1.39– 1.19 (m, 32 H), 1.49–1.39 (m, 4H,), 1.81–1.71 (m, 4H) , 3.93 (t, 4H, *J* = 6.6Hz,), 5.02 (s, 2H,), 6.41 (t, 2H, *J* = 2.3 Hz,) , 6.49 (d, 1H, *J* =2.4 Hz,) , 6.52 (d, 2H, *J* = 1.8 Hz,) , 6.60 (dd, 1H, *J* = 8.7, 2.3 Hz) 7.43 (d, 1H, *J* = 8.7 Hz,), 9.71 (s, 1H, CHO), 11.46 (s, 1H, OH); ^{13}C NMR (CDCl3, 125 MHz): 194.6 (CHO), 166.0, 164.6, 160.8, 137.9, 135.4, 115.8, 109.1, 105.8, 101.8, 101.1, 70.5, 68.2, 32.1–29.0, 22.8, 29.5, 26.2, 14.3.

2.5.8 Synthesis of C_{18}-2,4-sal ligand

A suspension of 2,4-dihyroxybenzaldehdye (0.897 g, 6.5 mmol), KI (0.080 g, 0.48 mmol) and $NaHCO_3$ (1.21 g, 14.43 mmol) in anhydrous MeCN (80 mL) was stirred at 70 °C for 15 minutes. A warm solution of 3,5-bis(octadecyloxy)benzyl bromide (3.00 g, 4.81 mmol) in dry THF (10 mL) was added slowly and stirred at reflux was continued for 3 days. The precipitate formed was filtered and washed with THF. The combined filtrate were evaporated in vacuum and the residue was purified by gradient column chromatography (SiO_2, hexane: ethylacetate = 9:1 and hexane:EtOAc 4:1) Yield = 0.935 g (32%), Calc; C, 78.48.47; H, 11.07; Found: C, 78.68; H, 11.37; ^{1}H NMR (400 MHz, $CDCl_3$)/δ ppm 0.91 (t, *J* = 1.00 Hz, 6 H) 1.16 - 1.59 (m, 60 H) 1.78 (d, *J* = 7.92 Hz, 4 H) 3.96 (t, *J* = 6.60 Hz, 4 H) 5.05 (s, 2 H) 6.42 - 6.46 (m, 1 H) 6.55 (d, *J* = 2.20 Hz, 3 H) 6.60 - 6.66 (m, 1 H) 7.45 (d, *J*=8.58 Hz, 1 H) 9.74 (s, 1 H) 11.47 (s, 1 H)

2.5.9 Synthesis of Cn-2,5-sal ligand

A suspension of 2,5-dihyroxybenzaldehdye (0.345 g, 2.5 mmol), KI (0.076 g, 0.46 mmol) and $NaHCO_3$(0.274 g, 3.24 mmol) in MeCN (60 mL) was stirred at 70 °C for 15 minutes. A warm solution of benzyl bromide (1.0 g, 0.536 mmol) in dry THF (10 mL) was added slowly and stirred at reflux was continued for 3 days. The precipitate formed was filtered and washed with THF. The combined filtrate were evaporated in vacuum and the residue was purified by gradient column chromatography.(SiO_2, hexane: ethylacetate = 9:1 and hexane:EtOAc 4:1) Yield = 0.086 g (8 %) ^{1}H NMR (400 MHz, $CDCl_3$)/δ ppm 0.85 - 0.95 (m, 6 H) 1.24 - 1.40 (m, 32 H) 1.40 - 1.50 (m, 4 H) 1.71 - 1.83 (m, 4 H) 3.94 (t, *J* = 6.60 Hz, 4 H) 4.99 (s, 1 H) 6.42 (t, *J* = 2.20 Hz, 1 H) 6.55 (d, *J*=2.20 Hz, 2 H) 6.94 (d, *J* = 9.02 Hz, 1 H) 7.07 (d, *J* = 3.08 Hz, 1 H) 7.22 (dd, *J* = 9.13, 2.97 Hz, 1 H) 9.84 (d, *J* = 0.44 Hz, 1 H) 10.66 (s, 1 H)

2.5.10 Synthesis of C_{12}-2,4-salphen •H_2O ligand

In a 100 ml RB flask, 2,4-sal (0.100 g, 0.167 mmol) was added with Abs. EtOH (25 mL). To this solution, 1,2-phenylenediamine (0.0906 g, 0.084 mmol) was added and the resulting mixture was refluxed for 24 hours with the addition of few drops (5/6 drops) of acetic acid. After 24 hours, the yellow solution was then cooled to room temperature and kept in freezer for overnight. The precipitate was filtered and washed with a cold ethanol. Yield = 0.240 g (76 %) Calc; C, 77.80; H, 9.87; N, 2.21; Found: C, 77.41; H, 10.30; N, 2.07. ^{1}H NMR (400 MHz, CHLOROFORM-*d*) 0.85 - 0.95 (m, 12 H) 1.24 - 1.52 (m, 72 H) 1.73 - 1.84 (m, 8 H) 3.96 (t, *J* = 6.60 Hz, 8 H) 5.03 (s, 4 H) 6.43 (t, *J* = 2.20 Hz, 2 H) 6.53 - 6.60 (m, 6 H) 6.63 (d, *J* = 2.20 Hz, 2 H) 7.21 - 7.26 (m, 2 H) 7.28 - 7.35 (m, 4 H) 8.56 (s, 2 H) 13.56 (s, 2 H)^{13}C NMR (101 MHz, CHLOROFORM-*d*) δ ppm 14.10 (s), 22.68 (s), 26.06 (s), 29.27 (s), 29.34 (s), 29.40 (s), 29.58 (s),

29.61 (s), 29.63 (s), 29.67 (s), 31.92 (s), 68.11 (s), 70.15 (s), 100.99 (s), 102.28 (s), 105.71 (s), 107.86 (s), 113.48 (s), 133.55 (s), 138.47 (s), 142.38 (s), 160.59 (s), 162.25 (s), 163.27 (s), 164.15 (s)

2.5.11 Synthesis of C_{18}-2,4-salphen • 0.75 H_2O ligand

In a 100 ml RB flask, 2,4-sal (0.100 g, 0.167 mmol) was added with Abs. EtOH (25 mL). To this solution, 1,2-phenylenediamine (0.0906 g, 0.084 mmol) was added and the resulting mixture was refluxed for 24 hours with the addition of few drops (5/6 drops) of acetic acid. After 24 hours, the yellow solution was then cooled to room temperature and kept in freezer for overnight. The precipitate was filtered and washed with a cold ethanol. Yield = 0.240 g (76 %) Calc; C, 78.78; H, 10.82; N, 1.73; Found: C, 78.42; H, 10.45; N, 1.99. ^{1}H NMR (400 MHz, $CDCl_3$) δ ppm 0.87 - 0.94 (m, 12 H) 1.23 - 1.40 (m, 112 H) 1.47 (br. s., 8 H) 1.74 - 1.84 (m, 8 H) 3.96 (t, *J*=6.49 Hz, 8 H) 5.05 (s, 4 H) 6.40 - 6.47 (m, 2 H) 6.59 (dd, *J*=12.87, 1.43 Hz, 6 H) 6.80 (d, *J*=7.92 Hz, 2 H) 7.01 - 7.13 (m, 2 H) 7.28 (s, 3 H) 8.55 (s, 2 H) 13.40 - 13.59 (m, 2 H)^{13}C NMR (101 MHz, CHLOROFORM-*d*) δ ppm 14.10 (s), 22.68 (s), 26.06 (s), 29.27 (s), 29.34 (s), 29.40 (s), 29.58 (s), 29.61 (s), 29.63 (s), 29.67 (s), 31.92 (s), 68.11 (s), 70.15 (s), 100.99 (s), 102.28 (s), 105.71 (s), 107.86 (s), 113.48 (s), 133.55 (s), 138.47 (s), 142.38 (s), 160.59 (s), 162.25 (s), 163.27 (s), 164.15 (s)

2.6 Synthesis of the Ti(IV) complexes using H_2salen ligand

2.6.1 Synthesis of [Ti(salen)Cl_2] 1

H_2salen (1.6603 g, 6.1 mmol) was dissolved in THF(25 ml). To this solution, $TiCl_4$ (0.65 ml, 6.0 mmol) in toluene (5 ml) was added immediately producing a yellow-red solution and precipitation was also observed (red color solid). Then the reaction mixture was stirred and

refluxed for 3 hours at 85 ºC. After the completion of the reaction, the mixture was filtered with fine glass frit. Yield = 2.310 (99%). FTIR (KBr , ν/cm-^{1}): 1611(s) (C=N), 1124 (s) (Ar-O); ^{1}H NMR (*CHLOROFORM-d*), δ/ppm = 4.25 (s), 6.87 (d, *J*=8.80 Hz), 7.08 (t, *J*=7.26 Hz), 7.50 (dd, *J*=7.30, 1.70 Hz), 7.54 - 7.59 (m), 8.37 (s)

2.6.2 Synthesis of [Ti(salen)(OPh-*m*-CH_3)$_2$] 2

In a 250 ml round bottom (RB) flask, [Ti($O^{i}Pr$)$_4$] (1.008 g, 1.050 ml, 3.55 mmol) was combined with a solution of CH_2Cl_2 (17 mL) of *meta*-cresol (0.7191 g, 695.5 µL, 6.65 mmol) in CH_2Cl_2 solution (17 mL), resulting in a yellow solution. To this reaction mixture, H_2salen (0.9028 g, 3.35 mmol) in CH_2Cl_2 (25 mL) was added, producing an orange-yellow solution. The reaction mixture was stirred for 10 minutes under argon at room temperature. After 10 minutes, the reaction mixture was concentrated in a rotary evaporator to dryness. The solid was sonicated with hot hexane (2 x 200 mL), filtered through a fine fritted funnel and washed with additional warm hexane. The residue was air dried; kept overnight in an oven set at 110 ˚C, and the dried product was collected. Yield = 1.53 g (86%). Single crystals suitable for X-ray crystallography were grown by the slow evaporation of the deuterated chloroform solution in an NMR tube at room temperature. Calc. for $C_{30}H_{28}N_2O_4Ti$: C, 68.19; H, 5.34; N, 5.30. Found: C, 68.23; H, 5.36; N, 5.33. FTIR (KBr , ν/cm^{-1}): 1626(s) (C=N); 1286(s) (C-O) ^{1}H NMR (400 MHz, $CDCl_3$): δ/ppm 2.01 (s), 3.70 (s), 6.04 (s), 6.40 (d, *J* = 7.70 Hz), 6.74 - 6.84 (m), 6.84 - 6.93 (m), 6.94 (d, *J* = 8.36 Hz), 7.41 (dd, *J* = 7.70, 1.76 Hz), 7.45 - 7.58 (m), 8.23 (s).

For complexes **3**, **4**, **5a, 6a**, **7a**, **8**, **9**, and **10**, the respective phenols (the number of moles = 6.05 mmol) was utilized.

2.6.3 Synthesis of [Ti(salen)(OPh-p-NO_2)$_2$] 3

Yield = 1.86 g (93%). Calc. for $C_{28}H_{22}N_4O_8Ti$: C, 56.97; H, 3.76; N, 9.49. Found: C, 56.26; H, 3.78; N, 9.03. FTIR (KBr , ν/cm^{-1}): 1625(s) (C=N); 1580 (s) (NO_2); 1280(s) (C-O). ^{1}H NMR (400 MHz, $CDCl_3$): δ/ppm 3.90 - 3.95 (m,4H), 6.30 - 6.35 (m, 4H), 6.94 (d, *J* = 8.14 Hz, 2H), 7.02 (dd, *J* = 14.97, 0.88 Hz, 2H), 7.47 (dd, *J* = 7.70, 1.54 Hz, 2H), 7.60 (ddd, *J* = 8.42, 7.10, 1.65 Hz, 2H), 7.83 - 7.91 (m, 4H), 8.36 - 8.41 (m, 2H). ^{49}Ti NMR (400 MHz, $CDCl_3$): δ/ppm, 1163.

2.6.4 Synthesis of [Ti(salen)(3,5-bis(trifluoromethyl)phenolate)$_2$]•0.375C_6H_{14} 4

Yield = 2.29 g (89%). Calc. for $C_{34.25}H_{25.25}F_{12}N_2O_4Ti$: C, 51.12; H, 3.16; N, 3.48. Found: C, 51.38; H, 2.64; N, 3.85. FTIR (KBr , ν/cm^{-1}): 1625 (C=N), 1282 (Ar-O). ^{1}H NMR (400 MHz, $CDCl_3$): δ/ppm 4.01(s,4H), 5.32 (s), 6.73(s, 4H), 6.92 (d, *J* = 8.36 Hz, 2H), 6.99 (m, *J* = 0.88 Hz, 2H), 7.07 (s,2H), 7.42 (dd, *J* = 7.81, 1.65 Hz, 2H), 7.55(m, 2H), 8.35(s, 2H), ^{19}F NMR:δ/ppm -62.44; ^{49}Ti NMR (400 MHz, $CDCl_3$): δ/ppm, 1163.

2.6.5 Synthesis of [Ti(salen)(OPh)$_2$] 5a and [Ti(salen)(OPh)](μ-O) 5b

Yield = 1.50 g (89%). Calc. for $C_{28}H_{24}N_2O_4Ti$: C, 67.21; H, 4.83; N, 5.60. Found: C, 67.41; H, 4.86; N, 5.59. FTIR (KBr , ν/cm^{-1}): 1606(s) (C=N), 1283(s) (Ar-O); ^{1}H NMR (400 MHz, $CDCl_3$): δ/ppm 3.70 (s, 4H), 6.25 (d, *J* = 7.26 Hz, 4H), 6.62 (t, *J* = 7.26 Hz, 2H), 6.90 - 7.01 (m, 8H), 7.46 (dd, *J* = 7.81, 1.65 Hz, 2H), 7.55 (m , 2H), 8.29 (s, 2H) ^{49}Ti NMR (400 MHz, $CDCl_3$): δ/ppm, 1163.

A portion of complex **5a** was dissolved in $CDCl_3$ in an NMR tube; then the ^{1}H spectrum was acquired as above. The solution was left for four weeks; then upon evaporation of $CDCl_3$ single crystals of compound **5b** were formed.

2.6.6 Synthesis of [Ti(salen)(OPh-o-F)$_2$]•0.25CH_2Cl_2 6a and [Ti(salen)(OPh-o-F)](μ-O) 6b

Yield = 1.70 g (89%). Calc. for $C_{28.25}H_{22.75}Cl_{0.5}F_2N_2O_4Ti$: C, 60.82; H, 4.07; N, 5.02. Found: C, 60.74; H, 4.15; N, 4.98. FTIR (KBr, ν/cm^{-1}): 1625m (C=N), 1495 (C-F), 745w (ortho disubstituted). ^{1}H NMR (400 MHz, $CDCl_3$): δ/ppm 3.94 (s. 4H), 6.50 (m, 4H), 6.55 - 6.67 (m, 4H), 6.86 - 6.95 (m, 4H), 7.35 - 7.40 (m, 4H), 7.46 - 7.52 (m, 4H), 8.28 (s, 4H). ^{19}F NMR:δ/ppm -133.30; ^{49}Ti NMR (400 MHz, $CDCl_3$): δ/ppm, 1162.

A portion of complex **6a** was dissolved in $CDCl_3$ in an NMR tube; then the ^{1}H spectrum was acquired as above. The solution was left for four weeks; then upon evaporation of $CDCl_3$ single crystals of compound **6b** were formed.

2.6.7 Synthesis of [Ti(salen)(OPh-*p*-CH_3)$_2$] 7a and [Ti(salen)(OPh-*p*-CH_3)] (μ-O) 7b

Yield = 1.56 g (88%). Calc. for $C_{30}H_{28}N_2O_4Ti$: C, 68.19; H, 5.34; N, 5.30. Found C, 68.75; H, 5.19; N, 5.13. FTIR (KBr, ν/cm^{-1}): 1625 (C=N), 1283 (Ar-O). ^{1}H NMR (400 MHz, $CDCl_3$): δ/ppm 2.14 (s), 3.66 (s), 6.06 - 6.18 (m), 6.72 (d, *J* = 8.36 Hz), 6.88 - 6.97 (m), 6.98 (d, *J* = 8.14 Hz), 7.28 (s), 7.46 (dd, *J* = 7.70, 1.98 Hz), 7.54 (ddd, *J* = 8.58, 6.93, 1.87 Hz), 8.28 (s) ^{49}Ti NMR (400 MHz, $CDCl_3$): δ/ppm, 1163.

A portion of complex **7a** was dissolved in $CDCl_3$ in an NMR tube; then the ^{1}H spectrum was acquired as above. The solution was left for four weeks; then upon evaporation of $CDCl_3$ single crystals of compound **7b** were formed.

2.6.8 Synthesis of [Ti(salen)(OPh-*o*-CH_3)$_2$] 8

Yield = 1.67 g (94 %). Calc. for $C_{30}H_{28}N_2O_4Ti$: C, 68.19; H, 5.34; N, 5.30. Found: C.67.39; H, 5.03; N, 5.39. ^{1}H NMR (400 MHz, $CDCl_3$): δ/ppm 1.80 (s,6H), 3.82 (s,4H), 6.26 (dd, *J* = 8.03,

1.0 Hz, 2H), 6.54 (td, *J* = 7.37, 1.10 Hz, 2H), 6.73 - 6.81 (m, 2H), 6.84 - 6.89 (m, 2H), 6.93 (m, *J*=1.76 Hz, 4H), 7.46 (dd, *J* = 7.70, 1.76 Hz, 2H), 7.53 (ddd, *J* = 8.42, 6.99, 1.76 Hz, 2H), 8.36 (s, 2H).

2.6.9 Synthesis of [Ti(salen)(OPh-*m*-F)$_2$] •0.25CH_2Cl_2 9

Yield = 1.75 g (97 %). Calc. for $C_{28.25}H_{22.75}Cl_{0.5}F_2N_2O_4Ti$: C, 60.82; H, 4.07; N, 5.02. Found: C, 60.55; H, 4.14; N, 4.91. FTIR (KBr, ν/cm^{-1}): 1627, (C=N), 1285 (Ar-O). ^{1}H NMR (400 MHz, $CDCl_3$): δ/ppm 3.79 (s,4H), 5.93 - 5.99 (m,2H), 6.04 (s,2H), 6.33 (s,2H), 6.82 - 6.89 (m,2H), 6.97 (d, *J* = 7.48 Hz,4H), 7.45 - 7.50 (m,2H), 7.54 - 7.60 (m,2H), 8.34 (s,2H). ^{49}Ti NMR (400 MHz, $CDCl_3$): δ/ppm, 1165.

2.6.10 Synthesis of [Ti(salen)(OPh-p-F)$_2$]•0.375CH_2Cl_2 10

Yield = 1.68 g (93 %). Calc. for $C_{28.375}H_{22.75}Cl_{0.75}F_2N_2O_4Ti$: C, 62.70; H, 4.13; N, 5.22. Found: C 60.24; H 4.08; N, 5.11. FTIR (KBr, ν/cm^{-1}): 1625 (C=N), 1288 (Ar-O). ^{1}H NMR (400 MHz, $CDCl_3$): δ/ppm 3.74 (s, 4H), 6.17 (dd, *J* = 9.02, 4.84 Hz,4H), 6.61 (t, *J* = 8.69 Hz,4H), 6.91 - 6.97 (m,4H), 7.46 (d, *J* = 6.40 Hz,2H), 7.56 (dt, *J* = 13.86, 5.50 Hz,2H), 8.31 (s,2H). ^{49}Ti NMR (400 MHz, $CDCl_3$): δ/ppm, 1166.

2.7 Synthesis of the Ti(IV) complexes using $C_nH_{2n+1}O$-salen ligand

2.7.1 Synthesis of [Ti($C_{16}H_{33}O$-salen)Cl_2] 11

$C_{16}H_{33}O$-salen (1.00 g, 1.33 mmol) was dissolved in THF (25 ml) and to that solution TiCl4 (0.253g, 0.147 ml, 1.24 mmol) in toluene (10 ml) was added resulting in immediate change into dark red color. The reaction mixture was then heated under reflux for 3 hours. Then the initial

volume of the solution was reduced to half under rotary evaporation. In the room temperature, the solid again formed a solution, thus the solution was again rotary evaporated to dryness. The viscous liquid was formed which was kept in freezer for overnight. The solid product was obtained was was further dried using nitrogen pump. Yield = 0.8139 g (80%). FTIR (KBr , ν/cm^{-1}): 2916, 2849s (CH), 1600(s) (C=N), 1187(s) (Ar-O); ^{1}H NMR (*$CDCl_3$*)/ δppm = 0.89 (t, *J* = 6.60 Hz), 1.27 (s), 4.00 (t, *J* = 6.49 Hz), 4.15 (s), 6.35 (d, *J* = 2.42 Hz), 6.60 (dd, *J* = 8.58, 2.42 Hz), 7.35 (d, *J* = 8.80 Hz), 8.21 (s).

2.7.2 Synthesis of [Ti($C_{18}H_{37}$O-salen)Cl_2] 12

$C_{18}H_{37}$O-salen (1.005 g, 1.24 mmol) was dissolved in THF (15 ml) and to that solution TiCl4 (0.136 ml, 1.24 mmol) in toluene (5 ml) was added resulting in immediate change into dark red color. The reaction mixture was then heated under reflux for 3 hours. Then the initial volume of the solution was reduced to half under rotary evaporation. The solution was then kept in the freezer for overnight forming a bright red color solid. The solid was then filtered and washed with additional toluene (15 ml). The product was dried under vacuum and dried product was obtained. Yield = 0.8139 g (71%). FTIR (KBr , ν/cm^{-1}): 2916, 2849s (CH), 1600(s) (C=N), 1187(s) (Ar-O); ^{1}H NMR (*CHLOROFORM-d*) δ/ppm = 0.89 (t, *J*=6.60 Hz), 1.27 (s), 4.00 (t, *J*=6.49 Hz), 4.15 (s), 6.35 (d, *J*=2.42 Hz), 6.60 (dd, *J*=8.58, 2.42 Hz), 7.35 (d, *J*=8.80 Hz), 8.21 (s)

2.8 Synthesis of Co(II), Ni(II), and Cu(II) complexes using C_n-salphen ligand

2.8.1 Synthesis of [Co(C_{12}-2,4,-salphen)]•C_2H_5OH•H_2O 13

In a 100 mL RB flask, C_{12}-2,4-salphen(0.100 g, 0.079 mmol) and $Co(CH_3CO_2)_2$•$4H_2O$ (0.020 g, 0.079 mmol) were added together and absolute EtOH (25 mL) were added together. The resultant mixture was then refluxed for 24 hours. After 24 hours, the solvent was removed by rotary evaporation and cooled to the room temperature. To the solid, absolute ethanol (15 mL) was added and sonicated. The solid were then obtained by filtration using fine glass frit, washed with cold ethanol, and dried under vacuum. Yield = 0.089 g (85 %) Calc. for $C_{82}H_{130}CoN_2O_{10}$: C, 72.76; H, 9.45; N, 2.02. Found C, 72.99; H, 9.20; N, 2.06.

2.8.2 Synthesis of [Ni(C_{12}-2,4-salphen)]•C_2H_5OH•H_2O 14

In a 100 ml RB flask, C_{12}-2,4-salphen (0.160 g, 0.126 mmol), $Ni(CH_3CO_2)_2$•$4H_2O$ (0.0314 g, 0.126 mmol) and abs EtOH (25 mL) were added together and refluxed for 24 hours. After 24 hours, the reaction mixture was cooled to room temperature and triturated. The solid product formed were obtained by filtration, washed with cold ethanol, and dried under vacuum. Yield = 0.1039 g (63 %) Calc. for $C_{82}H_{130}N_2NiO_{10}$: C, 72.76; H, 9.45; N, 2.02. Found C, 72.99; H, 9.20; N, 2.06. ^{1}H NMR (400 MHz, CHLOROFORM-*d*) δ/ppm 0.89 (t, *J* = 6.8 Hz, 12 H), 1.38 (m, 22 H), 1.27 (br. s., 26 H), 1.77 (m, 5 H), 3.95 (t, *J* = 6.5 Hz, 8 H), 4.97 (s, 4 H), 6.41 (m, 4 H), 6.55 (m, 4 H), 6.69 (m, 2 H), 7.20 (m, 8 H), 7.65 (dd, *J* = 6.2, 3.7 Hz, 2 H), 8.09 (s, 2 H)

2.8.3 Synthesis of [Cu(C_{12}-2,4-salphen)]•C_2H_5OH•H_2O 15

In a 100 ml RB flask, C_{12}-2,4-salphen (0.100 g, 0.079 mmol), $Cu(OAc)_2$•H_2O (0.016 g, 0.079 mmol) and abs EtOH (25 mL) were added together and refluxed for 24 hours. After 24

hours, the reaction mixture was cooled to room temperature and triturated. The solid product formed were obtained by filtration, washed with cold ethanol, and dried under vacuum. Yield = 0.084 g (80 %) Calc. for $C_{82}H_{130}N_2NiO_{10}$: C, 72.51; H, 9.42; N, 2.01. Found C, 72.45; H, 9.15; N, 2.06.

CHAPTER 3
RESULTS AND DISCUSSION

Synthesis, characterization, and mesomorphic studies of the ligands and complexes

The synthesis, characterization, and mesomorphic behavior of ligands and complexes are discussed in this section. This section is divided into various sub-sections, where the results are categorized based on the types of ligands used for the synthesis of the complexes.

The content of this chapter 3, sub-section 3.1, was reproduced with permission from Gurung, R. K.; McMillen, C. D.; Jarrett, W. L.; Holder, A. A. *Inorg. Chim. Acta* **2020,** *505*, 119496.

3.1 Synthesis and characterization of the titanium(IV) salen complexes using H_2salen ligand

Ligand H_2salen was prepared using a similar method as described in the literature [229-231]. The synthesis of complexes was carried out successfully by a slight modification of the original synthetic procedure, as reported by Gagne *et al.* [25]. The general synthetic procedure of all the titanium complexes is shown in scheme 3. All the complexes were characterized as either mononuclear or binuclear complexes.

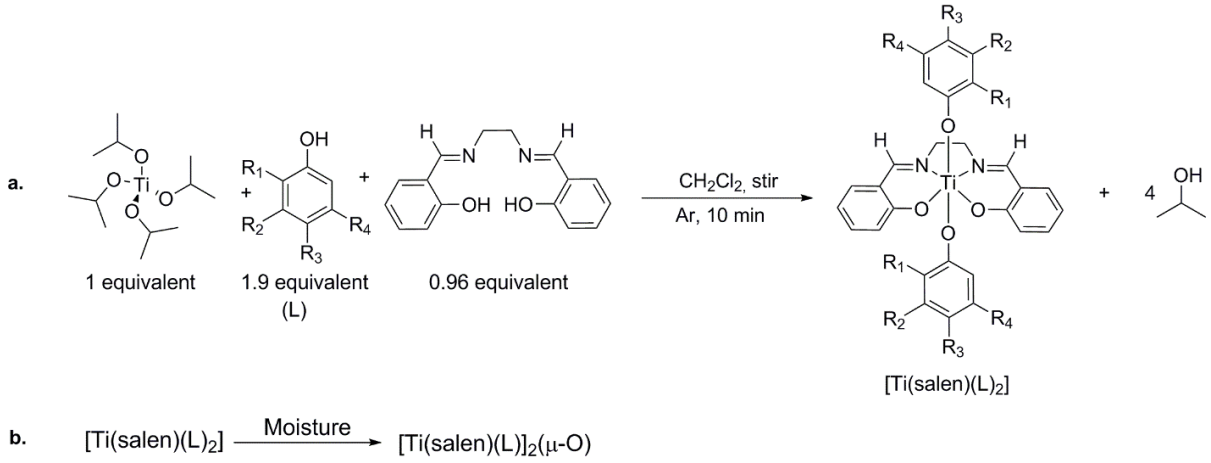

Scheme 3. Synthesis of the titanium(IV) Schiff base salen complexes (a) and formation of binuclear species due to hydrolysis (b).

3.1.1 Elemental Analysis, FTIR and NMR spectroscopic studies

Elemental analysis was carried out on complexes **2, 3, 4, 5a, 6a, 7a, 8, 9**, and **10.** The elemental analysis data for the percentages of N and H were within the error range of ±0.40% requirement, but the percentage found for C in complexes **4**, **6a, 9**, and **10** was not fully consistent with the calculated values. The percentages for carbon, hydrogen, and nitrogen in complex **4** were 51.38% H, 2.64%, and 3.85%, respectively. The elemental analysis data for the percentage of H found in complex **4** was 2.64% versus the calculated value of 3.16%. Since discrepancies could

likely due to the loss of solvates during the analytical procedure. Complexes **6a** and **9** were found to have 0.25 CH_2Cl_2 as a solvate, while complex **10** has 0.375 CH_2Cl_2 as a solvate.

FTIR and NMR spectra were acquired for the ligand and the respective complexes. FTIR spectra were acquired from 500-4000 cm^{-1}. The HC=N stretching frequencies are typically found between 1620-1640 cm^{-1} in the literature.[232] Based on the data for the assigned stretching frequencies, an imine ν(C=N) stretching frequency at 1635 cm^{-1} was observed for H_2Salen **1**; while for complexes 2, 3, 4, 5a, 6a, 7a, 8, 9, and 10, stretching frequencies were shifted to lower frequencies in the region of 1624 to 1630 cm^{-1} (Appendix A1-A10).

The ^{1}H NMR spectra were acquired for the ligand **1** and complexes 2, 3, 4, 5a, 6a, 7a, 8, 9, and 10 using $CDCl_3$ as a solvent (Appendix A11-S19). The presence of singlets at δ = 13.20 ppm and 8.36 ppm in the ^{1}H NMR spectra of ligand **1** was assigned for –OH and –N=CH (imine) protons, respectively. The disappearance and the shift of these proton signals signify the coordination of the ligand to the Ti(IV) metal center leading to the formation of the complexes. The –OH proton peak was not observed, while the imine proton was slightly shifted upfield. The coordination of the ligand to the Ti(IV) metal center occurred via *N,N'*- and *O,O'*-sites. In addition, the existence of additional aromatic peaks on ^{1}H NMR spectra of complexes was due to the presence of phenolic moiety at an axial position. Based on these results obtained from the ^{1}H NMR spectroscopy, it can be inferred that there is a successful synthesis of the complexes.

Fluorinated phenols were used to prepare complexes **4, 6a**, **9,** and **10**, respectively. The coordination of the ligand in the axial position was determined by ^{19}F NMR spectroscopic studies. In complex **4,** ^{19}F NMR chemical shift was very small, ranging from -62.51 ppm in free ligand to -62.44 ppm after coordination. Similarly, for complex **6a**, the coordination of the "free" ligand to

a titanium(IV) metal center resulted in the change in the chemical shift from -140.8 ppm to -133.3 ppm. Shifts in ^{19}F NMR spectra were also observed for the complexes **9** and **10**.

Table 6. NMR spectroscopic data for ligand H_2salen and the titanium(IV) complexes.

	^1H, δ/ppm				^{19}F, δ/ppm
	-OH	HC=N	$-CH_2$	$-CH_3$	
H_2salen	13.20	8.36	3.94	-	-
2	-	8.23	3.70	-	-
3	-	8.36	3.90	2.01	-
4	-	8.35	4.01		-62.44
5a	-	8.29	3.70		
6a	-	8.28	3.94		-133.3
7a	-	8.28	3.66	2.14	-
8	-	8.36	3.82	1.80	
9	-	8.34	3.79		-112.8
10		8.31	3.74		-124.5

3.1.2 ^{49}Ti NMR spectroscopic studies

In addition to ^1H NMR spectroscopy, we acquired ^{49}Ti NMR spectra of the complexes. To study the electronic effect of the ligand on the titanium(IV) metal center, ^{49}Ti NMR spectroscopy is a perfect spectroscopic tool. The result obtained from the ^{49}Ti NMR spectroscopic studies will help establish the influence of the salen ligand and the substituent phenol on the titanium(IV) metal center.

In this study, we acquired ^{49}Ti NMR spectra for complexes **3**, **4**, **5a**, **6a**, **7a**, **9**, and **10** in solution. ^{49}Ti NMR spectra were not acquired for complexes **2** and **8**. Such spectra were not determined as complexes **2** and **8** exhibited very low solubility in deuterated chloroform.

In what is to our knowledge, this is the first report of ^{49}Ti NMR spectra of titanium(IV) complexes with Schiff bases as ligands in solution. Kidd *et al*. [8] had reported the $^{47/49}$Ti NMR chemical shifts for tetrahedral titanium halide compounds like $TiCl_4$, $TiBr_4$ and the effect of the electronegativity of the halogen atoms. In previous studies, most of the ^{49}Ti NMR spectra reported in the literature were based on titanium(IV)-containing species with a tetrahedral geometry [2, 8, 233]. The correlation between shielding/deshielding effect and ligand electronegativity of ^{49}Ti NMR was studied by Traill *et al.*[233]. In their study, when the chloride ligand in $TiCl_4$ (δ = 0.00 ppm) is substituted by ethoxide (EtO^-) ligand, it resulted in the shielding effect. The chemical shift decreases from δ = 0.00 ppm (for $TiCl_4$) to δ = -858 ppm (for $[Ti(OEt)_4]$) [233]. Contrastingly, an opposite behavior was observed in the experiment as reported by Sarsfield *et al.* [6] and Berger *et al*. [234], where the central titanium(IV) metal center became more deshielded when the chloride ion was replaced by electron donating methyl group. For example, the chemical shift for $[TiCl_3(CH_3)]$ was observed at +613 ppm, while all the halogens were replaced with methyl group $[Ti(CH_3)_4]$, the peaks were deshielded and observed at δ = +1325 ppm [234]. Thus, the ^{49}Ti NMR signals were not only dependent on the nature of ligand surrounding the titanium(IV) metal center. Along with the nature of the ligand, the symmetry of the respective titanium(IV) complex and the molecular complexity also affected the chemical shift in ^{49}Ti NMR spectrum [1].

In our study, complexes **3**, **4**, **5a**, **6a**, **7a**, **9**, and **10** have octahedral geometries where salen ligand occupies an equatorial region providing a similar electronic environment around the titanium(IV) metal center; while the axial position are occupied by various substituent phenol groups. All the titanium(IV) salen complexes were found to resonate approximately in the range of δ = +1160 ppm to +1170 ppm. The only subtle change in the chemical shift is noticed due to the various axial substituted phenol groups. Interestingly, we only observed the peaks for ^{49}Ti

NMR active nucleus (**Figure 33**) for some of the titanium(IV) salen complexes (**3**, **4**, **5a**, **6a**, **7a**, **9**, and **10**). The lack of a ^{47}Ti NMR chemical shift can be attributed to greater quadrupolar broadening and the size of the complex as the size increases, the peak will be too broad to be observed.[1] The ^{49}Ti NMR spectroscopic data obtained for the series of complexes are shown in Table 7, along with reported titanium(IV)-containing species.

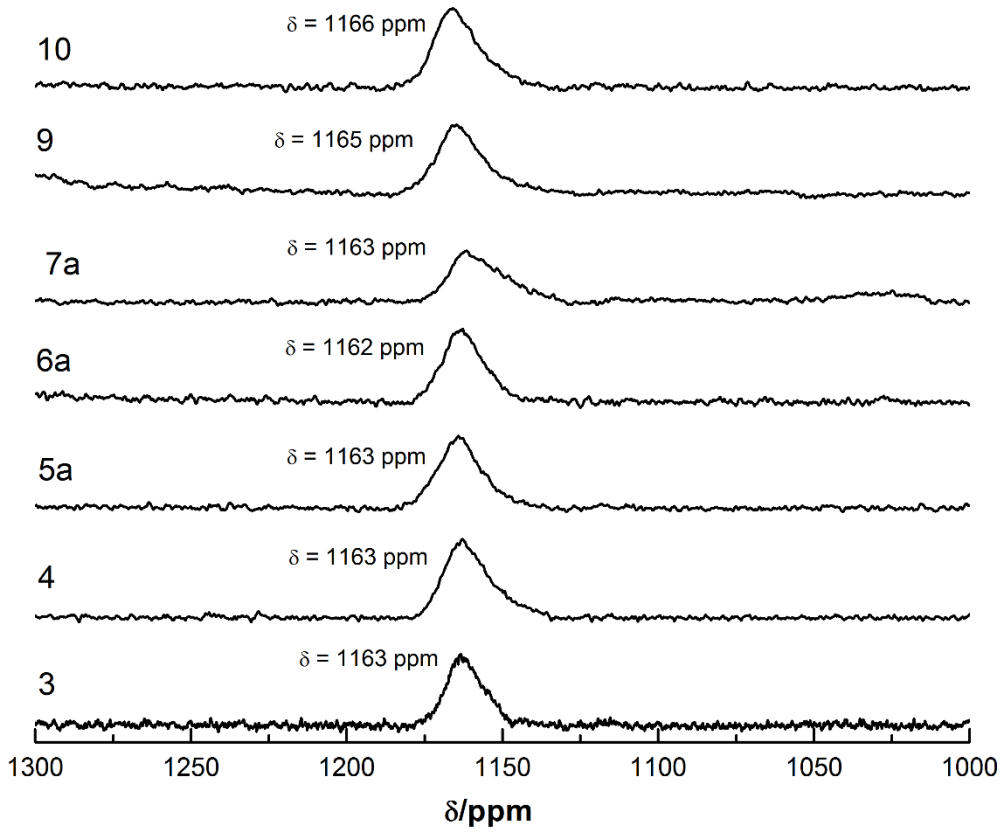

Figure 33. ^{49}Ti NMR spectra of titanium(IV) salen complexes in $CDCl_3$.

Table 7. ^{49}Ti NMR spectral data of selected titanium(IV) species.

Compound	Solvent	Shift/ppm	Reference
$TiCl_4$	Neat	0	[7]
TiF_4	48% aq. HF	+1177	[8]
$TiBr_4$	Melt (50 °C)	+482	[7]
TiI_4	C_6D_6	+1278	[7]
$[Ti(O^iPr)_4]$	$CDCl_3$	-854	[5]
$[Ti(OEt)_4]$	Neat	-858	[233]
$[TiCl(OEt)_3]$	CD_2Cl_2	-750	[233]
$[TiCl_2(OEt)_2]$	CD_2Cl_2	-560	[233]
$[TiCl_3(OEt)]$	CD_2Cl_2	-360	[233]
$[Ti(\eta\text{-}C_5(CH_3)_5)(CH_3)Cl_2]$	CD_2Cl_2	+143	[6]
$[Ti(\eta\text{-}C_5(CH_3)_5)(CH_3)_2Cl]$	CD_2Cl_2	+343	[6]
$[Ti(\eta\text{-}C_5(CH_3)_5)(CH_3)_2(C_6F_5)]$	CD_2Cl_2	+484	[6]
$[Ti(\eta\text{-}C_5(CH_3)_5)(CH_3)_3]$	CD_2Cl_2	+551	[6]
$[TiCl_3(CH_3)]$	$CDCl_3$	+613	[234]
$[TiCl_2(CH_3)_2]$	$CDCl_3$	+906	[234]
$[TiCl(CH_3)_3]$	$CDCl_3$	+1211	[234]
$[Ti(CH_3)_4]$	$CDCl_3$	+1325	[234]
$[Ti(CH_2C(CH_3)_2(C_6H_5))_4]$	C_6D_6	+1375	[1]
[Ti(salen)(OPh-*p*-NO_2)$_2$] **3**	$CDCl_3$	+1163	This work
[Ti(salen)(OPh-3,5-$(CF_3)_2$)$_2$] **4**	$CDCl_3$	+1163	This work
[Ti(salen)(OPh)$_2$] **5a**	$CDCl_3$	+1163	This work
[Ti(salen)(OPh-*o*-F)$_2$] **6a**	$CDCl_3$	+1162	This work
[Ti(salen)(OPh-*p*-CH_3)$_2$] **7a**	$CDCl_3$	+1163	This work
[Ti(salen)(OPh-*m*-F)$_2$] **9**	$CDCl_3$	+1165	This work
[Ti(salen)(OPh-*p*-F)$_2$] **10**	$CDCl_3$	+1166	This work

3.2.3 X-ray Crystallographic Studies

Single crystals suitable for X-ray crystallography were grown by the slow evaporation of a deuterated chloroform solution in NMR tubes at room temperature. The X-ray crystallography data confirmed the existence of mononuclear and binuclear octahedral titanium(IV) species. The titanium(IV) metal center is coordinated by the salen ligand in the equatorial position and a substituted phenolato ligand in the axial position. Complexes **2**, **3**, and **4** are mononuclear species; while the crystal structures obtained from complexes **5a**, **6a**, and **7a** are binuclear species in nature. Crystals of complexes **3** and **6b** were found to have chloroform solvates, containing 0.5 and 0.67 molecules of $CHCl_3$ per formula unit, respectively. The crystal structures of the complexes are shown in **Figure 34**, while their crystallographic data are summarized in Tables 8 and 9.

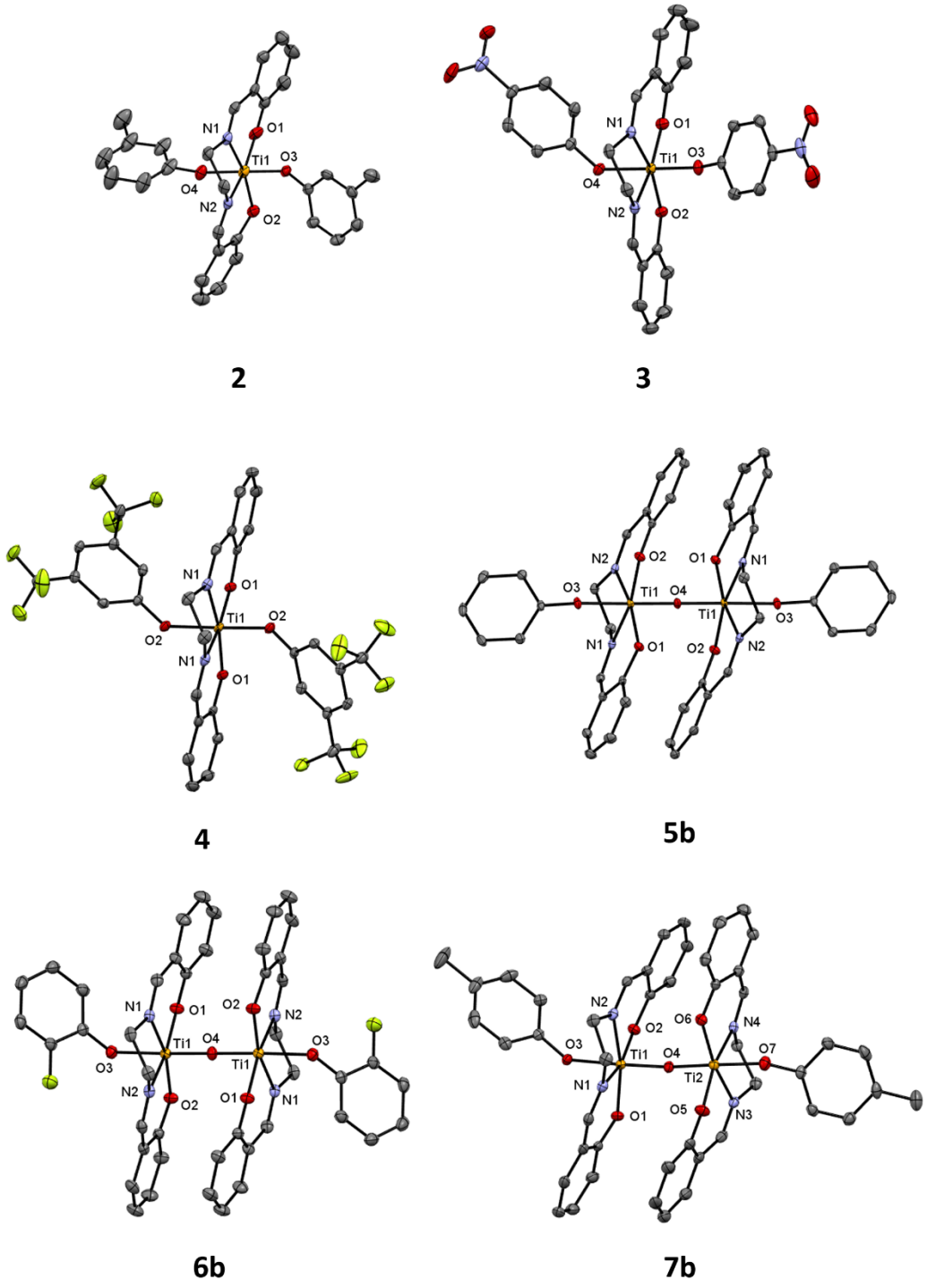

Figure 34. Crystal structures of titanium(IV) salen complexes, shown as 50% probability ellipsoids.

Table 8. Crystal structure data for mononuclear Ti(IV) complexes.

	2 **[Ti(salen)(OPh-*m*-CH_3)$_2$]**	**3** **[Ti(salen)(OPh-*p*-NO_2)$_2$] •½$CHCl_3$**	**4** **[Ti(salen)(OPh-*3,5*-(CF_3)$_2$)$_2$]**
Chemical formula	$C_{30}H_{28}N_2O_4Ti$	$C_{28.50}H_{22.50}Cl_{1.50}N_4O_8Ti$	$C_{32}H_{20}F_{12}N_2O_4Ti$
Formula wt. (g/mol)	528.44	650.08	772.40
Crystal size (mm)	0.14 x 0.15 x 0.42	0.02 x 0.11 x 0.24	0.10 x 0.12 x 0.32
Crystal system	orthorhombic	monoclinic	monoclinic
Space group	*Pca*2_1	*P*2_1/*c*	*C*2/*c*
a (Å)	27.5068(13)	20.5225(14)	21.074(3)
b (Å)	13.3852(6)	6.5429(4)	10.0002(11)
c (Å)	14.2391(6)	21.3756(14)	17.235(2)
α (°)	90	90	90
β (°)	90	94.309(3)	124.428(4)
γ (°)	90	90	90
Volume ($Å^3$)	5242.6(4)	2862.1(3)	2996.0(6)
Z	8	4	4
D (calc., g/cm^3)	1.339	1.509	1.712
Abs. coeff. (mm^{-1})	0.365	0.497	0.404
Theta range (deg.)	2.06 to 25.25	2.65 to 25.50	2.34 to 26.50
Reflections collected	43025	55824	25675
Data / restraints / param.	9191 / 103 / 671	5301 / 0 / 370	3098 / 0 / 231
R(int) [indep. refl.]	0.0466 [9191]	0.0465 [5301]	0.0503 [3098]
R1, wR2 [(I>2σ(I)]	0.0562, 0.1471	0.0329, 0.0797	0.0385, 0.0960
R1, wR2 (all data)	0.0627, 0.1529	0.0429, 0.0865	0.0496, 0.1009
Goodness of fit	1.053	1.033	1.105
Abs. str. param. (Flack)	-0.001(8)	-	-
Largest diff. peak/hole (eA^{-3})	0.772/-0.506	0.243/-0.367	0.383/-0.616
CCDC deposition no.	1958627	1958628	1958629

Table 9. Crystal structure data for binuclear Ti(IV)complexes.

	5b **[Ti(salen)(OPh)]$_2$ (μ-O)**	**6b** **[Ti(salen)(OPh-*o*-F)]$_2$(μ-O) •2/3CHCl$_3$**	**7b** **[Ti(salen)(OPh-*p*-CH$_3$)]$_2$ (μ-O)**
Chemical formula	$C_{44}H_{38}N_4O_7Ti_2$	$C_{44.67}H_{36.67}Cl_2F_2N_4O_7Ti_2$	$C_{46}H_{42}N_4O_7Ti_2$
Formula wt. (g/mol)	830.58	946.14	858.63
Crystal size (mm)	0.10 x 0.25 x 0.38	0.10 x 0.19 x 0.27	0.08 x 0.14 x 0.28
Crystal system	monoclinic	triclinic	trigonal
Space group	$P2_1/n$	P-1	$P3_1$
a (Å)	12.642(2)	14.8264(13)	15.7502(4)
b (Å)	10.8265(19)	16.2782(14)	15.7502(4)
c (Å)	14.037(2)	16.5069(14)	14.1347(4)
α (°)	90	113.138(3)	90
β (°)	100.660(6)	113.233(2)	90
γ (°)	90	98.136(3)	120
Volume (Å^3)	1888.1(6)	3152.3(5)	3036.61(18)
Z	2	3	3
D (calc., g/cm^3)	1.461	1.495	1.409
Abs. coeff. (mm^{-1})	0.483	0.573	0.453
Theta range (deg.)	2.39 to 27.50	2.28 to 28.36	2.08 to 27.49
Reflections collected	47228	165134	27574
Data / restraints / param.	4334 / 0 / 259	15700 / 0 / 838	8294 / 1 / 534
R(int) [indep. refl.]	0.0420 [4334]	0.0362 [15700]	0.0455 [8294]
R1, wR2 [(I>2σ(I)]	0.0276, 0.0694	0.0364, 0.0940	0.0327, 0.0664
R1, wR2 (all data)	0.0314, 0.0715	0.0415, 0.0977	0.0397, 0.0689
Goodness of fit	1.037	1.038	1.042
Abs. str. param. (Flack)	-	-	-0.006(9)
Largest diff. peak/hole (eA^{-3})	0.340/-0.382	1.389/-1.141	0.250/-0.274
CCDC deposition no.	1958630	1958631	1958632

The coordinated salen ligands that form the equatorial plane of the complexes exhibit acute N-Ti-N bond angles ranging from 75.18(11)° to 76.34(6)°, and obtuse O-Ti-O bond angles ranging from 111.98(6)° to 114.61(16)° for both the mononuclear and binuclear complexes. The Ti-N bonds to the salen ligand are longer than the Ti-O bonds, with Ti-N bond lengths ranging from 2.1392(15) Å to 2.170(3) Å, and Ti-O bond lengths ranging from 1.8570(12) Å to 1.9053(13) Å. These bond lengths and angles are within the range reported for other structures having octahedral titanium coordinated by the salen ligand (N-Ti-N = 74.31° to 79.71°; O-Ti-O = 110.87° to 114.96°; Ti-N = 2.068 Å to 2.194 Å; Ti-O = 1.755 Å to 1.987 Å) [235]. In the binuclear species, the salen ligands coordinated to each titanium center are arranged to facilitate partial overlap of their respective pi systems from the aromatic components (centroid···centroid = 3.747 Å to 4.039 Å).

The salen ligands in complex **7b** are twisted slightly more about the Ti-O-Ti bridging axis than those of complexes **5b** and **6b**, causing the pi systems of only one side of each ligand in complex **7b** to have partial overlap with one another.

The Ti-O bonds to the phenolato ligands range from 1.862(4) Å to 1.9672(13) Å. In the binuclear complexes, the bridging Ti-O bonds are consistently shorter than those to the ligands, ranging from 1.811(2) Å to 1.846(2) Å. These bridging interactions are linear, with Ti-O-Ti of 169.33(14)° in **7b**, and rigidly enforced to 180° by the inversion symmetry of **5b** and **6b**. The *trans*- O-Ti-O angles between phenolato ligands of the mononuclear species (168.73(6))° to 174.92(18)°), or between phenolato ligands and bridging oxides of the binuclear species (166.84(4)° to 170.43(4)°) are also generally linear.

The packing of the complexes appears to be governed by steric considerations and relatively weak intermolecular interactions, both of which are influenced by the mononuclear versus binuclear nature of the complexes as well as the nature of the phenolato ligands. Selected

packing diagrams are shown in (**Figure 35**). In complex **2**, H···pi interactions between the salen and $^{-}$OPh-*m*-CH_3 ligands of neighboring molecules connect the complexes in three dimensions.

Complex **2** features partial overlap of the pi systems of the salen ligands of neighboring molecules along the *c*-axis (C···C = 3.383 Å), combined with weak C-H···F interactions between the salen ligands and OPh-3,5-$(CF_3)_2$ ligands of neighboring complexes along the *a*- and *b*-axes. Packing is further reinforced by H···pi interactions alternating between salen and $^{-}$OPh-3,5-$(CF_3)_2$ ligands of neighboring molecules along the *b*- and *c*-axes. In complex **3**, the oxygen atoms of one of the NO_2 groups act as weak hydrogen bond acceptors from the salen ligand of a neighboring complex along the *a*-axis, while those of the second NO_2 group interact with the pi system of the salen ligand of a neighboring complex along the *c*-axis.

The binuclear complex **5a** features H···pi interactions between salen and $^{-}$OPh ligands of neighboring molecules, as well as weak C-H···O interactions between neighboring salen ligands, to form sheets parallel to (10-1). The packing of complex **6a** creates a framework built from weak C-H···F interactions along the *a*-axis, weak C-H···O interactions along the *c*-axis, and H···pi interactions along the *b*-axis. The framework possesses voids accommodating the $CHCl_3$ solvent molecules, which are pinned in place by weak C-H···Cl and H···pi interactions. Complex **7b** also forms a three-dimensional framework built from H···pi and weak C-H···O interactions.

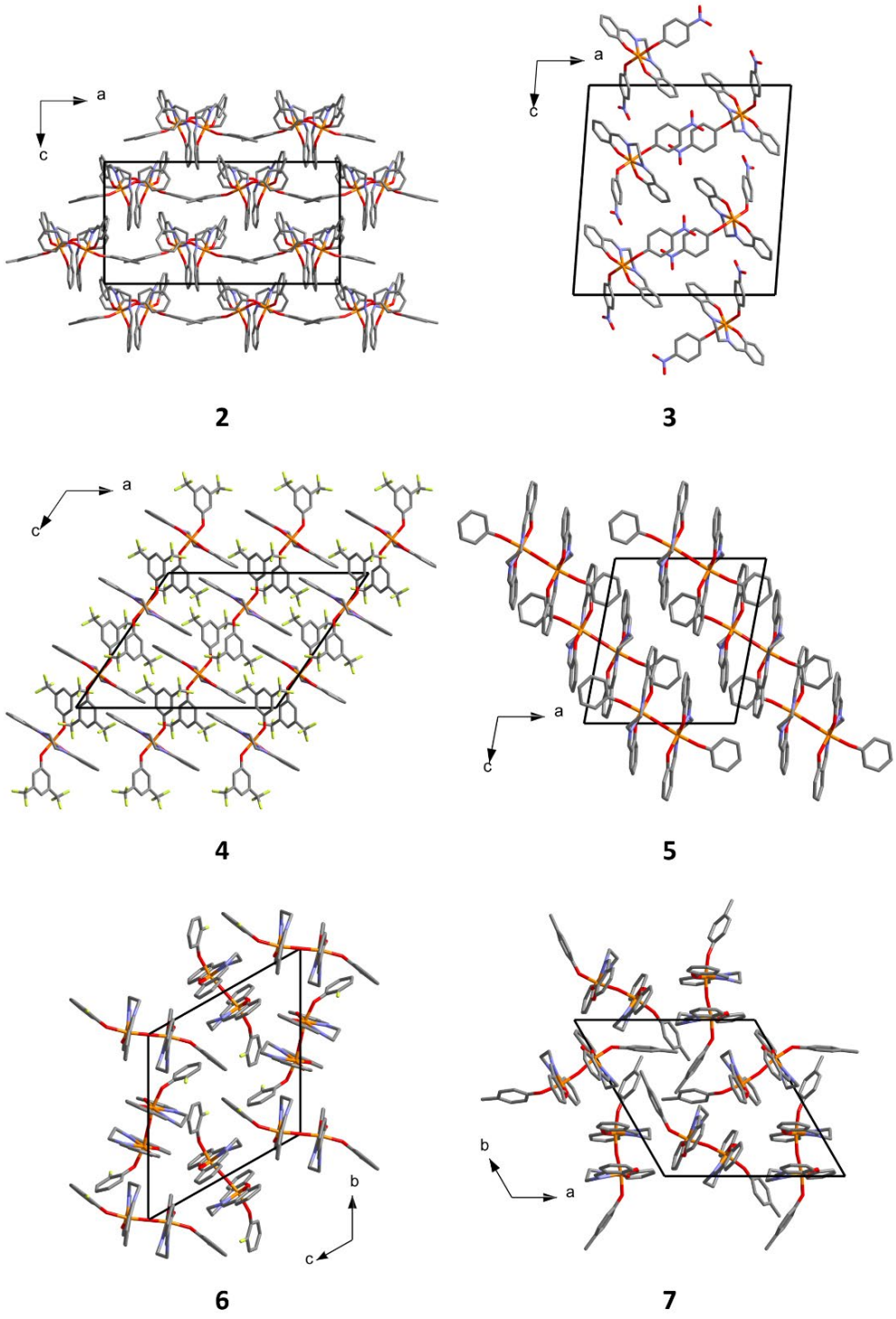

Figure 35. Selected projections of the packing arrangements of complexes **2-7**. Color scheme: Ti = orange, O = red, N = purple, F = yellow, C = grey. Hydrogen atoms and solvent molecules are omitted for clarity.

These complexes are believed to be relatively water sensitive and can form oxo-bridged binuclear complexes, which were crystallized out from $CDCl_3$ after several weeks under ambient atmosphere. In an independent report, Tzubery *et al.* [111] and Nielson *et al.* [117, 230] previously published the formation of binuclear species ($[Ti_2L_2(\mu\text{-}O)]$ where L = mono(alkoxide)bis(phenolato) salen ligand) and ([Ti(OEt)L-O-Ti(OEt)L], (where L = diaminebis(phenolato) ligand), respectively.

While growing crystals for X-ray crystallography from $CDCl_3$ in NMR tubes, it is believed that a sufficient amount of atmospheric water could be present during the prolonged crystal growth period, thus initiating the formation of hydrolyzed species, followed by the formation of binuclear species [10, 117]. It is one of the characteristic features of titanium(IV) complexes to undergo hydrolysis, and eventually form species with Ti-O bonds as in $[Ti(salen)(OPh)]_2(\mu\text{-}O)$. [10]

3.2 Synthesis and characterization of titanium(IV) Schiff base complexes using the $C_nH_{2n+1}O$-salen ligand

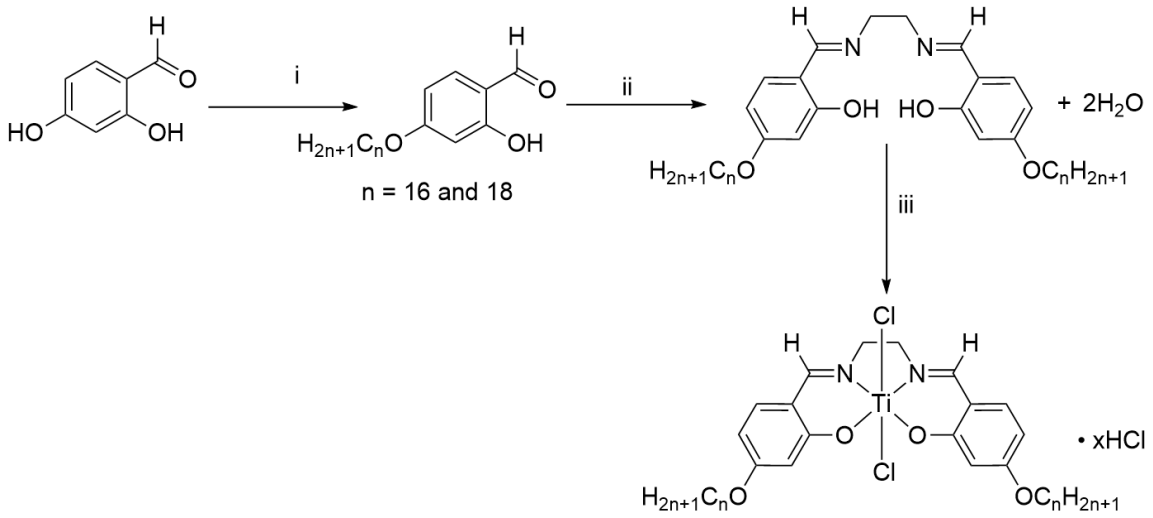

Scheme 4. Synthesis of titanium(IV) Schiff base ligand and complexes. (i) EtOH, KOH, $C_nH_{2n+1}Br$, Reflux, 24 h, 47-51%, (ii) Ethylenediamine, EtOH, CH_3COOH, Reflux, 24 h, 70-90 %, (iii) $TiCl_4$, THF, stir, RT, 3 h, 71-80%.

The ligands and complexes were synthesized by the analogous method reported in the literature.[25] Symmetrically disubstituted six-coordinate titanium(IV) Schiff base complexes can be prepared via two different routes: by direct addition of ligand to a suitable metal precursor or substitution of a Ti-salen complex.[25] The successful synthesis of the complex was achieved by the direct addition of $C_nH_{2n+1}O$-salen with titanium tetrachloride in THF at ambient temperature with good yield. All the complexes synthesized have good solubility in $CHCl_3$, allowing to characterize by NMR spectroscopy.

3.2.1 Elemental Analysis, FTIR, and NMR spectroscopic studies

Elemental analysis was carried out on $C_{18}H_{37}O$-salen ligand and [Ti($C_{18}H_{37}O$-salen)Cl_2] complex. The elemental analysis data for the percentage of C, H, and N were consistent with the

% calculated for the ligand, but the percentage found for C in the complex was not fully consistent with the calculated values. The percentages for carbon, hydrogen, and nitrogen in the complex were 67.74%, 9.40%, and 3.04%, respectively. The elemental analysis data for the percentage of C found in the complex was 66.76% versus the calculated value of 67.74%. The discrepancies could likely be due to the loss of solvates during the analytical procedure. The complex was found to have 0.5 HCl as a solvate.

FTIR and NMR spectra were acquired for the ligands and the respective complexes. FTIR spectra were acquired from 500-4000 cm^{-1}. The HC=N stretching frequencies are typically found between 1620-1640 cm^{-1} in the literature. Based on the data for the assigned stretching frequencies, an imine ν(C=N) stretching frequency at 1635 cm^{-1} was observed for Salen ligands; while for complexes [Ti(C_nH_{2n+1}O-salen)Cl_2] (n = 16 and 18), stretching frequencies were shifted to lower frequencies in the region of 1624 to 1630 cm^{-1} (Table 10).

Table 10. Important IR peaks of salen type ligands and its complexes.

Compounds	**ν (CH)/cm^{-1}**	**ν (C=O)/cm^{-1}**	**ν (C=N)/cm^{-1}**	**ν (Ar-O)/cm^{-1}**
$C_{16}H_{33}$O-sal	2915	1676	-	-
$C_{16}H_{33}$O-salen	1915	-	1625	1144
$C_{18}H_{37}$O-sal	2954	-	1625	1145
$C_{18}H_{33}$O-salen	2954		1625	1145
$C_{14}H_{29}$O-2,5-ester-en	2952	1727	1637	1202
[Ti($C_{16}H_{33}$O-salen)Cl_2] **11**	2954	-	1606	1205
[Ti($C_{18}H_{37}$O-salen)Cl_2] **12**	2954	-	1600	1187

The ^{1}H NMR spectra were acquired for the ligands and complexes using $CDCl_3$ as a solvent. (**Figure 36** and **Figure 37**). For ligands $C_nH_{2n+1}O$-salen, the presence of singlet at δ = 13.20 ppm and 8.36 ppm in the ^{1}H NMR spectra were assigned for phenolic and imine protons, respectively. The phenolic proton was disappeared in the complex while the shift of the imine proton signifies the coordination for ligand with the Ti(IV) metal center leading to the formation of the complexes. The important peaks observed area tabulated below (Table 11). The symmetric structure of the ligands and the complexes were also established by the NMR spectroscopy. Diagnostic of the symmetric structure is a singlet methylene proton at 3.8 - 4.0 ppm region, assigned to the four equivalent bridging methylene protons. These complexes were stable to moisture present in the atmosphere.

Table 11. Selected spectroscopic data for the ligands and the complexes.

	^{1}H, δ/ppm					^{13}C, δ/ppm
Compound	-OH	CHO	HC=N	CH_2-CH_2	-CH_3	HC=N
$C_{16}H_{33}O$-Sal	11.48	9.71	-		0.89	
$C_{18}H_{37}O$-Sal	11.48	9.71	-		0.89	
$C_{16}H_{33}O$-Salen	13.64	-	8.18	3.86	0.89	164.1
$C_{18}H_{37}O$-Salen	16.67	-	8.20	3.86	0.89	164.1
$C_{14}H_{29}O$-2,5-ester-en	-	-	8.29	3.97	0.89	164.1
[Ti($C_{16}H_{33}O$-salen)Cl_2] **11**	-	-	8.28	4.13	0.89	163.5
[Ti($C_{18}H_{37}O$-salen)Cl_2] **12**	-	-	8.28	4.14	0.89	163.4

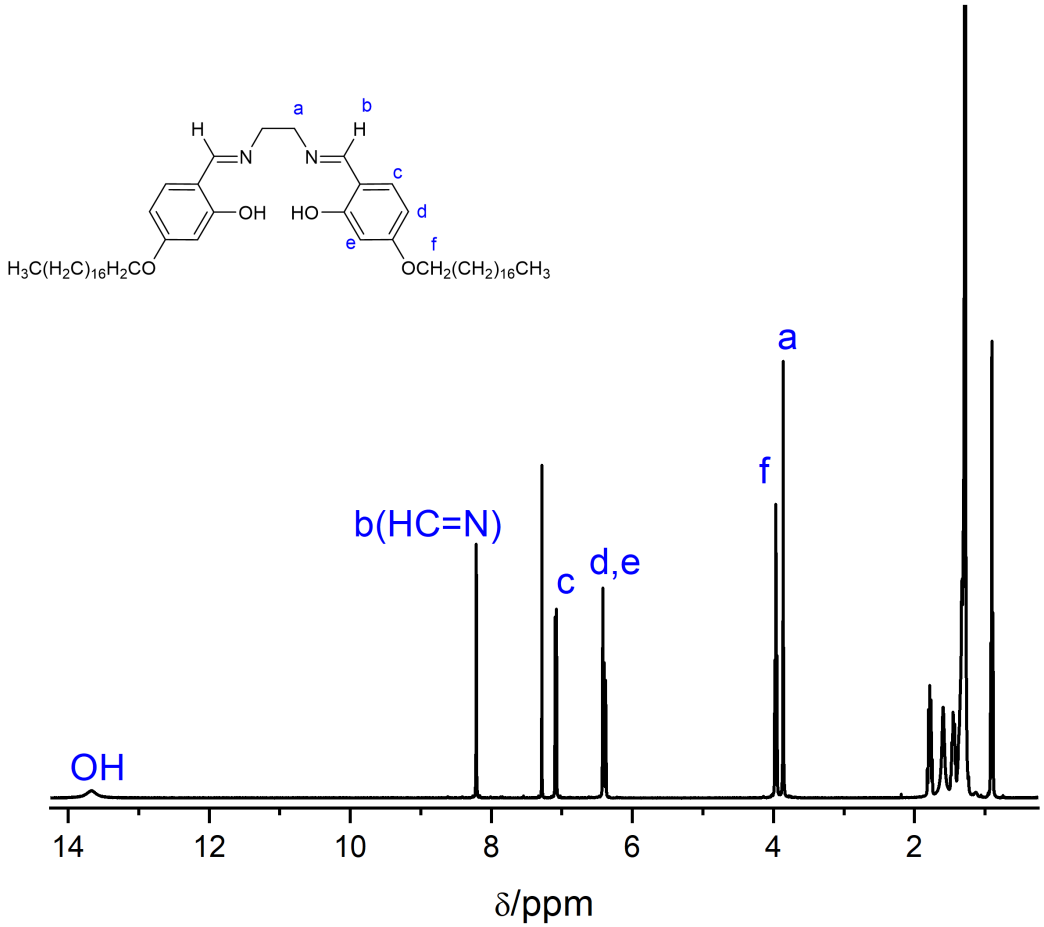

Figure 36. ^{1}H NMR spectra of $C_{18}H_{37}O$-salen ligand in $CDCl_3$.

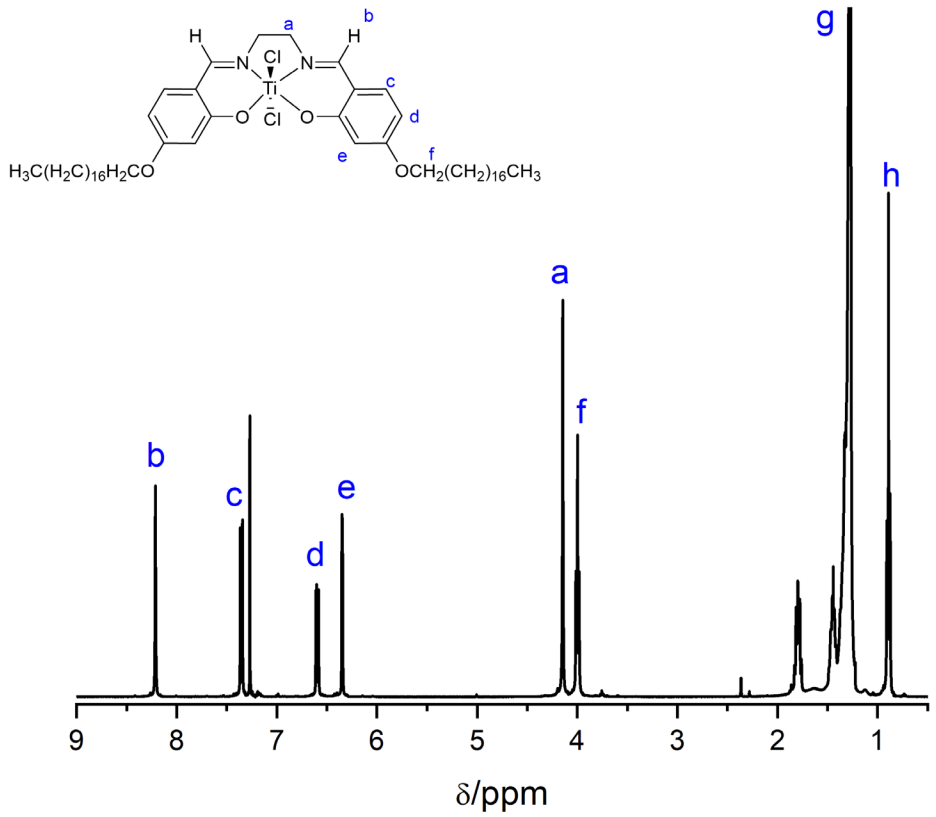

Figure 37. ^{1}H NMR spectrum of complex **12** in $CDCl_3$.

3.2.2 Liquid crystal studies of the ligands and the Ti(IV) complexes

The thermal and the optical behavior of the free ligands and the complexes were investigated by the cross polarizer optical microscope, and differential scanning calorimetry (DSC). The ligands were sandwich in between two glass slides and slowly heated until it melts. Once the melting of the ligands occurred, the slide was observed via cross-polarized using an optical microscope. Upon cooling, textures (**Figure 38**) were observed and based upon the shape of texture the arrangement of the mesophase were predicated.

Two of the ligands, $C_nH_{2n+1}O$-salen (where n = 16 and 18) exhibit liquid crystalline behavior. Textures observed for $C_nH_{2n+1}O$-salen (where n = 16 and 18) under cross polarizer showed a broken fan-like texture which is one of the characteristic features of the columnar mesophase, but the titanium(IV) complexes upon investigation were non-mesogenic as none of texture were developed under cross polarizer. In this case, these complexes were not planar due to their six coordinated octahedral geometry. Due to this coordination, the interaction between the neighboring molecule was hindered preventing the mesophase formation.

The mesophases generated for all the ligand were all columnar mesophases, as predicted by optical techniques and using the complementary shape approach. On cooling the compounds, the viscosity of the compound increased, and the textures were observed.

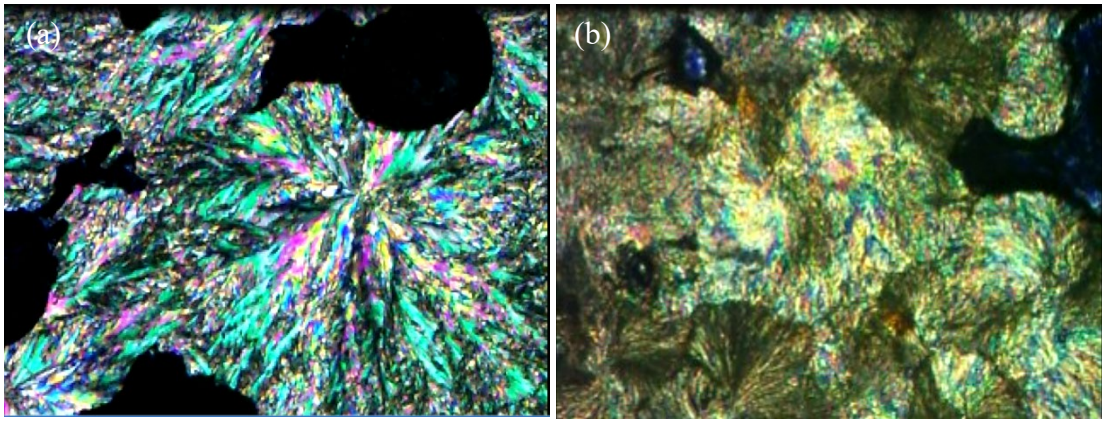

Figure 38. Optical texture observed for the ligands (a) $C_{16}H_{33}O$-salen and (b) $C_{18}H_{37}O$-salen.

Table 12. Liquid crystal properties analysis

Structure	**Comments**	**LC**
$C_{16}H_{33}O$-salen	LC. Very narrow range Cr 90.7 °C LC 101 °C I	Yes
$C_{18}H_{33}O$-salen	LC. arrow range. Cr 41.9 LC 96 I.	Yes
$C_{14}H_{29}O$-2,5-ester-en	Crystalline. No LC phase was observed	**No**
[Ti($C_{16}H_{33}O$-salen)Cl_2] **11**	Crystalline. Melts to isotropic at 91°C on cooling supercooled to 61°C and crystallizes	No
[Ti($C_{18}H_{37}O$-salen)Cl_2] **12**	Crystalline Cr 102 I	No

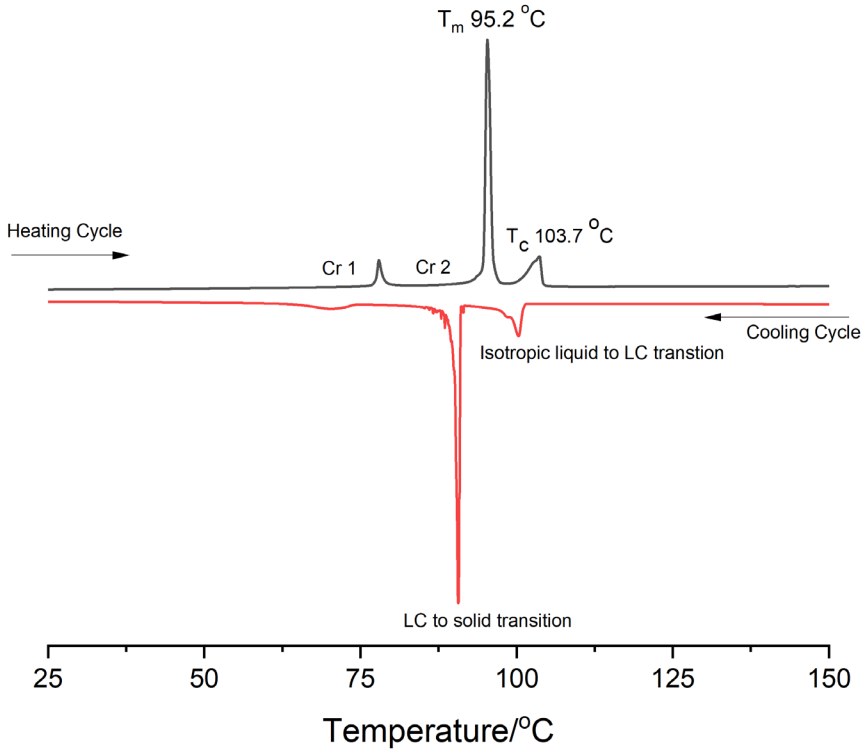

Figure 39. DSC thermogram of the $C_{16}H_{33}O$-salen ligand.

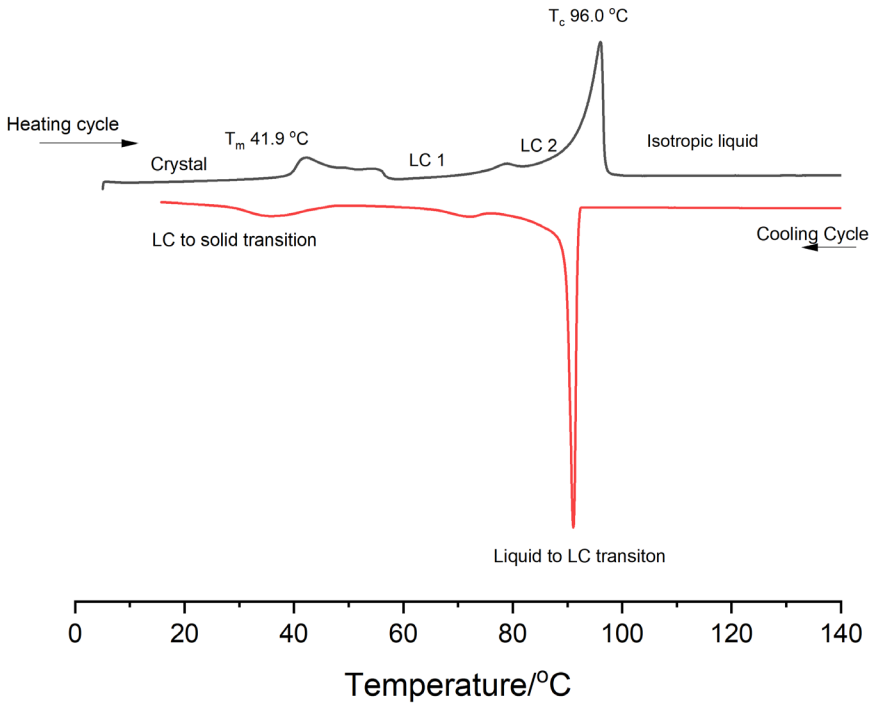

Figure 40. DSC thermogram of the $C_{18}H_{37}O$-salen ligand.

The melting temperature of this series of ligands was detected by DSC. DSC thermogram of $C_{16}H_{33}O$-salen (**Figure 39**) showed three endothermic peaks in the first heating cycle, which are due to crystal to crystal transition at 74.6 °C, crystal to mesophase at 95.2 °C, and mesophase to isotropic liquid at 103.7 °C. During the cooling cycle, a similar pattern exothermic peaks were observed with identical enthalpy change for the ligand, where transition to liquid crystal state occurred at 101.0 °C and the liquid crystal state to crystalline state at 91.7 °C. The ligand exhibit mesophase behavior at very narrow range of only approximately 10 °C. Likewise, during the heating cycle of $C_{18}H_{37}O$-salen (**Figure 40**), four endothermic peaks were observed. Crystal to liquid crystalline transition occurs at 41.9 °C. Similarly, two very small endothermic peak at 58.1 °C and 79.8 °C was observed indicating the various mesogenic phase transition, and liquid

crystalline to isotropic liquid transition occurred 96.0 °C during the first heating cycle. On cooling cycle, only three exothermic peaks are observed. The transition from the isotropic liquid phase to the liquid crystal phase was observed at 91.2 °C, and the transition to the mesophase to crystal occurred at 35.4 °C. In the above case, both the experiment was repeated to ensure reproducibility. On the second cycle of heating, similar phases transition was observed, confirming the reproducibility.

On the other hand, the liquid crystal phase transition was not observed for the complexes, which is an agreement with POM studies, as no texture was noticed for complexes. The DSC traces showed only the melting temperature for the complexes. The transition temperature of the ligands and the complexes are listed in scheme 5.

Scheme 5. The transition temperatures of ligands and the complexes.

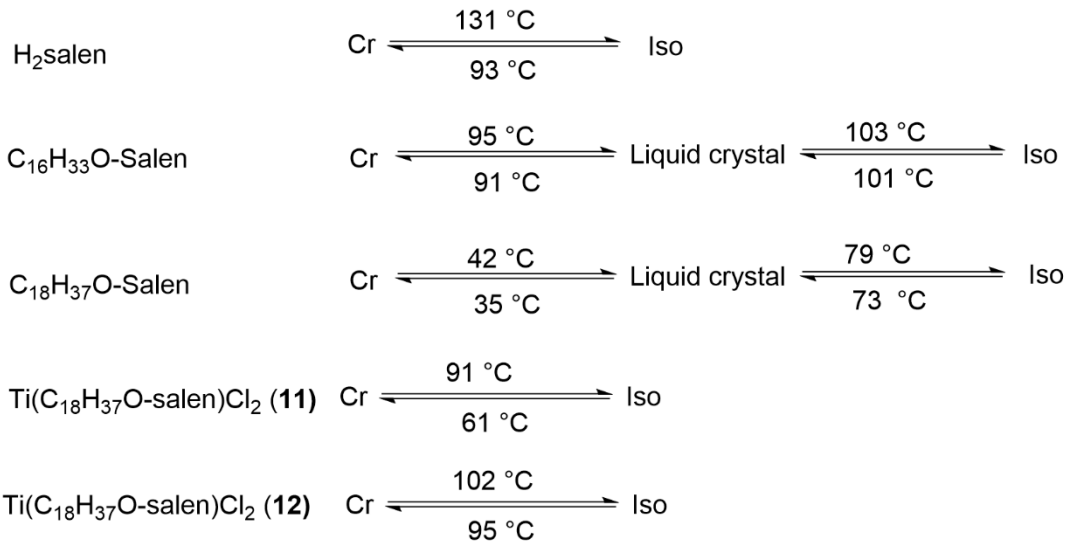

***Cr1 = crystal, Iso = Isotropic liquid phase*

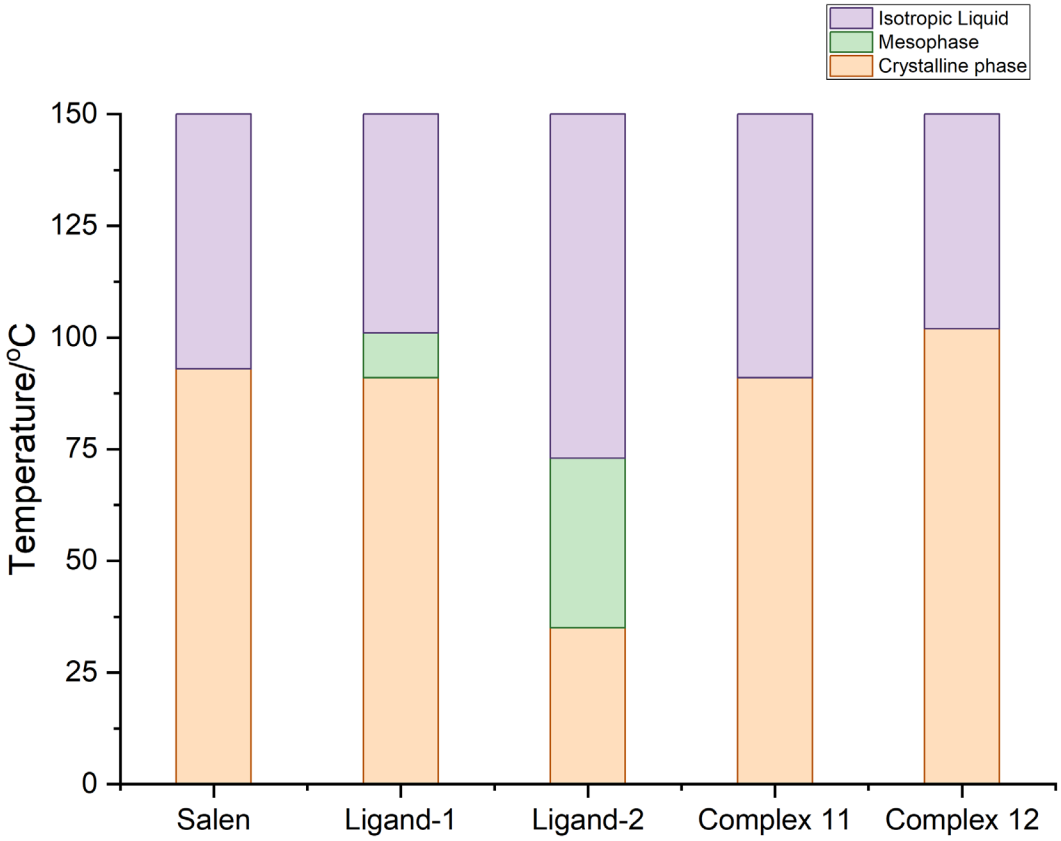

Figure 41. Melting Behavior of ligands and the complexes. Ligand-1 = $C_{16}H_{33}O$-salen, and Ligand-2 = $C_{18}H_{37}O$-salen

3.3 Synthesis, characterization and mesomorphic studies of the C_n-2,4-salphen ligand and its complexes

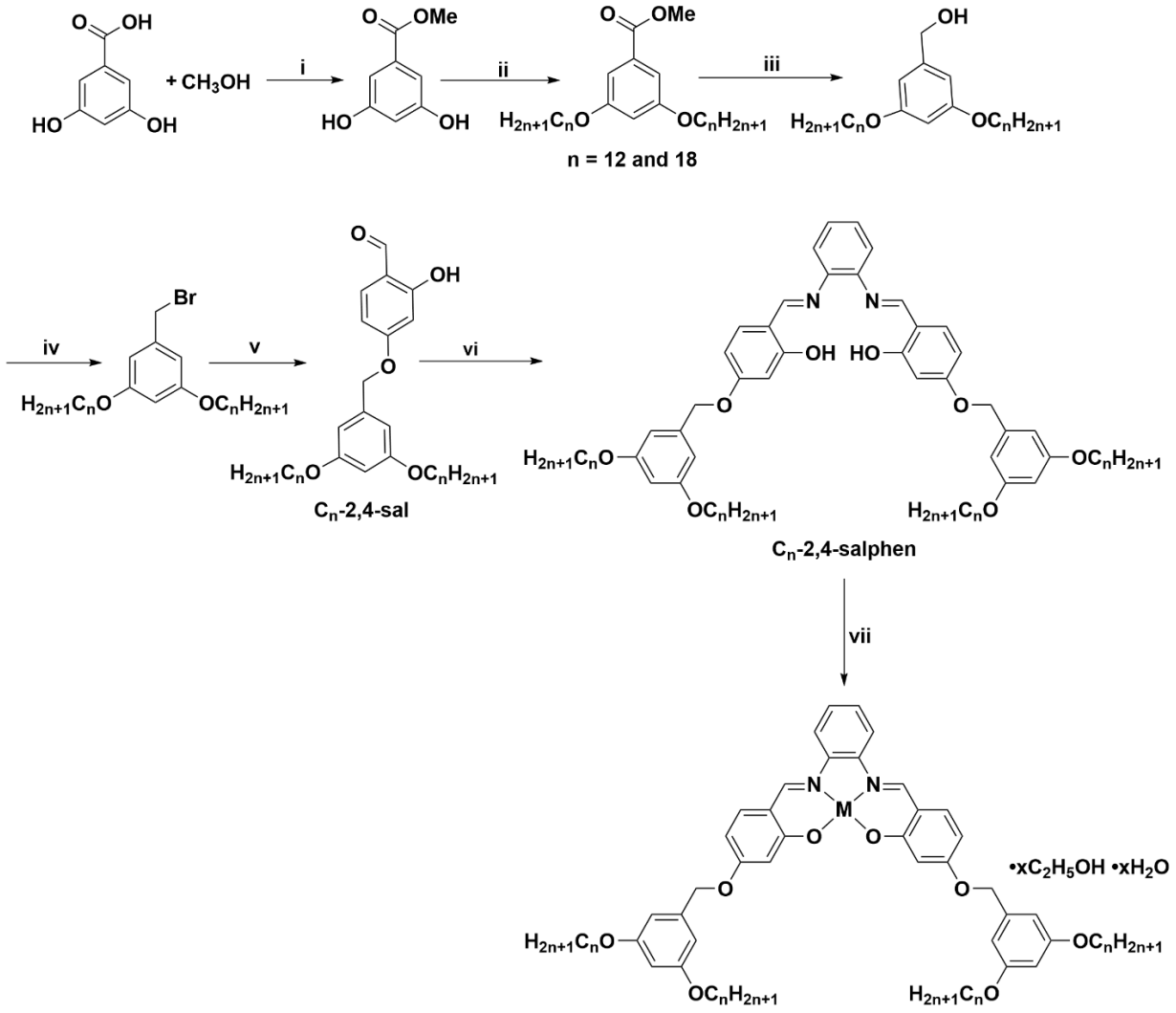

Scheme 6. The general method for the synthesis of the ligands and the complexes. (i) Conc. H_2SO_4, MeOH, Reflux, 2h, 90%, (ii) K_2CO_3, $C_nH_{2n+1}Br$, 2-butanone, 90 °C, (iii) $LiAlH_4$, THF, 75 °C, 90-95%, (iv) CBr_4, DCM, RT, 4 h, 81 %, (v) 2,4-dhydroxybenzaldehyde, MeCN/THF, $NaHCO_3$, KI, Reflux, 3d, 65-71%, (vi) *ortho*-phenylenediamine, CH_3COOH, EtOH, Reflux, 24, 65-85%, (vii) $M(COOCH_3)_2$ •xH_2O (M = Co^{2+}, Ni^{2+}, and Cu^{2+}), absolute EtOH, Reflux, 24 h, 63-85%

As shown in Scheme 4, the synthesis of the C_n-2,4-salphen ligand required multi-step synthesis followed by purification and appropriate characterizations. 2,4-dihyrdoxybenzoic acid was used as a starting material to synthesize the target ligands. Esterification followed by nucleophilic substitution of 2,4-dihydroxybenzoic acid with alkyl bromide generate methyl-3,5-bis(alkoxy)benzoate, which was subsequently reduced by lithium aluminum hydride and finally again a nucleophilic reaction to give precursor ligand 3,5-bis(alkoxy)benzyl bromide

Various commercially available disubstituted dihydroxy benzaldehyde was used to generate C_n-2,4-sal and C_n-2,5-sal, respectively. The purpose of using disubstituted dihydroxy benzaldehyde was to design a target ligand, either a rod-like structure or a half disc-like structure. The rod-like structure can be achieved by the nucleophilic substitution of 2,5-dihydroxybenzaldehyde with bis(alkoxy)benzyl bromide. Due to the formation of various side products, which were confirmed by TLC and NMR spectroscopy, the synthesis with 2,5-dihdyroxybenzaldehye was not investigated further (Appendix, A25). Meanwhile, the half disc-like or bent structure was obtained by the reaction of 2,4-dihydroxybenzaldehyde with bis(alkoxy)benzyl bromide.

Finally, the desired target ligand was synthesized by the condensation reaction of precursor C_n-2,4-sal ligand with *ortho*-phenylenediamine. The synthesis was straight forward reaction with a decent yield. The synthesis of the complex was achieved by using the appropriate metal precursor via the ligand substitution mechanism. The target ligands were purified by recrystallization using absolute ethanol as a solvent.

All the ligands and the complexes were characterized by elemental analysis, FTIR, NMR, ESI MS, and UV-visible spectroscopy, where appropriate.

3.3.1 Elemental analysis, FTIR, and ESI MS studies

Elemental analysis was carried out on precursor ligands C_{12}-2,4-sal, C_{18}-2,4-sal, C_{12}-2,4-salphen, C_{18}-2,4-salphen and the complexes [Co(C_{12}-salphen)] **13**, [Ni(C_{12}-salphen)] **14** and [Cu(C_{12}-salphen)] **15**. The percentage of C and H found for C_{12}-2,4-sal, and C_{18}-2,4-sal precursor ligands were in close agreement with the percentage calculated. Meanwhile, the percentage of C found in C_{12}-2,4-salphen ligand was 76.93 % vs. the calculated value of 77.80 %. Likewise, the percentage of C found in C_{18}-2,4-salphen ligand was 78.42% vs. the calculated value of 79.45 %. The elemental analysis data for the percentage of C is not fully consistent with the calculated value, but other spectroscopic methods confirmed the identity of ligands. Since the discrepancy is only in carbon, it is likely due to the loss of water as solvate during the analytical procedure. Ligand C_{12}-2,4-salphen and C_{18}-2,4-salphen were found to have 1.0 and 0.75 H_2O molecules as a solvate, respectively.

Similarly, the elemental analysis was carried out only on the complexes of **13**, **14,** and **15**. The percentage of C found for the **13**, **14,** and **15** were 72.47%, 72.99%, and 72.45% versus. the calculated 74.45 %, 74.47 %, and 74.20%, respectively. Due to the fact that the discrepancy is only in the carbon, it is likely due to the loss of ethanol and water as solvate during the analytical procedure. Complexes **13**, **14,** and **15** were found to have 1.0 mol of ethanol and 1.0 mol of water as a solvate, respectively.

FT IR spectra of precursor ligands were acquired, and important stretching frequencies are presented in table 12 (Appendix A20). The FTIR spectra of C_{12}-2,4-Sal and C_{18}-2,4-Sal ligands exhibit characteristic bands that correspond to various functional groups in different energy regions. The most significant bands in the 4000-500 cm^{-1} region are found between 1680-1730 (C=O), and 1150-1230 (Ar-O). Subsequently, C_{12}-2,4-Sal and C_{18}-2,4-Sal react with *ortho*-

phenylenediamine to form a Schiff base ligand. The significant change is the formation of imine bond formation (C=N), which is very important in the identification of Schiff base ligands. The new bond formed is found between 1580-1630 (C=N) (**Figure 42**).

Infrared spectra of all the complexes (Appendix , A54) show a shift in the stretching frequency of imine bond as compared to the free ligands. In addition to this shift in the vibrational stretching frequency, an additional band at 434 cm^{-1} for ν(Ni-N) confirms the coordination with the Ni^{2+} metal ion. The shift and addition of a new peak are indicative of the involvement of the imine nitrogen and phenolic oxygen atoms in the chelation. From this analysis, it suggests that the ligands coordinate with the metal center in a tetradentate form via the imine nitrogen and the phenolic oxygens in all the complexes.

Table 13. FTIR spectroscopic data (ν/cm^{-1}) for the ligands.

Compound	V(CH_3)	ν(C=O)	ν(C=N)	ν(C-O)	ν(M-O)	ν(M-N)
C_{12}-2,4-Sal	2928 (s)	1631 (s)	-	1180 (s)	-	-
C_{18}-2,4-Sal	2928 (s)	1635 (s)	-	1180 (s)	-	-
C_{12}-2,4-Salphen	2928 2918 (s) 2952 (s)	-	1624 1600 (s)	1180 1166(s)		-
C_{18}-2,4-Salphen	291828 (s) 2952 (s)	-	1624 (s)	1180 (s)	-	-
13	2918 (s) 2952 (s)	-	1606	1166	508 (w)	429 (m)
14	2918(s) 2853 (s)	-	1604	1164 (s)	512 (w)	434 (m)
15	2918 (s) 2952 (s)	-	1607	1164	501 (w)	-

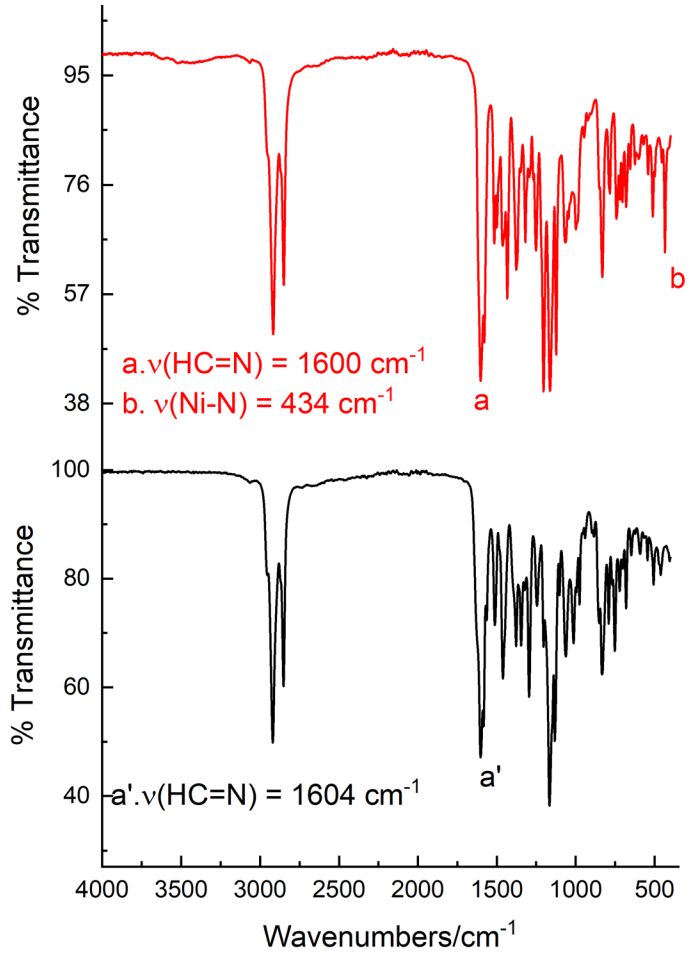

Figure 42. FT IR spectra of C_{12}-2,4-salphen ligand (black) and a complex **14** (red).

ESI-MS spectra were acquired for only precursor ligand C_{12}-2,4-sal (Appendix, A21-22). The ligand C_{12}-2,4-salphen ligand and complexes are insoluble in the preferred solvent. Thus, the mass spectrum was acquired for only precursor ligand. The mass spectrum of the precursor ligand was acquire using HPLC grade methanol in positive ion mode. In the mass spectrum, we have assigned M as the molecular ion. A base peak for C_{12}-2,4-sal occurred as m/z = 597.8, which is indicative of the presence of the [**M** + $\mathbf{H}^+$] species.

3.3.2 NMR spectroscopic studies

In an NMR spectroscopy study, ^{1}H, ^{13}C, and 2-D (Appendix, A23-24) spectra were acquired for the precursor ligands and a complex **14** in $CDCl_3$ at ambient temperature where appropriate. For the compound C_{12}-2,4-Sal, the presence singlets at δ = 11.46 ppm and δ = 9.73 ppm represent the phenolic proton and the proton from the aldehyde group, respectively (**Figure 43**). After the reaction of C_{12}-2,4-Sal with the *ortho*-phenylenediamine, the Schiff base C_{12}-2,4-salphen ligand was synthesized. The singlet peaks at δ = 13.55 ppm and δ = 8.55 ppm in the ^{1}H NMR spectra of C_{12}-2,4-salphen were assigned for phenol and imine protons, respectively. In addition, 2-D (hsqc) (Appendix, A 23-24) NMR spectroscopy was utilized to complete the peak assignment of C_{12}-2,4-sal and C_{12}-2,4-salphen ligands**.** Upon complexation, the lack of proton signal corresponding to the OH group of the free ligands and the upfield shift of the imine proton further attested the coordination of azomethine-N. Due to the paramagnetic nature, the useful NMR spectra for Co(II) and Cu(II) complexes were unable to be obtained. The coordination of the ligand to the metal centers occurred via *N,N'*- and *O,O'*-sites. Based on these results obtained from the ^{1}H NMR spectroscopy, it can be inferred that there is a successful synthesis of the complexes.

.

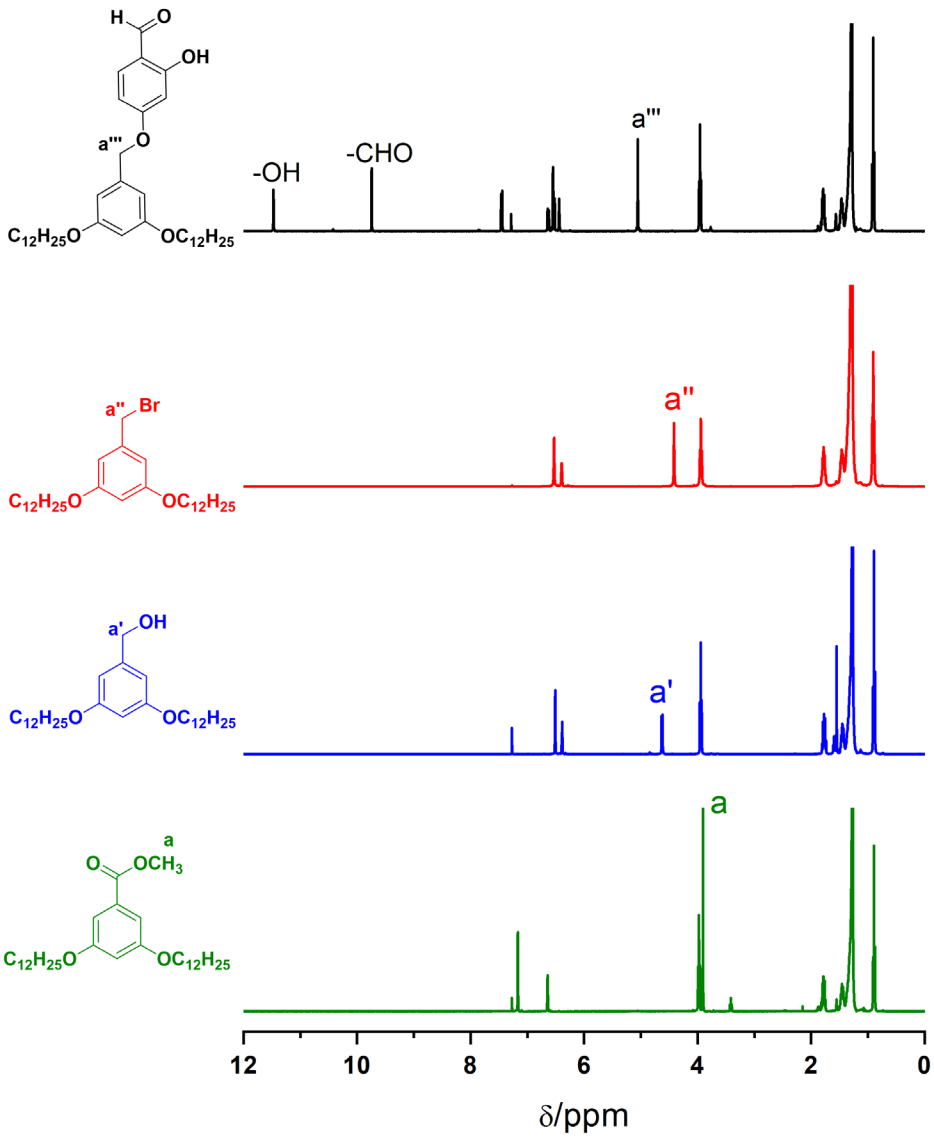

Figure 43. ^{1}H NMR spectra precursor ligand in $CDCl_3$.

The ^{13}C NMR spectra for precursor ligands are shown in below (**Figure 44**). For Methyl-bis(dodecyloxy)benzoate (**Figure 44**, green), the two important peaks noticed were at δ = 167.0 ppm (a), which was due carbonyl carbon of the ester group, and at δ = 52.0 ppm (b) was due to the methyl carbon. Likewise, for bis(dodecyloxy)phenylmethanol (**Figure 44**, blue), the important peak observed was at δ = 65.5 ppm (a'), which was due to methylene carbon directly

bonded with -OH function group. Bis(dodecyloxy)benzylbromide (**Figure 44**, red) was prepared by the nucleophilic substitution reaction of bis(dodecyloxy)phenylmethanol, the important peak observed was at δ = 33.7 ppm (a'') due to the methylene carbon bonded with the bromide functional group. And for the precursor ligand C_{12}-2,4-Sal (**Figure 44**, black), the peak at δ = 194.4 ppm is the characteristic peak for the carbonyl carbon.

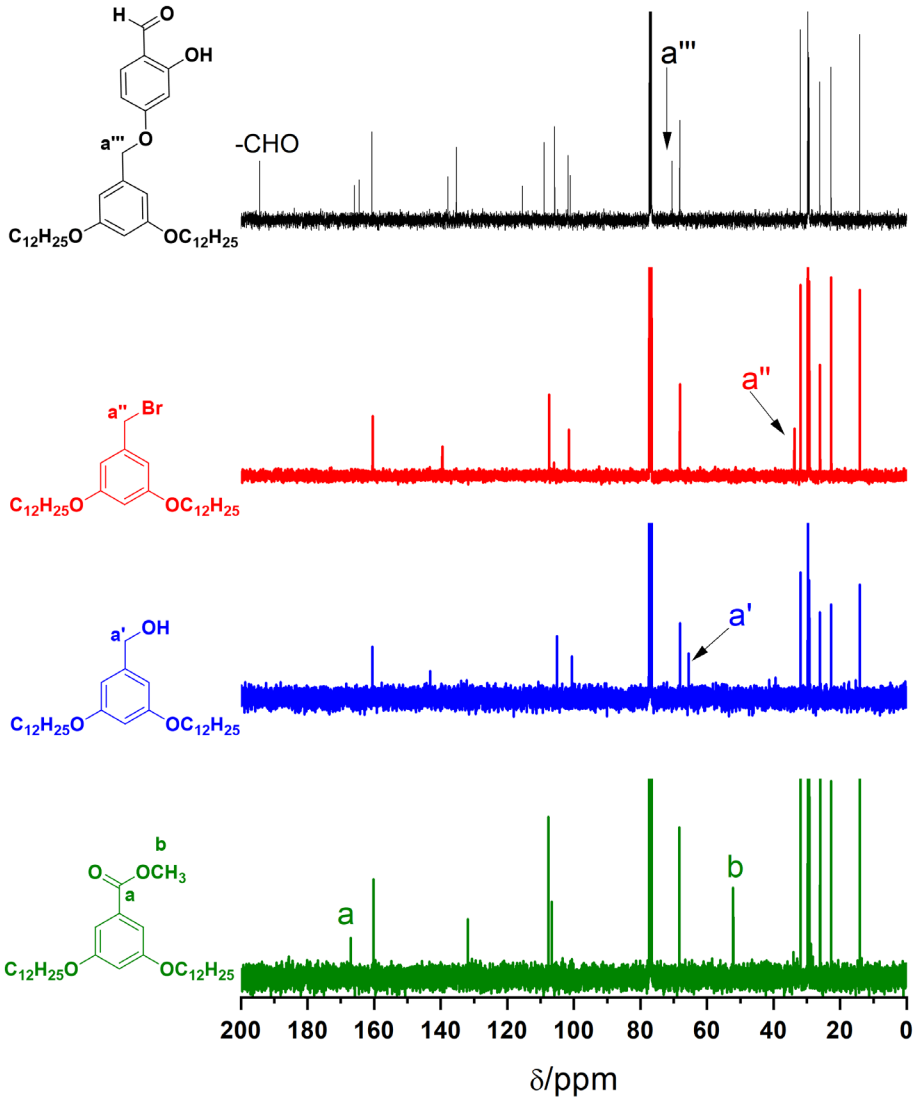

Figure 44. ^{13}C NMR spectra of the precursor ligand in $CDCl_3$.

The synthesis of the target ligand, i.e., C_{12}-2,4-salphen was a straightforward reaction. Precursor ligand C_{12}-2,4-sal undergoes the condensation reaction with *ortho*-phenylenediamine to produce C_{12}-2,4-salphen ligand. Thus, the synthesized ligand was purified by recrystallization using absolute ethanol as a solvent. The important shift in ^{1}H NMR observed was the presence of the imine peak at 8.56 ppm and at 13.5 ppm (**Figure 45**), which was due to the phenolic proton. Likewise, the important chemical shift observed in the ^{13}C NMR is the peak at δ = 193 ppm, which is a characteristic peak for carbonyl carbon for precursor ligand (C_{12}-2,4-sal) disappeared, and a new peak at 162.0 ppm (a) (**Figure 46**) appeared. The peak at 162.0 ppm was due to the imine carbon confirming the formation of the desired product. All the peaks were assigned using hsqc NMR spectroscopy (Appendix, A23-24).

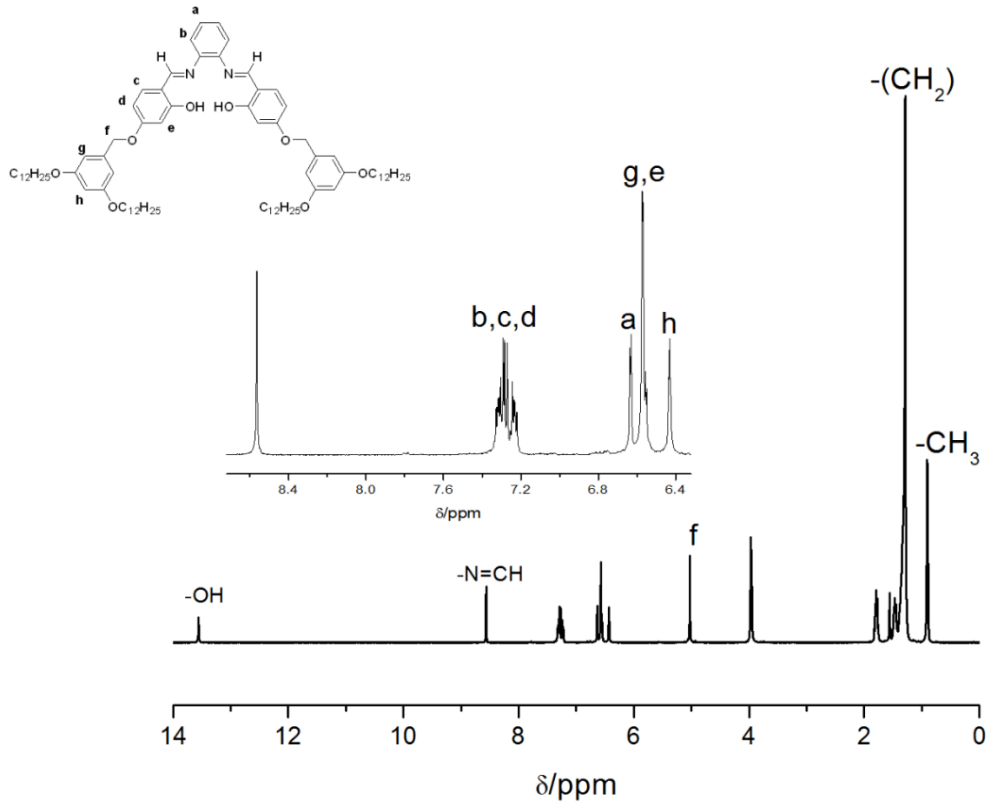

Figure 45. ^{1}H NMR spectra of C_{12}-2,4-salphen in $CDCl_3$.

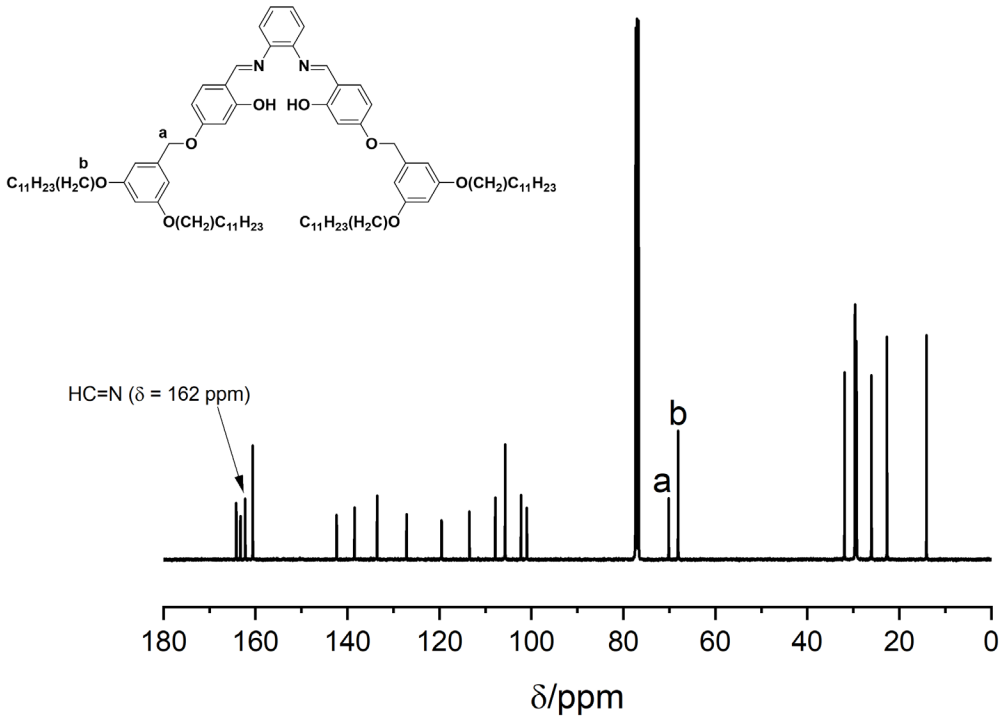

Figure 46. ^{13}C NMR spectrum of the C_{12}-2,4-salphen in $CDCl_3$.

The desired complexes were obtained by the reaction of C_{12}-2,4-salphen ligand and respective metal precursors. All the complexes were purified using recrystallization techniques and characterized using elemental analysis, UV-visible spectroscopy and NMR spectroscopies. Due to paramagnetic nature, standard NMR spectra for Co(II) and Cu(II) complexes were not very practical. NMR spectroscopy was only applicable wtih the Ni(II) complex. The proton from phenolic group deprotonated and bind with Ni(II) ion via *O,O'* and *N,N'* forming an square planar complex. This was confirmed by NMR spectroscopy, as phenolic peak disappeared and there was a shift in imine peak (**Figure 47**). Likewise, in the ^{13}C NMR spectra the shift is imine carbon was observed (**Figure 48**).

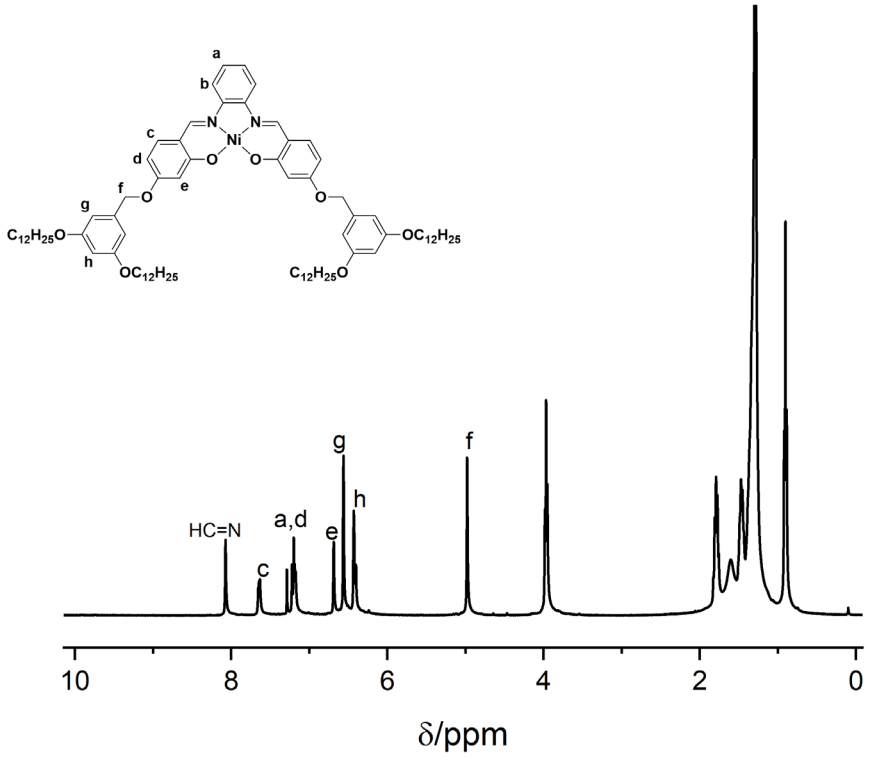

Figure 47. ^{1}H NMR spectrum of a complex **14** in $CDCl_3$.

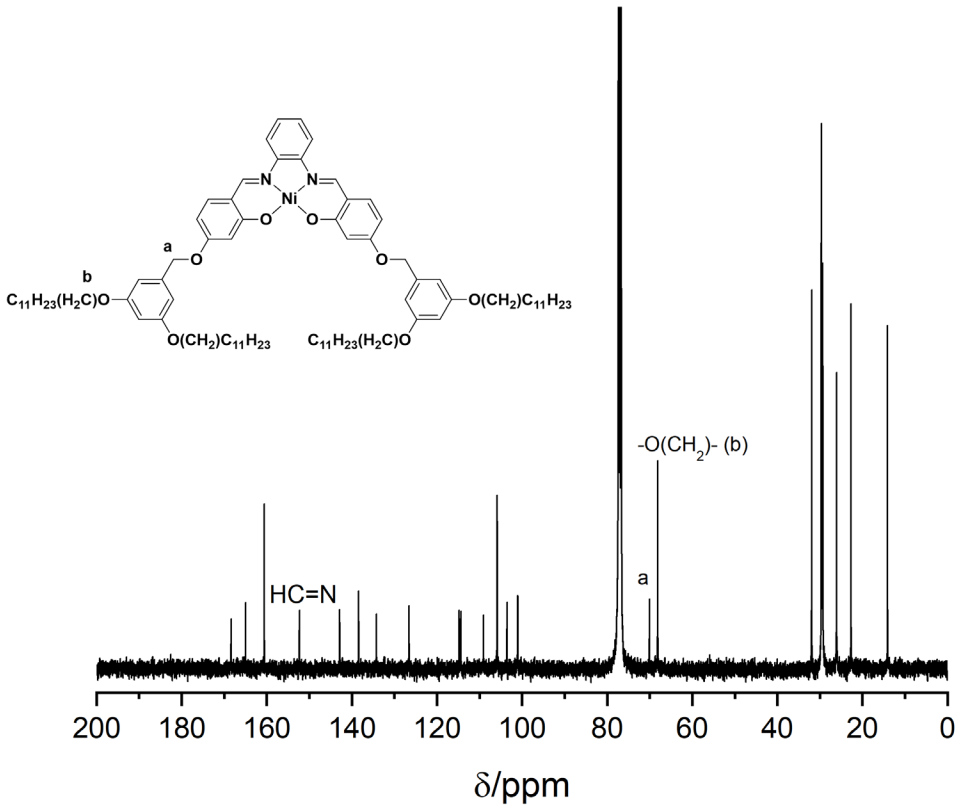

Figure 48. ^{13}C NMR spectrum of a complex **14** in $CDCl_3$.

Table 14. ^{1}H NMR spectroscopic data (δ/ppm) for the ligands and the complex.

Compound	^{1}H, δ/ppm					^{13}C, δ/ppm	
	OH	CHO	HC=N	ArO-CH_2-Ar	OCH_2	C=O	C=N
C_{12}-2,4-sal	11.46	9.73	-	5.04	3.94	194	-
C_{18}-2,4-sal	11.47	9.74	-	5.04	3.96	194.3	-
C_{12}-2,5-sal	10.68	9.86	-	5.01	3.97	196.0	-
C_{12}-2,4-salphen	13.55	-	8.55	5.01	3.95	-	162.0
C_{18}-2,4-salphen	13.57	-	-8.55	5.07	3.96	-	163.0
14	-	-	8.09	4.96	3.95	-	152.3

3.3.3 UV-visisble spectroscopy

The absorption spectra of the C_{12}-2,4-salphen ligand and complexes **13**, **14**, and **15** were acquired in dichloromethane solution at ambient temperature (Table 15). Absorption spectra of the free ligand exhibit two bands (**Figure 49**) at 287 nm and 332 mn correspond to characteristic intraligand π-π* electronic transitions of the aromatic rings and the imine unit. After coordination, all the absorption bands were shifted significantly to longer wavelengths. The absorption spectra of complexes **13**, **14**, and **15** are shown in below (Figure 49). The first two bands in the complexes were bathochromically shifted with respect to free ligands. For the Ni^{2+} complex, the peak featuring at 452nm is believed to be of ligand to metal charge transfer band. The excitation of filled d orbital electrons into the empty antibnding π orbital of the ligand.[180] The absorption peak featured at 561 nm in the case of complex **13**, 557 nm for complex **14,** and 556 nm for complexes **15** are attributed to d-d transition, respectively.

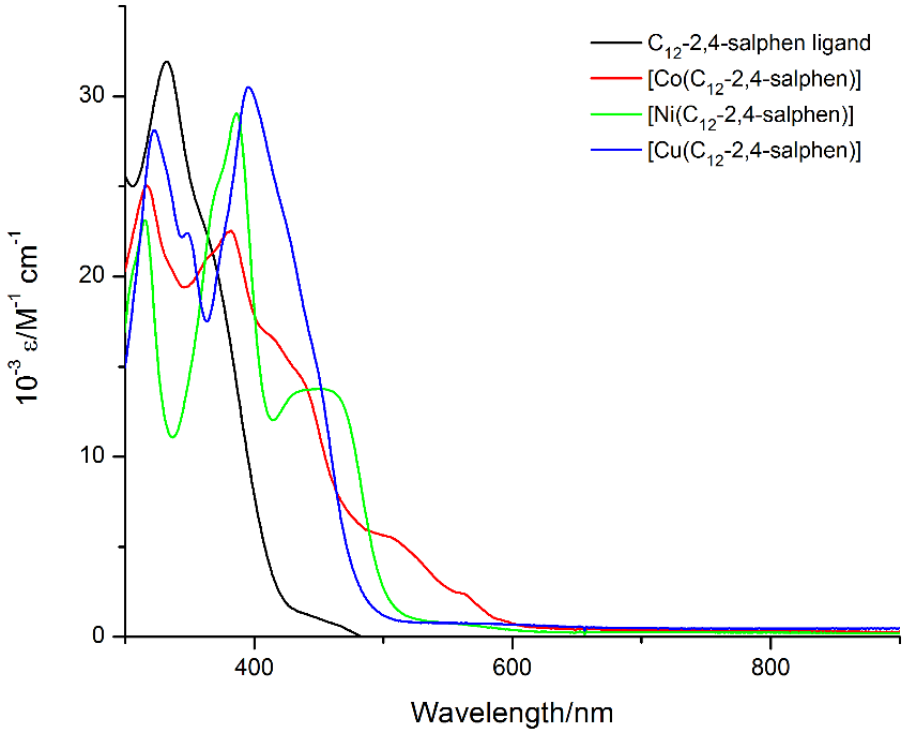

Figure 49. UV-visible spectra of the ligand and metal complexes in CH_2Cl_2.

Table 15. UV-visible spectra data of the ligand and metal complexes.

Compound	λ_{abs}; $\varepsilon/10^3$ (M^{-1} cm^{-1})
C_{12}-2,4-salphen	287 (29.2), 332 (31.9)
[Co(C_{12}-2,4-salphen)]•C_2H_5OH•H_2O **13**	382 (22.5),504 (55.5), 561 (24.2)
[Ni(C_{12}-2,4-salphen)] •C_2H_5OH•H_2O **14**	315 (23.13), 386 (29.0) , 452 (13.7) 557 (0.57)
[Cu(C_{12}-2,4-salphen)] •C_2H_5OH•H_2O **15**	322 (28.1) 395(30.5),556 (0.42)

3.3.4 Liquid crystal studies of the ligands and its complexes

The liquid crystalline properties are generally studied using polarized optical microscopy and differential scanning calorimetry. To confirm the mesophase structure XRD measurement are perfomed. In our study, C_{12}-2,4-salphen ligand was taken as a representative example to be analyzed by Small-angle X-ray diffraction. In some case, the sticky nature of the complexes hindered the study using XRD techniques. Hence, herein follows the discussion on the mesomorphic properties of the ligands and their complexes.

The texture of the ligands were observed between the cross polarizers using optical microscope upon cooling from an isotropic melt. The ligands exhibit birefringence which is the characteristic feature of the mesomorphic materials. The textures between the cross polarizer of the optical microscope were of fan-like defects and grainy patterns for C_{12}-2,4-salphen and C_{18}-2,4-salphen, respectively. These types of defect are characteristics feature of columnar mesophases.[180, 236] At first glance, the images (**Figure 50)** suggest that C_{12}-2,4-salphen (a and b) and C_{18}-2,4-salphen (c and d) exhibit the columnar phase. The straight-line defect textures and a grainy textures of the hexagonal columnar phase (Col_h) were observed under cross polarizer. In the POM image, the dark spots indicate the hemi-disc-like molecules were oriented

homeotropically, which means the discs were oriented face-on to the glass substrate.[203, 237] In addition to the optical texture, the mesophase was identified as a hexagonal columnar phase through an XRD study (**Figure 52**). The grainy texture of C_{18}-2,4-salphen that was developed upon cooling from the isotropic melt remained unaltered down to room temperature. Althought, the texture was observed for the C_{18}-2,4-salphen, but the transition temperature was unable to predict by DSC. Only one endothermic peak was observed during the heating cycle, and similar peak observed upon cooling.

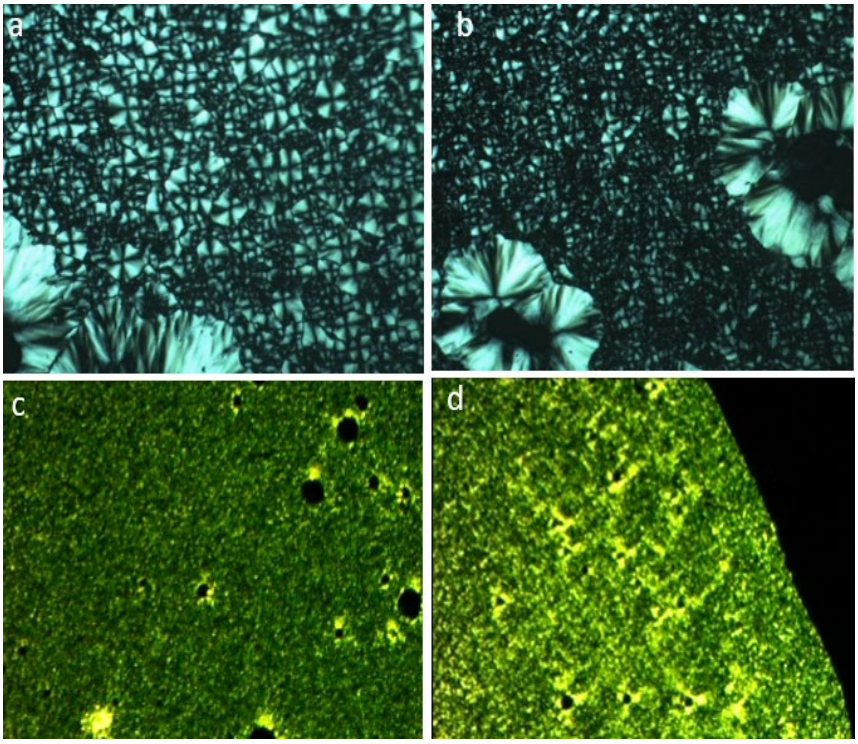

Figure 50. Polarographic Optical Image of the C_{12}-2,4-salphen (a and b) and C_{18}-2,4-salphen (c and d) under cooling condition.

The transition temperature and enthalpy of ligands were recorded on the DSC scan cycles. The DSC thermogram of the ligand is shown in Figure 51. The ligand with the shorter chain length upon heating showed two endothermic peaks at 91 °C, representing the melting

from crystal to liquid crystal phase, and upon further heating, another small peak was observed at 175 °C, which was due to the transition of liquid crystal phase into an isotropic liquid phase. Upon cooling, two exothermic peaks were observed, which indicates the enantiotropic nature of the liquid crystal, which means it can change into the liquid crystal state from either raising the temperature of the solid or lowering the temperature of the liquid.

Likewise, a ligand with the longer chain length C_{18}-2,4-salphen melted close to the room temperature, i.e., the onset temperature during the heating cycle was observed at 33.8 °C. In this case, the increase in the chain length does not favor the mesomorphic behavior of the ligand. The DSC trace for both the ligands was repeatable during the second heating cycle, displaying sharp peaks for phase transitions. Thus, from the optical and thermal studies, it is clear that the mesophase for ligand with shorter chain length is more stabilized relative to ligand with longer chain length.

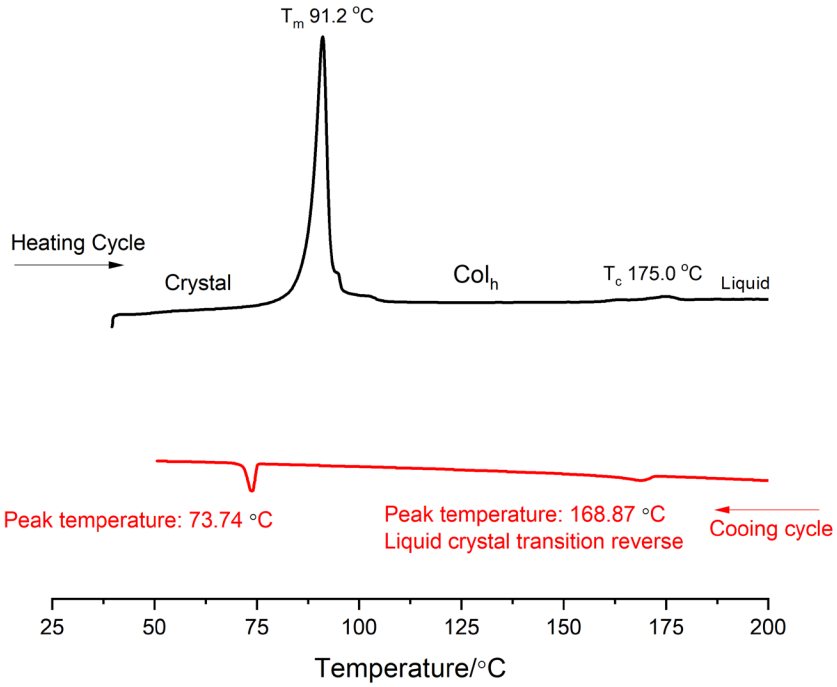

Figure 51. DSC thermogram of the C_{12}-2,4-salphen ligand.

To confirm the mesophase, C_{12}-2,4-salphen ligand was selected as representative examples for temperature-dependent powder X-ray diffraction measurements. The columnar nature of the mesophase observed by POM was confirmed by variable-temperature powder XRD studies. The diffractograms of the C_{12}-2,4-salphen ligand displayed a series of three peaks in the low-angle region with a reciprocal d-spacing ration of 1: $1/\sqrt{3}$:$1/\sqrt{4}$, which can be indexed at the d(10), d(11), and d(20) reflections of the columnar hexagonal mesophase (**Figure 52**). This is the characteristics feature for the discotic columnar (Col_h) phase. The sharpness of the small angel reflections suggested a highly ordered mesophase structure. The two half-disc-shape molecules arrange in an antiparallel to cover the surface area of the lattice.

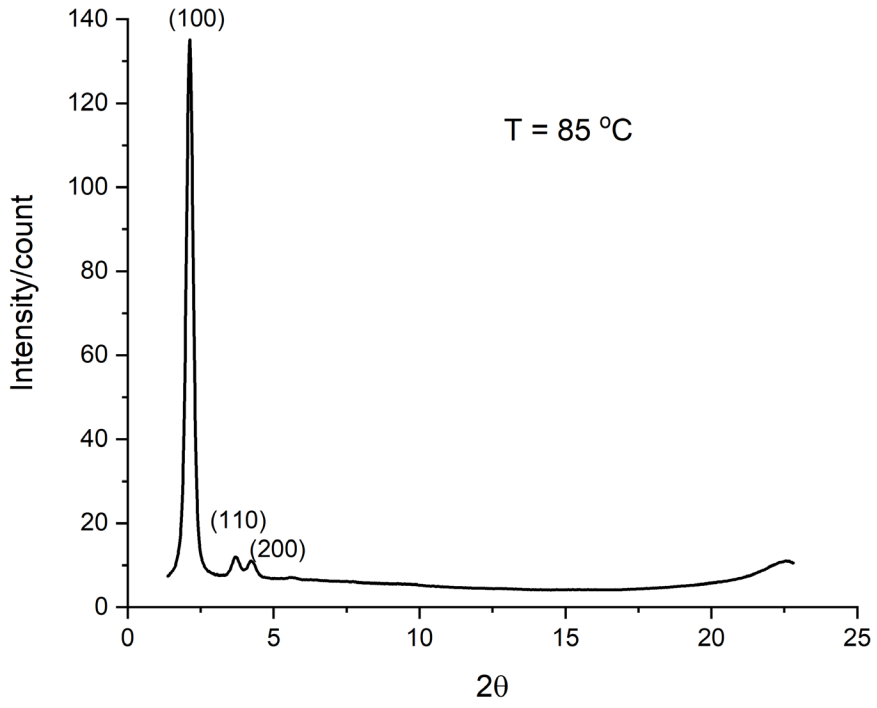

Figure 52. XRD of the C_{12}-2,4-salphen ligand at 85 °C.

Table 16. *d*-spacings and lattice parameter for a C_{12}-2,4-salphen ligand with hexagonal mesophase.

	d-spacing(obs)/Å	Miller indices[*hkl*]	parameters[a]
	35.15	10	T = 85 °C
C_{12}-2,4-salphen	22.62	11	a = 40.6 Å
	19.56	20	

[a] The Col_h lattice parameter $a = 2\langle d_{10}\rangle/\sqrt{3}$.

In a wide-angle region, the presence of another broad peak indicates the formation of the dimer along the axis of the column. The lattice constant of the columnar phase of C_{12}-2,4-salphen is a = 40.6 Å. The semi disc-like molecules, thus arranged in an anti-parallel manner. The rigid core of salphen-type ligands were stacked along the axis, thereby forming a column which was expected to self-organized to generate a columnar hexagonal arrangement. The schematic representation of the formation of column and self-organization is shown below (**Figure 53)**.

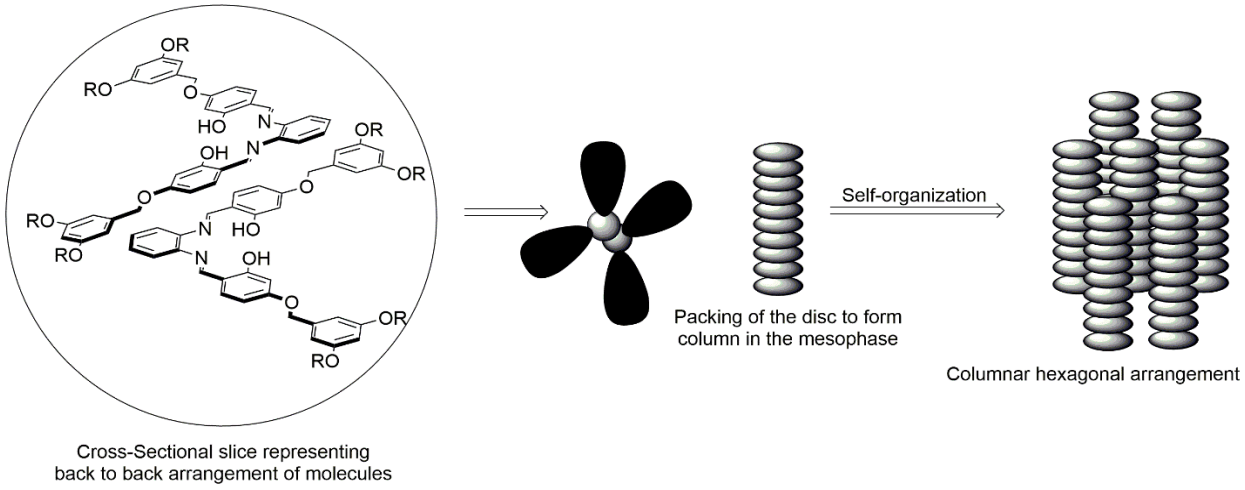

Figure 53. Schematic representation of the liquid crystal ligand and its self-organization.

The mesomorphic behavior of the complexes **13**, **14**, and **15** were also studied optically and thermally. The result obtained from the optical and thermal studies are shown in below (**Figure**

54, Figure 55, and **Figure 56**). For complex **13**, optically and thermally results obtained were not as anticipated. While cooling from the isotropic melt, there does not appear a texture, but it was very viscous. From DSC traces also, the conclusive results were not obtained (Appendix A26). The reason behind cobalt(II) complexes not behaving as a liquid crystal requires further research, but one of the possibilities can be due to its geometrical arrangement. To support this belief, further investigation is required for which single-crystal X-ray crystallography can be an excellent method.

For complexes **14** and **15,** optical textures were observed between crossed polarizers using an optical microscope. The focal conic texture was observed for complex **14**, while the texture observed for complex **15** was obscure**.** Thus, for complex **15**, its liquid crystal nature was verified using DSC. The defects are commonly associated due to the phase transition in liquid crystal. For both the complexes, the textures observed remain unchanged upon cooling down to ambient temperature.

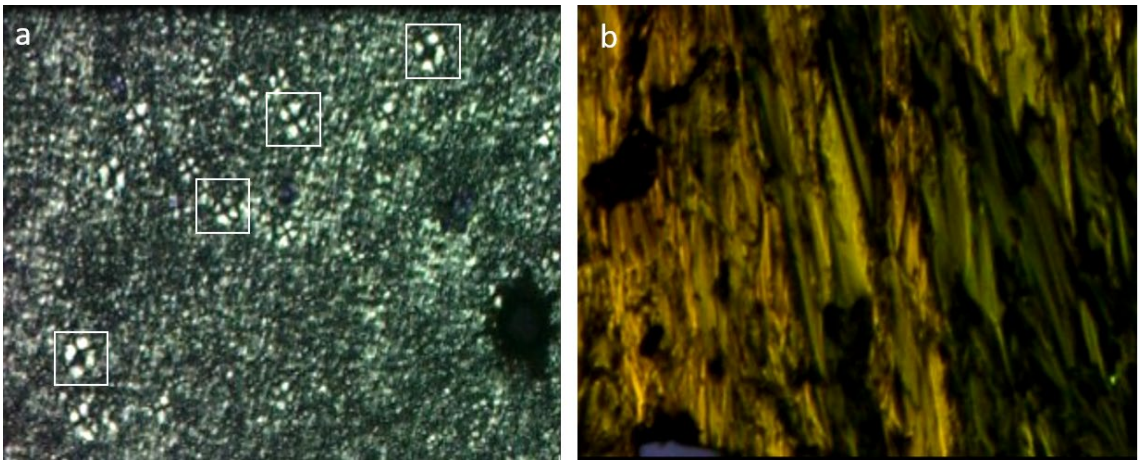

Figure 54. Texture observed between cross polarizer using optical microscopy. a. Complex **14,** and b. Complex **15.**

Likewise, DSC was utilized to confirm the liquid crystal properties of the complexes and to acquire the phase transition temperatures. In the DSC thermogram, complex **14 (Figure 55)** was observed melted into a liquid crystal phase at 31.3 °C and cleared at 112.0 °C. In the cooling cycle, peaks pertaining to clearing and melting temperature were observed, confirming the reversibility of the process. As discussed earlier, complex **15,** when analyzed by crossed polarizer using an optical microscope, melted into a mesomorphic phase although the texture was unclear. To support the result obtained by the polarized microscope, DSC thermogram was acquired. The complex **15,** showed two endothermic peaks, at 41.9 °C due to crystal to liquid crystal transition and completely melt into an isotropic liquid at 80.3°C (**Figure 56**). The reversibility of the process was confirmed during the cooling cycle. Thus, the liquid crystal behaviour of the complexes were established using polarigraphic optical microscope and differential scanning calorimetry.

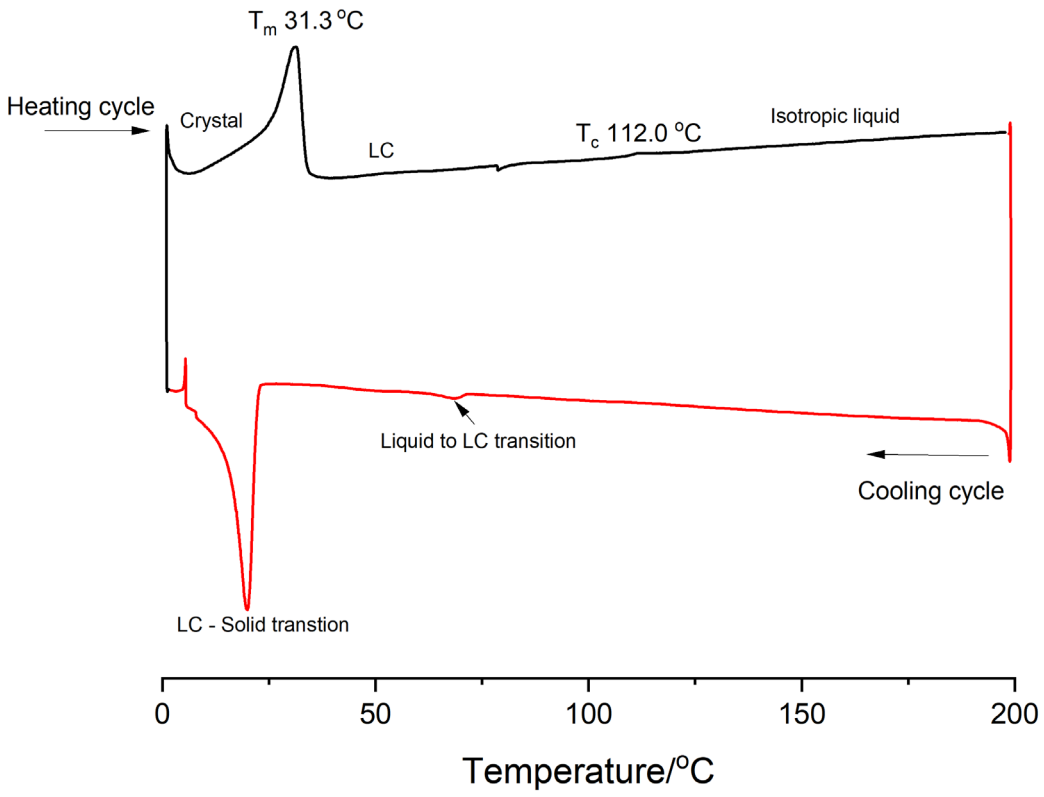

Figure 55. DSC thermograph of a complex **14** at the rate of 10 °C min^{-1}.

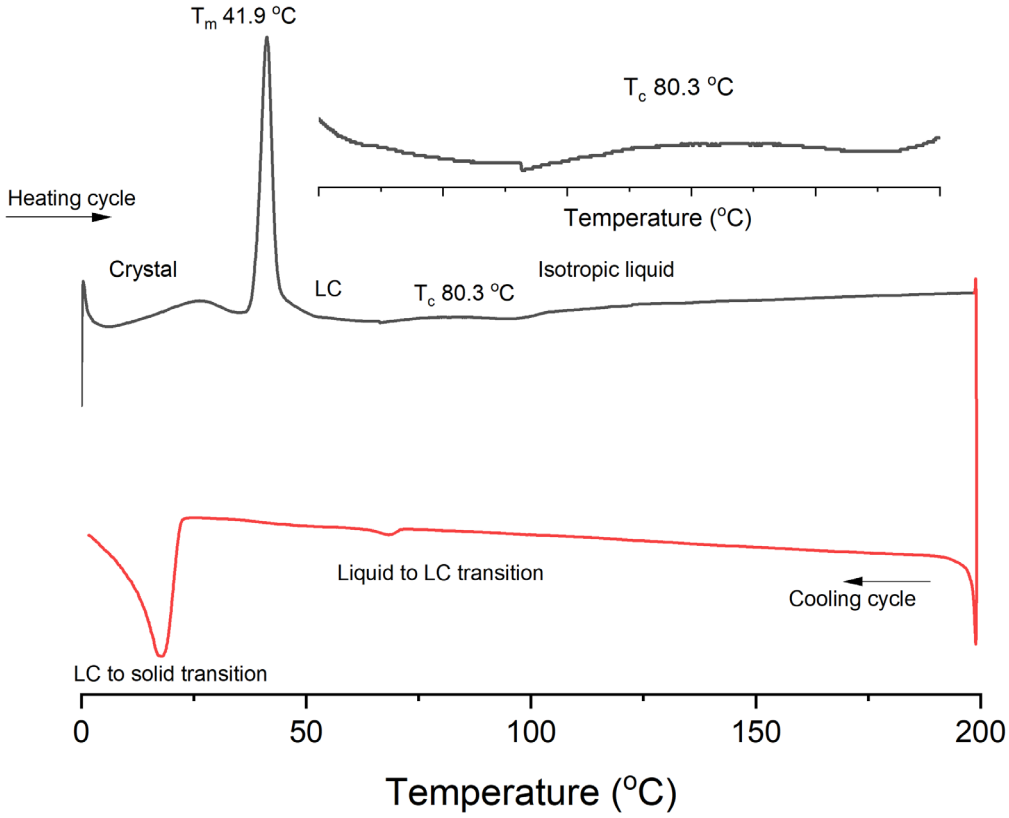

Figure 56. DSC thermograph of complex **15** at the rate of 10 °C min^{-1}.

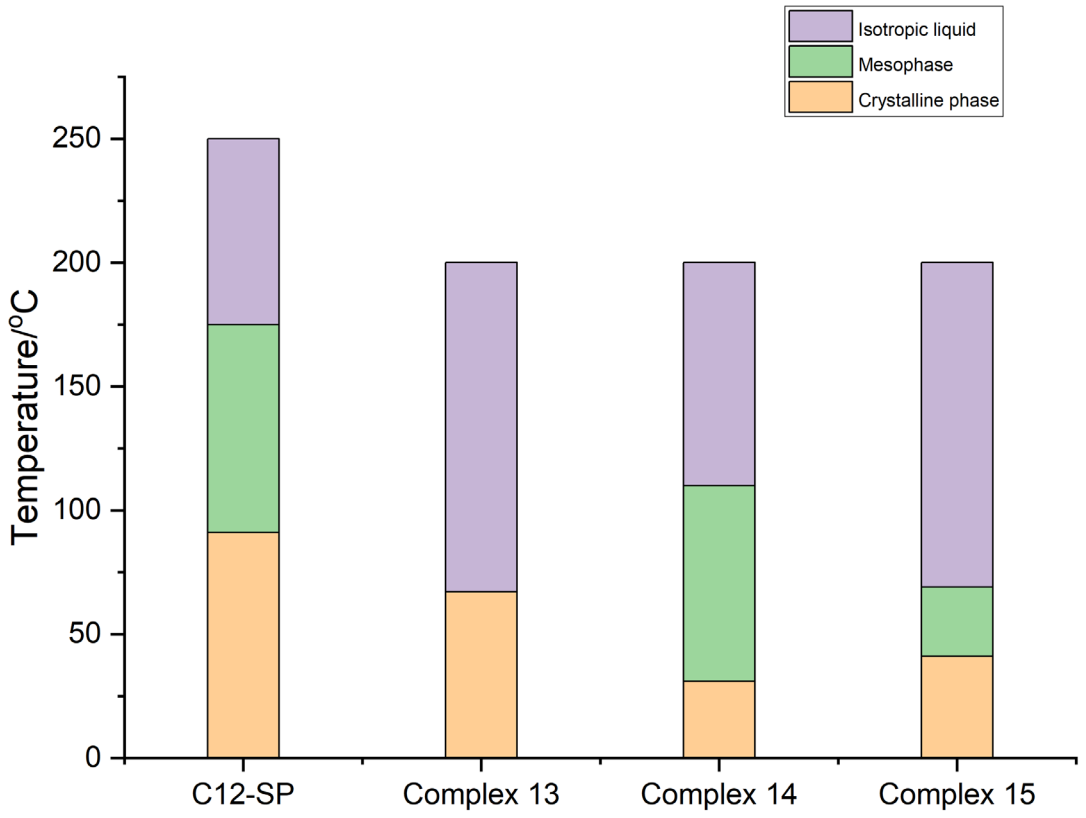

Figure 57. Melting Behavior of ligand (C12-SP = C_{12}-2,4-salphen) and the complexes.

The decrease in the melting temperature was observed in the complexes as compared to that of the ligand. However, the range in which the complex behaves as a liquid crystal was narrowed. When the metal ion is incorporated in the organic liquid crystal, it enhances the intermolecular coordination, thus providing an exciting opportunity to create supramolecular assemblies. In this study, Ni^{2+} and Cu^{2+} metal ions with symmetrical Schiff base ligand behave as mesogens. Interestingly, the complex of Co^{2+} did not show any mesomorphism. Thus, from this result, it can be inferred the rationale design of the ligand and the appropriate choice of metal center can be used to tune the mesomorphic characteristics of the liquid crystals.

CHAPTER 4

CONCLUSIONS

This dissertation presents a fundamental understating of the development of liquid crystal material based on the nature of the ligands and the geometry of the complexes. We have studied and found the effect of the design of the ligands is mostly responsible for the liquid crystal exhibiting various phases. The rod-like molecules are responsible for the nematic or smectic phase liquid crystals, while the disc-like molecules are responsible for the discotic columnar phase. A summary of the significant findings in each project is described below.

In the first project, we have successfully synthesized and fully characterized a series of new titanium(IV) salen complexes. The protocol used for the synthesis of the octahedral titanium(IV) salen complex was adjusted and optimized, resulting in a high yield of the desired product. The tetradentate H_2salen ligand coordinates to titanium(IV) metal center while surrounding the equatorial position via [*ONNO*] sites. The substituted phenol ligand occupied the axial position leading to the octahedral geometry of the complexes. The X-ray crystallographic structure of the complexes confirmed the geometry of the complexes. From our observation, the presence of the moisture affected the structure, and the stability of the mononuclear titanium(IV) salen complex, as well as the stability of the complexes, were greatly influenced by the substituent group present in the axial position. The bulkier substituent group in the phenol in axial position enhanced the formation of the mononuclear complex regardless of the atmospheric condition, while the less bulky counterpart hydrolyzed in the formation of the binuclear species. From the X-ray crystallographic study, the octahedral complex with the bulkier ligand on the axial position was mononuclear, while the less bulky group produced a binuclear complex bridged via an oxo-bridge. In both conditions, the complexes were

symmetrical as only a single set of the NMR peaks were observed. In conclusion, we have demonstrated an easier method for the preparation of the titanium(IV) salen complexes and the effect of substituents of the phenols on the structures of the complexes.

Secondly, Schiff base salen ligands $C_nH_{2n+1}O$-salen (where n = 16 and 18) derived from salicylaldimine have been synthesized. Ethylenediamine was used to bridge two groups along with various carbon side chains that were used to prepare the target ligands. Subsequently, we successfully prepared six coordinated octahedral titanium(IV) complex via a direct method where the ligand was mixed with the metal precursors in an appropriate solvent. The ligands and the complexes were well characterized, and liquid crystalline behaviors were analyzed. Upon thermal and optical analysis, only ligands exhibit the mesomorphic character. The ligands, when observed between the cross polarizer using an optical microscope, have a broken fan-like texture, which could be indicative of the lamellar or columnar mesophase. DSC technique was utilized to obtain the transition temperature of the liquid crystal. Unfortunately, the complexes prepared using these ligands do not have mesomorphic characteristics. Under POM, the complexes $[Ti(C_nH_{2n+1}O\text{-salen})Cl_2]$ (where n = 16 and 18), do not exhibit mesomorphic characteristics.

The complexes lacking liquid crystal properties may be due to various factors. The possible reasons that complexes lack the mesomorphic behavior may be due to the flexibility of the complexes, formation of various isomers, and its geometry.

The third project was in conjunction with the earlier projects, where a first row transition metal, i.e., Co^{2+}, Ni^{2+}, and $Cu^{2+,}$ were used to prepare the complexes along with the salicylamide Schiff bases salphen ligand. The ligands prepared were modified from its predecessor. The key factor based on the π-conjugated salphen framework was using a phenyl spacer, which enhances

the rigidity of the ligand favoring the intercolumnar stacking. The column arranges again into hexagonal form due to the self-assembly phenomenon generating a mesomorphism. The important aspect of modification was to alter the salicylideneimine units or in the aryl bridging group or altering the number of the carbon side chain. Here, the modification was done in two areas using the phenyl space as a bridging group and addition of the disubstituted aryl group, which tuned the mesophase properties of the ligands. Incorporating metal in a square planar geometry was another essential modification during the preparation of the metallomesogens.

In summary, we have prepared a new series of symmetric salphen-type ligand and their 1:1 metal complex with Co^{2+}, Ni^{2+}, and Cu^{2+} metal ions. The complexes have square planar geometry. The square planar geometry of the complexes enables the arrangement in a well organized hexagonal network of a column, in which the molecules were stacked with a high degree of intracolumnar order. The compounds exhibited interesting mesomorphic properties. It was true that the rod-like molecules were responsible for the nematic or smectic phases, while the disc-like molecules can generate the discotic phases. The complexes which were prepared using this ligand exhibited the discotic liquid crystal phase. The transition temperature for the complexes **14** and **15** were determined using the thermal technique. The complex **13,** doesnot have texture when observed between the cross polarizers using an optical microscope, in addition the transition temperature was unable to be determined using the DSC thermograms. These results show that the mesomorphic behavior of the ligands and the complexes can be obtained by modifying the nature of the ligands and the geometries of the complexes.

In the future, a series of the salphen ligands can be extending by using various carbon side chains. By extending this series, the nature of the liquid crystal and the phase they adapt can be investigated. In addition, the ligands can be utilized to prepare complexes, where nickel(II)

metal center can be chosen as the nickel complex are fairly easier to characterized using with NMR spectroscopy. Also, another important aspect of nickel(II) complex is due to its square planar geometry which is favorable situations for the complex to stack together to form a column and ultimately a column mesophase. For paramagnetic metal centers like cobalt(II) and copper(II), EPR spectroscopy can be utilized for their characterization. Beside this, the ligands and the complexes can be properly characterized by temperature-dependent XRD, and high resolution polarized optical microscopy will provide an insight into the nature of geometry formed by various mesophases.

REFERENCES

1. Foris, A. *Magn. Reson. Chem.* **2000,** *38* (12), 1044-1046.
2. Rossini, A. J.; Hung, I.; Schurko, R. W. *J. Phys. Chem. Lett.* **2010,** *1* (20), 2989-2998.
3. Lucier, B. E. G.; Huang, Y. *Annu. Rep. NMR Spectrosc.* **2016,** *88*, 1-78.
4. Koch, R.; Bruhn, T. *J. Mol. Model.* **2006,** *12* (5), 723-729.
5. Ballesteros, R.; Fajardo, M.; Sierra, I.; Force, C.; del Hierro, I. *Langmuir* **2009,** *25* (21), 12706-12712.
6. Sarsfield, M. J.; Ewart, S. W.; Tremblay, T. L.; Roszak, A. W.; Baird, M. C. *J. Chem. Soc., Dalton Trans.* **1997,** (18), 3097-3104.
7. Hao, N.; Sayer, B. G.; Denes, G.; Bickley, D. G.; Detellier, C.; McGlinchey, M. J. *J. Magn. Reson.* **1982,** *50* (1), 50-63.
8. Kidd, R. G.; Matthews, R. W.; Spinney, H. G. *J. Amer. Chem. Soc.* **1972,** *94* (19), 6686-9.
9. Ashbrook, S. E.; Sneddon, S. *J. Am. Chem. Soc.* **2014,** *136* (44), 15440-15456.
10. Cotton, F. A.; Wilkinson, G.; Murillo, C. A.; Bochmann, M.; Grimes, R., *Advanced inorganic chemistry*. Wiley New York: 1999; Vol. 5.
11. Koelle, U.; Koelle, P. *Angew. Chem., Int. Ed.* **2003,** *42* (37), 4540-4542.
12. Zolnhofer, E. M.; Wijeratne, G. B.; Jackson, T. A.; Fortier, S.; Heinemann, F. W.; Meyer, K.; Krzystek, J.; Ozarowski, A.; Mindiola, D. J.; Telser, J. *Inorg. Chem.* **2020,** *59* (9), 6187-6201.
13. Horrer, G.; Krahfuss, M. J.; Lubitz, K.; Krummenacher, I.; Braunschweig, H.; Radius, U. *Eur. J. Inorg. Chem.* **2020,** *2020* (3), 281-291.
14. Edema, J. J. H.; Duchateau, R.; Gambarotta, S.; Hynes, R.; Gabe, E. *Inorg. Chem.* **1991,** *30* (2), 154-6.
15. Araya, M. A.; Cotton, F. A.; Matonic, J. H.; Murillo, C. A. *Inorg. Chem.* **1995,** *34* (22), 5424-8.
16. Barroso, S.; Madeira, F.; Calhorda, M. J.; Ferreira, M. J.; Duarte, M. T.; Martins, A. M. *Inorg. Chem.* **2013,** *52* (16), 9427-9439.
17. McMurry, J. E. *Acc. Chem. Res.* **1974,** *7* (9), 281-6.
18. Knecht, E. *Ber. Dtsch. chem. Ges.* **1903,** *36*, 166-69.
19. Large, N. R.; Stubbs, F. J.; Hinshelwood, C. N. *J. Chem. Soc.* **1954**, 2736-43.
20. Tachikawa, H.; Ichikawa, T.; Yoshida, H. *J. Am. Chem. Soc.* **1990,** *112* (3), 977-82.
21. Hartmann, M.; Clark, T.; Van Eldik, R. *J. Phys. Chem. A* **1999,** *103* (48), 9899-9905.
22. LaPierre, E. A.; Patrick, B. O.; Manners, I. *J. Am. Chem. Soc.* **2019,** *141* (51), 20009-20015.
23. Wang, T.-H.; Navarrete-Lopez, A. M.; Li, S.; Dixon, D. A.; Gole, J. L. *J. Phys. Chem. A* **2010,** *114* (28), 7561-7570.
24. Gao, M.-Y.; Fang, W.-H.; Wen, T.; Zhang, L.; Zhang, J. *Cryst. Growth Des.* **2017,** *17* (7), 3592-3595.
25. Chen, H.; White, P. S.; Gagné, M. R. *Organometallics* **1998,** *17* (24), 5358-5366.
26. Tzubery, A.; Tshuva, E. Y. *Inorg. Chem.* **2011,** *50* (17), 7946-7948.
27. Miller, M.; Tshuva, E. Y. *Eur. J. Inorg. Chem.* **2014,** *2014* (9), 1485-1491.
28. Tzubery, A.; Melamed-Book, N.; Tshuva, E. Y. *Dalton Trans.* **2018,** *47* (11), 3669-3673.

29. Liu, X.-H.; Nurul Abser, M.; Bruce, D. W. *J. Organomet. Chem.* **1998,** *551* (1-2), 271-280.
30. Elliott, J. M.; Chipperfield, J. R.; Clark, S.; Sinn, E. *Inorg. Chem.* **2001,** *40* (25), 6390-6396.
31. Lai, C. K.; Chang, C.-h.; Tsai, C.-h. *J. Mater. Chem.* **1998,** *8* (3), 599-602.
32. Lawrence, M. A. W.; McMillen, C. D.; Gurung, R. K.; Celestine, M. J.; Arca, J. F.; Holder, A. A. *J. Chem. Crystallogr.* **2015,** *45* (8-9), 427-433.
33. Lawrence, M. A. W.; Celestine, M. J.; Artis, E. T.; Joseph, L. S.; Esquivel, D. L.; Ledbetter, A. J.; Cropek, D. M.; Jarrett, W. L.; Bayse, C. A.; Brewer, M. I.; Holder, A. A. *Dalton Trans.* **2016,** *45* (25), 10326-10342.
34. Liao, C.-M.; Hsu, C.-C.; Wang, F.-S.; Wayland, B. B.; Peng, C.-H. *Polym. Chem.* **2013,** *4* (10), 3098-3104.
35. Bakac, A.; Brynildson, M. E.; Espenson, J. H. *Inorg. Chem.* **1986,** *25* (23), 4108-4114.
36. Dori, Z.; Gray, H. B. *Inorg. Chem.* **1968,** *7* (5), 889-892.
37. Mondal, A. K.; Mondal, A.; Konar, S. *Magnetochemistry* **2019,** *5* (1), 12.
38. Massoud, S. S.; Fischer, R. C.; Mautner, F. A.; Parfait, M. M.; Herchel, R.; Travnicek, Z. *Inorg. Chim. Acta* **2018,** *471*, 630-639.
39. Osborne, S. J.; Wellens, S.; Ward, C.; Felton, S.; Bowman, R. M.; Binnemans, K.; Swadzba-Kwasny, M.; Gunaratne, H. Q. N.; Nockemann, P. *Dalton Trans.* **2015,** *44* (25), 11286-11289.
40. Yi, G.; Cui, H.; Zhang, C.; Zhao, W.; Chen, L.; Zhang, Y.-Q.; Chen, X.-T.; Song, Y.; Yuan, A. *Dalton Trans.* **2020,** *49* (7), 2063-2067.
41. Smith, A. L.; Clapp, L. A.; Hardcastle, K. I.; Soper, J. D. *Polyhedron* **2010,** *29* (1), 164-169.
42. Pogany, L.; Moncol, J.; Gal, M.; Salitros, I.; Boca, R. *Inorg. Chim. Acta* **2017,** *462*, 23-29.
43. Hicks, J.; Jones, C. *Organometallics* **2015,** *34* (11), 2118-2121.
44. Yang, X.-J.; Fan, X.; Zhao, Y.; Wang, X.; Liu, B.; Su, J.-H.; Dong, Q.; Xu, M.; Wu, B. *Organometallics* **2013,** *32* (23), 6945-6949.
45. Dugan, T. R.; Sun, X.-R.; Rybak-Akimova, E. V.; Olatunji-Ojo, O.; Cundari, T. R.; Holland, P. L. *J. Am. Chem. Soc.* **2011,** *133* (32), 12418-12421.
46. Cropek, D. M.; Metz, A.; Müller, A. M.; Gray, H. B.; Horne, T.; Horton, D. C.; Poluektov, O.; Tiede, D. M.; Weber, R. T.; Jarrett, W. L.; Philips, J. D.; Holder, A. A. *Dalton Trans.* **2012,** *41* (42), 13060-13073.
47. Constable, E. C.; Housecroft, C. E. *Chem. Soc. Rev.* **2013,** *42* (4), 1429-1439.
48. Chakrabarty, R.; Das, B. K. *J. Mol. Catal. A: Chem.* **2004,** *223* (1-2), 39-44.
49. Chakrabarty, R.; Das, B. K.; Clark, J. H. *Green Chem.* **2007,** *9* (8), 845-848.
50. Chakrabarty, R.; Kalita, D.; Das, B. K. *Polyhedron* **2007,** *26* (6), 1239-1244.
51. Chakrabarty, R.; Sarmah, P.; Saha, B.; Chakravorty, S.; Das, B. K. *Inorg. Chem.* **2009,** *48* (14), 6371-6379.
52. Furenlid, L. R.; Renner, M. W.; Szalda, D. J.; Fujita, E. *J. Am. Chem. Soc.* **1991,** *113* (3), 883-92.
53. James, T. L.; Cai, L.; Muetterties, M. C.; Holm, R. H. *Inorg. Chem.* **1996,** *35* (14), 4148-4161.
54. Jarchow, O.; Schulz, H.; Nast, R. *Angew. Chem., Int. Ed.* **1970,** *9* (1), 71.

55. Broring, M.; Prikhodovski, S.; Brandt, C. D. *Inorg. Chim. Acta* **2004,** *357* (6), 1733-1738.
56. Cotton, F. A.; Goodgame, D. M. I. *J. Am. Chem. Soc.* **1960,** *82*, 5771-4.
57. Zhang, C.-P.; Wang, H.; Klein, A.; Biewer, C.; Stirnat, K.; Yamaguchi, Y.; Xu, L.; Gomez-Benitez, V.; Vicic, D. A. *J. Am. Chem. Soc.* **2013,** *135* (22), 8141-8144.
58. Corker, J. M.; Evans, J.; Levason, W.; Spicer, M. D.; Andrews, P. *Inorg. Chem.* **1991,** *30* (2), 331-4.
59. Lin, C.-Y.; Power, P. P. *Chem. Soc. Rev.* **2017,** *46* (17), 5347-5399.
60. Tschugaew, L. *Ber. Dtsch. chem. Ges.* **1905,** *38*, 2520-22.
61. Bridgeman, A. J. *Dalton Trans.* **2008,** (15), 1989-1992.
62. Chakraborty, S.; Prasad, S. K.; Rao, D. S. S.; Bhattacharjee, C. R. *Liq. Cryst.* **2019,** *46* (6), 872-883.
63. Jacques, P.-A.; Artero, V.; Pecaut, J.; Fontecave, M. *Proc. Natl. Acad. Sci. U. S. A.* **2009,** *106* (49), 20627-20632.
64. Collins, T. J.; Nichols, T. R.; Uffelman, E. S. *J. Am. Chem. Soc.* **1991,** *113* (12), 4708-9.
65. Zheng, B.; Tang, F.; Luo, J.; Schultz, J. W.; Rath, N. P.; Mirica, L. M. *J. Am. Chem. Soc.* **2014,** *136* (17), 6499-6504.
66. Waterman, R.; Hillhouse, G. L. *J. Am. Chem. Soc.* **2003,** *125* (44), 13350-13351.
67. Wiese, S.; McAfee, J. L.; Pahls, D. R.; McMullin, C. L.; Cundari, T. R.; Warren, T. H. *J. Am. Chem. Soc.* **2012,** *134* (24), 10114-10121.
68. Iluc, V. M.; Miller, A. J. M.; Anderson, J. S.; Monreal, M. J.; Mehn, M. P.; Hillhouse, G. L. *J. Am. Chem. Soc.* **2011,** *133* (33), 13055-13063.
69. Balamurugan, R.; Palaniandavar, M.; Gopalan, R. S. *Inorg. Chem.* **2001,** *40* (10), 2246-2255.
70. Shimizu, I.; Morimoto, Y.; Faltermeier, D.; Kerscher, M.; Paria, S.; Abe, T.; Sugimoto, H.; Fujieda, N.; Asano, K.; Suzuki, T.; Comba, P.; Itoh, S. *Inorg. Chem.* **2017,** *56* (16), 9634-9645.
71. Barbier, J. P.; El Biyyadh, A.; Kappenstein, C.; Mabiala, N. D.; Hugel, R. P. *Inorg. Chem.* **1985,** *24* (22), 3615-20.
72. Crutchley, R. J.; Hynes, R.; Gabe, E. J. *Inorg. Chem.* **1990,** *29* (24), 4921-4928.
73. Sharma, M.; Ganeshpandian, M.; Majumder, M.; Tamilarasan, A.; Sharma, M.; Mukhopadhyay, R.; Islam, N. S.; Palaniandavar, M. *Dalton Trans.* **2020,** *49* (24), 8282-8297.
74. DiMucci, I. M.; Lukens, J. T.; Chatterjee, S.; Carsch, K. M.; Titus, C. J.; Lee, S. J.; Nordlund, D.; Betley, T. A.; MacMillan, S. N.; Lancaster, K. M. *J. Am. Chem. Soc.* **2019,** *141* (46), 18508-18520.
75. Rosen, B. M.; Jiang, X.; Wilson, C. J.; Nguyen, N. H.; Monteiro, M. J.; Percec, V. *J. Polym. Sci., Part A: Polym. Chem.* **2009,** *47* (21), 5606-5628.
76. Cheng, B.; Yi, H.; He, C.; Liu, C.; Lei, A. *Organometallics* **2015,** *34* (1), 206-211.
77. Rostovtsev, V. V.; Green, L. G.; Fokin, V. V.; Sharpless, K. B. *Angew. Chem., Int. Ed.* **2002,** *41* (14), 2596-2599.
78. Wang, C.; Wang, D.; Yu, S.; Cornilleau, T.; Ruiz, J.; Salmon, L.; Astruc, D. *ACS Catal.* **2016**, Ahead of Print.
79. Demko, Z. P.; Sharpless, K. B. *Angew. Chem., Int. Ed.* **2002,** *41* (12), 2113-2116.
80. Levi, G.; Biasin, E.; Dohn, A. O.; Jónsson, H. *Phys. Chem. Chem. Phys.* **2020,** *22* (2), 748-757.

81. Green, K.-A.; Hoover, J. M. *ACS Catal.* **2020,** *10* (3), 1769-1782.
82. Magini, M. *Inorg. Chem.* **1982,** *21* (4), 1535-8.
83. Leite, S. M. G.; Lima, L. M. P.; Gama, S.; Mendes, F.; Orio, M.; Bento, I.; Paulo, A.; Delgado, R.; Iranzo, O. *Inorg. Chem.* **2016,** *55* (22), 11801-11814.
84. Hurtado, M.; Sankpal, U. T.; Chhabra, J.; Brown, D. T.; Maram, R.; Patel, R.; Gurung, R. K.; Simecka, J.; Holder, A. A.; Basha, R. *Invest. New Drugs* **2018**, Ahead of Print.
85. Hurtado, M.; Sankpal, U. T.; Kaba, A.; Mahammad, S.; Chhabra, J.; Brown, D. T.; Gurung, R. K.; Holder, A. A.; Vishwanatha, J. K.; Basha, R. *Cell. Physiol. Biochem.* **2018,** *51* (4), 1894-1907.
86. Hussain, A.; AlAjmi, M. F.; Rehman, M. T.; Amir, S.; Husain, F. M.; Alsalme, A.; Siddiqui, M. A.; AlKhedhairy, A. A.; Khan, R. A. *Sci. Rep.* **2019,** *9* (1), 1-17.
87. Filomeni, G.; Cerchiaro, G.; Da Costa Ferreira, A. M.; De Martino, A.; Pedersen, J. Z.; Rotilio, G.; Ciriolo, M. R. *J. Biol. Chem.* **2007,** *282* (16), 12010-21.
88. Schiff, H. *Ann. Chim.(Paris)* **1864,** *131*, 118.
89. Tidwell, T. T. *Angew. Chem. Int. Ed.* **2008,** *47* (6), 1016-1020.
90. Al Zoubi, W.; Al-Hamdani, A. A. S.; Kaseem, M. *Appl. Organomet. Chem.* **2016**.
91. Sinha, D.; Tiwari, A. K.; Singh, S.; Shukla, G.; Mishra, P.; Chandra, H.; Mishra, A. K. *Eur. J. Inorg. Chem.* **2008,** *43* (1), 160-165.
92. Basa, P. N.; Bhowmick, A.; Schulz, M. M.; Sykes, A. G. *J. Org. Chem.* **2011,** *76* (19), 7866-7871.
93. Yang, J.; Shi, R.; Zhou, P.; Qiu, Q.; Li, H. *J. Mol. Struct.* **2016,** *1106*, 242-258.
94. HoLM, R.; Everett Jr, G. *Prog. Inorg. Chem.* **2009,** *7*, 83.
95. Balsells, J.; Carroll, P. J.; Walsh, P. J. *Inorg. Chem.* **2001,** *40* (22), 5568-5574.
96. Verma, P.; Erimban, S.; Kumar, N.; Daschakraborty, S.; Nayak, A.; Kumar, S. *J. Phys. Chem. C* **2019,** *123* (27), 16681-16689.
97. Kumar, S.; Dhar, D. N.; Saxena, P. *J Sci Ind Res* **2009,** *68* (3), 181-187.
98. Kigoshi, S.; Kanazawa, A.; Kanaoka, S.; Aoshima, S. *J. Polym. Sci., Part A: Polym. Chem.* **2019,** *57* (9), 989-996.
99. Shah, K.; Chhabra, S.; Shrivastava, S. K.; Mishra, P. *Med. Chem. Res.* **2013,** *22* (11), 5077-5104.
100. Ansari, K. I.; Kasiri, S.; Grant, J. D.; Mandal, S. S. *J. Biomol. Screening* **2011,** *16* (1), 26-35.
101. Binnemans, K.; Lodewyckx, K.; Donnio, B.; Guillon, D. *Chem. - Eur. J.* **2002,** *8* (5), 1101-1105.
102. Chico, R.; Dominguez, C.; Donnio, B.; Coco, S.; Espinet, P. *Dalton Trans.* **2011,** *40* (22), 5977-5983.
103. Verquin, G.; Fontaine, G.; Bria, M.; Zhilinskaya, E.; Abi-Aad, E.; Aboukaïs, A.; Baldeyrou, B.; Bailly, C.; Bernier, J.-L. *J. Bio. Inorg. Chem.* **2004,** *9* (3), 345-353.
104. Peng, Y.; Zhong, H.; Chen, Z.-F.; Liu, Y.-C.; Zhang, G.-H.; Qin, Q.-P.; Liang, H. *Chem. Pharm. Bull.* **2014,** *62* (3), 221-228.
105. Terenzi, A.; Loetsch, D.; van Schoonhoven, S.; Roller, A.; Kowol, C. R.; Berger, W.; Keppler, B. K.; Barone, G. *Dalton Trans.* **2016,** *45* (18), 7758-7767.
106. Anderson, D. J.; Eisenberg, R. *Inorg. Chem.* **1994,** *33* (24), 5378-9.
107. Mandal, S.; Poria, D. K.; Seth, D. K.; Ray, P. S.; Gupta, P. *Polyhedron* **2014,** *73*, 12-21.

108. Pramanik, H. A. R.; Chanda, S.; Bhattacharjee, C. R.; Paul, P. C.; Mondal, P.; Prasad, S. K.; Shankar Rao, D. S. *Liq. Cryst.* **2016,** *43* (11), 1606-1615.
109. Würtenberger, I.; Follia, V.; Lerch, F.; Cwikla, C.; Fahrner, N.; Kalchschmidt, C.; Flögel, B.; Kircher, B.; Gust, R. *J. Med. Chem.* **2014,** *58* (2), 588-597.
110. Tzubery, A.; Tshuva, E. Y. *Inorg. Chem.* **2011,** *51* (3), 1796-1804.
111. Tzubery, A.; Tshuva, E. Y. *Eur. J. Inorg. Chem.* **2017,** *2017* (12), 1695-1705.
112. Barroso, S.; Coelho, A. M.; Gomez-Ruiz, S.; Calhorda, M. J.; Zizak, Z.; Kaludjerovic, G. N.; Martins, A. M. *Dalton Trans.* **2014,** *43* (46), 17422-17433.
113. Hanif, M.; Hartinger, C. G. *Future Med. Chem.* **2018,** *10* (6), 615-617.
114. Tshuva, E. Y.; Miller, M. *Met. Ions Life Sci.* **2018,** *18* (Metallo-Drugs: Development and Action of Anticancer Agents), 219-250.
115. Meker, S.; Manna, C. M.; Peri, D.; Tshuva, E. Y. *Dalton Trans.* **2011,** *40* (38), 9802-9809.
116. Meker, S.; Braitbard, O.; Margulis-Goshen, K.; Magdassi, S.; Hochman, J.; Tshuva, E. Y. *Molecules* **2015,** *20* (10), 18526-18538.
117. Nielson, A. J.; Waters, J. M. *Polyhedron* **2010,** *29* (7), 1715-1726.
118. Gupta, K.; Sutar, A. K. *Coord. Chem. Rev.* **2008,** *252* (12), 1420-1450.
119. Kleij, A. W. *Chem. Eur. J.* **2008,** *14* (34), 10520-10529.
120. Li, Z.; Fernández, M.; Jacobsen, E. N. *Org. Lett.* **1999,** *1* (10), 1611-1613.
121. Chen, Z.; Yakura, K.; Matsunaga, S.; Shibasaki, M. *Org. Lett.* **2008,** *10* (15), 3239-3242.
122. Qin, W.; Long, S.; Panunzio, M.; Biondi, S. *Molecules* **2013,** *18* (10), 12264-12289.
123. Giroud-Godquin, A. M.; Maitlis, P. M. *Angew. Chem. Int. Ed.* **1991,** *30* (4), 375-402.
124. Kato, T.; Uchida, J.; Ichikawa, T.; Sakamoto, T. *Angew. Chem., Int. Ed.* **2018,** *57* (16), 4355-4371.
125. Goossens, K.; Lava, K.; Bielawski, C. W.; Binnemans, K. *Chem. Rev. (Washington, DC, U. S.)* **2016,** *116* (8), 4643-4807.
126. Bruce, D. W. *Acc. Chem. Res.* **2000,** *33* (12), 831-840.
127. Reinitzer, F. *Liq. Cryst.* **1989,** *5* (1), 7-18.
128. Donnio, B.; Bruce, D. W., Metallomesogens. In *Liq. Cryst.*, Springer: 1999; pp 193-247.
129. Hogan, B. T.; Kovalska, E.; Craciun, M. F.; Baldycheva, A. *J. Mater. Chem. C* **2017,** *5* (43), 11185-11195.
130. Date, R. W.; Iglesias, E. F.; Rowe, K. E.; Elliott, J. M.; Bruce, D. W. *Dalton Trans.* **2003,** (10), 1914-1931.
131. Hudson, S. A.; Maitlis, P. M. *Chem. Rev.* **1993,** *93* (3), 861-885.
132. Woltman, S. J.; Jay, G. D.; Crawford, G. P. *Nat. Mater.* **2007,** *6* (12), 929-938.
133. Torroba, J.; Bruce, D.; Reedijk, J.; Poeppelmeier, K., Elsevier Ltd: Amsterdam: 2013; Vol. 8, pp 837-917.
134. Giroud-Godquin, A. M. In *Metal-containing liquid crystals*, Wiley-VCH Verlag GmbH: 1998; pp 901-932.
135. Blunk, D.; Bierganns, P.; Bongartz, N.; Tessendorf, R.; Stubenrauch, C. *New J. Chem.* **2006,** *30* (12), 1705-1717.
136. Donnio, B. *Curr. Opin. Colloid Interface Sci.* **2002,** *7* (5,6), 371-394.
137. Sonin, A. S. *J. Mater. Chem.* **1998,** *8* (12), 2557-2574.
138. Drug delivery systems. In *Strategies to Modify the Drug Release from Pharmaceutical Systems*, Bruschi, M. L., Ed. Woodhead Publishing: 2015; pp 87-194.

139. Donnio, B. *Inorg. Chim. Acta* **2014,** *409* (PB), 53-67.
140. Binnemans, K. In *Physical properties of metallomesogens*, John Wiley & Sons Ltd.: 2010; pp 61-141.
141. Goodby, J. W.; Collings, P. J.; Kato, T.; Tschierske, C.; Gleeson, H. F.; Raynes, P.; Editors, *Handbook of Liquid Crystals, Volume 1: Fundamentals of Liquid Crystals, 2nd Edition*. Wiley-VCH Verlag GmbH & Co. KGaA: 2014; p 490 pp.
142. Chiang, I. H.; Chuang, W.-T.; Lu, C.-L.; Lee, M.-T.; Lin, H.-C. *Chem. Mater.* **2015,** *27* (13), 4525-4537.
143. Vorlander, D.; Apel, A.; Galka, W. *Ber. Dtsch. Chem. Ges. B* **1932,** *65B*, 1101-9.
144. Srinivasan, M. V.; Kannan, P.; Roy, A. *New J. Chem.* **2013,** *37* (5), 1584-1590.
145. Trisovic, N.; Antanasijevic, J.; Toth-Katona, T.; Kohout, M.; Salamonczyk, M.; Sprunt, S.; Jakli, A.; Fodor-Csorba, K. *RSC Adv.* **2015,** *5* (80), 64886-64891.
146. Zhang, C.; Diorio, N.; Lavrentovich, O. D.; Jakli, A. *Nat. Commun.* **2014,** *5*, 4302/1-4302/6.
147. Cavero, E.; Lydon, D. P.; Uriel, S.; de la Fuente, M. R.; Serrano, J. L.; Gimenez, R. *Angew. Chem., Int. Ed.* **2007,** *46* (27), 5175-5177.
148. Laschat, S.; Baro, A.; Steinke, N.; Giesselmann, F.; Haegele, C.; Scalia, G.; Judele, R.; Kapatsina, E.; Sauer, S.; Schreivogel, A.; Tosoni, M. *Angew. Chem., Int. Ed.* **2007,** *46* (26), 4832-4887.
149. Chandrasekhar, S.; Sadashiva, B. K.; Suresh, K. A. *Pramana* **1977,** *9* (5), 471-80.
150. Chandrasekhar, S.; Madhusudana, N. V. *Annu. Rev. Mater. Sci.* **1980,** *10*, 133-55.
151. Bushby, R. J.; Lozman, O. R. *Curr. Opin. Colloid Interface Sci.* **2002,** *7* (5,6), 343-354.
152. Wöhrle, T.; Wurzbach, I.; Kirres, J.; Kostidou, A.; Kapernaum, N.; Litterscheidt, J.; Haenle, J. C.; Staffeld, P.; Baro, A.; Giesselmann, F.; Laschat, S. *Chem. Rev.* **2016,** *116* (3), 1139-1241.
153. Chandrasekhar, S.; Ranganath, G. S. *Rep. Prog. Phys.* **1990,** *53* (1), 57-84.
154. Chico, R.; de Domingo, E.; Dominguez, C.; Donnio, B.; Heinrich, B.; Termine, R.; Golemme, A.; Coco, S.; Espinet, P. *Chem. Mater.* **2017,** *29* (17), 7587-7595.
155. Chico, R.; Dominguez, C.; Donnio, B.; Heinrich, B.; Coco, S.; Espinet, P. *Cryst. Growth Des.* **2016,** *16* (12), 6984-6991.
156. Tritto, E.; Chico, R.; Sanz-Enguita, G.; Folcia, C. L.; Ortega, J.; Coco, S.; Espinet, P. *Inorg. Chem.* **2014,** *53* (7), 3449-3455.
157. Zhao, K.-Q.; Bai, X.-Y.; Xiao, B.; Gao, Y.; Hu, P.; Wang, B.-Q.; Zeng, Q.-D.; Wang, C.; Heinrich, B.; Donnio, B. *J. Mater. Chem.* **2015,** *3* (44), 11735-11746.
158. Cuerva, C.; Campo, J. A.; Cano, M.; Schmidt, R. *J. Mater. Chem. C* **2019,** *7* (33), 10318-10330.
159. Tan, S.; Wang, C.; Wu, Y. *J. Mater. Chem. A* **2013,** *1* (4), 1022-1025.
160. Goossens, K.; Lava, K.; Bielawski, C. W.; Binnemans, K. *Chem. Rev.* **2016,** *116* (8), 4643-4807.
161. Ovejero, P.; Asensio, E.; Heras, J. V.; Campo, J. A.; Cano, M.; Torres, M. R.; Nunez, C.; Lodeiro, C. *Dalton Trans.* **2013,** *42* (6), 2107-2120.
162. Serrette, A.; Carroll, P. J.; Swager, T. M. *J. Am. Chem. Soc.* **1992,** *114* (5), 1887-9.
163. El-ghayoury, A.; Douce, L.; Skoulios, A.; Ziessel, R. *Angew. Chem., Int. Ed.* **1998,** *37* (16), 2205-2208.
164. Zou, G.; Zhao, L.; Zeng, L.; Luo, K.; Ni, H.; Wang, H.; Li, Q.; Yu, W.; Li, X. *Inorg. Chem.* **2019,** *58* (1), 861-869.

165. Marcos, M., Design and Synthesis of Low Molecular Weight Metallomesogens. In *Metallomesogens*, Wiley-VCH Verlag GmbH: 2007; pp 235-299.
166. Gimenez, R.; Lydon, D.; Serrano, J. *Curr. Opin. Solid State Mater. Sci.* **2002,** *6* (6), 527-535.
167. Liu, T.-M.; Lin, K.-T.; Li, F.-J.; Lee, G.-H.; Chen, M.-C.; Lai, C. K. *Tetrahedron* **2015,** *71* (45), 8649-8660.
168. Akiyoshi, R.; Hirota, Y.; Kosumi, D.; Tsutsumi, M.; Nakamura, M.; Lindoy, L. F.; Hayami, S. *Chem. Sci.* **2019,** *10* (22), 5843-5848.
169. Guo, L.-X.; Xing, Y.-B.; Wang, M.; Sun, Y.; Zhang, X.-Q.; Lin, B.-P.; Yang, H. *J. Mater. Chem. C* **2019,** *7* (16), 4828-4837.
170. Ilis, M.; Micutz, M.; Circu, V. *J. Organomet. Chem.* **2017,** *836-837*, 81-89.
171. Kong, F. K.-W.; Tang, M.-C.; Wong, Y.-C.; Chan, M.-Y.; Yam, V. W.-W. *J. Am. Chem. Soc.* **2016,** *138* (19), 6281-6291.
172. Kim, D.-Y.; Kang, D.-G.; Lee, M.-H.; Kim, J.-S.; Lee, C.-R.; Jeong, K.-U. *Chem. Commun.* **2016,** *52* (87), 12821-12824.
173. Wu, X.; Xie, G.; Cabry, C. P.; Xu, X.; Cowling, S. J.; Bruce, D. W.; Zhu, W.; Baranoff, E.; Wang, Y. *J. Mater. Chem. C* **2018,** *6*, 3298.
174. Pana, A.; Chiriac, F. L.; Secu, M.; Pasuk, I.; Ferbinteanu, M.; Micutz, M.; Circu, V. *Dalton Trans.* **2015,** *44* (32), 14196-14199.
175. Dobrun, L. A.; Kovshik, A. P.; Ryumtsev, E. I.; Galyametdinov, Y. G.; Knyazev, A. A. *Phys. Solid State* **2017,** *59* (4), 815-819.
176. Piguet, C.; Buenzli, J.-C. G.; Donnio, B.; Guillon, D. *Chem. Commun. (Cambridge, U. K.)* **2006,** (36), 3755-3768.
177. Liao, C. T.; Chen, H. H.; Hsu, H. F.; Poloek, A.; Yeh, H. H.; Chi, Y.; Wang, K. W.; Lai, C. H.; Lee, G. H.; Shih, C. W. *Chemistry-A European Journal* **2011,** *17* (2), 546-556.
178. Mironov, V. S.; Galyametdinov, Y. G.; Ceulemans, A.; Gorller-Walrand, C.; Binnemans, K. *J. Chem. Phys.* **2002,** *116* (11), 4673-4685.
179. Jacobsen, E. N.; Zhang, W.; Guler, M. L. *J. Am. Chem. Soc.* **1991,** *113* (17), 6703-6704.
180. Chakraborty, S.; Mondal, P.; Prasad, S. K.; Rao, D. S. S.; Bhattacharjee, C. R. *Eur. J. Inorg. Chem.* **2016,** *2016* (28), 4604-4614.
181. Cozzi, P. G. *Chem. Soc. Rev.* **2004,** *33* (7), 410-421.
182. Battistini, P.; Carcelli, M.; Dalcanale, E.; Pelizzi, C.; Pelizzi, G.; Righini, L. *Mol. Cryst. Liq. Cryst. Sci. Technol., Sect. A* **1998,** *309*, 167-188.
183. Borbone, F.; Grizzuti, N.; Pasquino, R.; Ricciotti, L.; Roviello, A.; Roviello, G. *Liq. Cryst.* **2015,** *42* (7), 1003-1012.
184. Debnath, S.; Srour, H. F.; Donnio, B.; Fourmigue, M.; Camerel, F. *RSC Adv.* **2012,** *2* (10), 4453-4462.
185. Greenbank, W. A.; McGrath, K. M. *J. Photochem. Photobiol., A* **2014,** *279*, 52-58.
186. Lee, Y. H.; Harrowfield, J. M.; Shin, J. W.; Won, M. S.; Rukmini, E.; Hayami, S.; Min, K. S.; Kim, Y. *Int. J. Mol. Sci.* **2013,** *14* (10), 20729-20743, 15 pp.
187. Lin, C.-H.; Kao, H.-C.; Sung, W.-T.; Cheng, Y.-W.; Wang, W.-J. *J. Chin. Chem. Soc. (Weinheim, Ger.)* **2015,** *62* (1), 26-32.
188. Giroud, A. M.; Mueller-Westerhoff, U. T. *Mol. Cryst. Liq. Cryst.* **1977,** *41* (1), 11-13.
189. Horie, H.; Takagi, A.; Hasebe, H.; Ozawa, T.; Ohta, K. *J. Mater. Chem.* **2001,** *11* (4), 1063-1071.

190. Chou, C.-T.; Pai, Y.-F.; Lin, C.-C.; Misra, T. K.; Liu, C.-Y. *J. Chromatogr. A* **2004,** *1043* (2), 255-263.
191. Ohta, K.; Hasebe, H.; Moriya, M.; Fujimoto, T.; Yamamoto, I. *Mol. Cryst. Liq. Cryst.* **1991,** *208*, 33-41.
192. Wu, I. T.; Chaing, P.-Y.; Chang, W.-J.; Sheu, H.-S.; Lee, G.-H.; Lai, C. K. *Tetrahedron* **2011,** *67* (38), 7358-7369.
193. Senthilkumar, N.; Raghavan, A.; Narasimhaswamy, T.; Kim, I.-J. *Inorg. Chim. Acta* **2013,** *397*, 129-139.
194. Davidson, M. Microscopy The Source for microscopy eduation. https://www.microscopyu.com/techniques/polarized-light/polarized-light-microscopy.
195. Andrienko, D. *J. Mol. Liq.* **2018,** *267*, 520-541.
196. Torralba, M. C.; Cano, M.; Campo, J. A.; Heras, J. V.; Pinilla, E.; Torres, M. R. *J. Organomet. Chem.* **2006,** *691* (4), 765-778.
197. Cuerva, C.; Campo, J. A.; Cano, M.; Schmidt, R. *Dalton Trans* **2016,** *46* (1), 96-105.
198. Sindhu, R.; Binod, P.; Pandey, A. In *Microbial poly-3-hydroxybutyrate and related copolymers*, Elsevier B.V.: 2015; pp 575-605.
199. Nikolić, V.; Ilić-Stojanović, S.; Petrović, S.; Tačić, A.; Nikolić, L., Administration Routes for Nano Drugs and Characterization of Nano Drug Loading. In *Characterization and Biology of Nanomaterials for Drug Delivery*, Mohapatra, S. S.; Ranjan, S.; Dasgupta, N.; Mishra, R. K.; Thomas, S., Eds. Elsevier: 2019; pp 587-625.
200. Bruce, D. W.; O'Hare, D.; Walton, R. I.; Editors, *Molecular Materials*. John Wiley & Sons Ltd.: 2010; p 360 pp.
201. Serrano, J. L.; Editor, *Metallomesogens: Synthesis, Properties, and Applications*. VCH: 1996; p 498 pp.
202. Pelzl, G.; Hauser, A. *Phase Transitions* **1991,** *37* (1), 33-62.
203. Goodby, J. W.; Collings, P. J.; Kato, T.; Tschierske, C.; Gleeson, H. F.; Raynes, P.; Editors, *Handbook of Liquid Crystals, Volume 2: Smectic and Columnar Liquid Crystals, 2nd Edition*. Wiley-VCH Verlag GmbH & Co. KGaA: 2014; p 779 pp.
204. Kim, M. J.; Park, J. H.; Yamamoto, J.; Kim, Y. S.; Scalia, G. *Phys. Status Solidi RRL* **2016,** *10* (5), 397-403.
205. Cuerva, C.; Campo, J. A.; Cano, M.; Schmidt, R.; Lodeiro, C. *J. Mater. Chem. C* **2018,** *6* (36), 9723-9733.
206. Conejo-Rodriguez, V.; Cuerva, C.; Schmidt, R.; Bardaji, M.; Espinet, P. *J. Mater. Chem. C* **2019,** *7* (3), 663-672.
207. Edell, D. J.; Farrell, B. Implantable devices having a liquid crystal polymer substrate. US20020198582A1, 2002.
208. Cong, Y.; Gu, W.; He, X.; Zhang, B. *Zhongguo Cailiao Jinzhan* **2015,** *34* (1), 79-83.
209. Lv, M.; Guo, H. A liquid crystal epoxy resin-carbon fiber composite material and its preparation method. CN103602042A, 2014.
210. Bravo Vasquez, J. P.; Hill, R. H. Method for the deposition of materials from mesomorphous films. US20020197415A1, 2002.
211. Alison, L. M.; Owain, L. P. Photopolymerizable chiral reactive mesogen mixtures for electronic and optical applications. EP2218764A1, 2010.
212. Cuerva, C.; Campo, J. A.; Cano, M.; Arredondo, B.; Romero, B.; Oton, E.; Oton, J. M. *New J. Chem.* **2015,** *39* (11), 8467-8473.

213. Wang, Y.; Shi, J.; Chen, J.; Zhu, W.; Baranoff, E. *J. Mater. Chem. C* **2015,** *3* (31), 7993-8005.
214. Ziessel, R.; Camerel, F.; Donnio, B. *Chem. Rec.* **2009,** *9* (1), 1-23.
215. Cuerva, C.; Campo, J. A.; Ovejero, P.; Torres, M. R.; Oliveira, E.; Santos, S. M.; Lodeiro, C.; Cano, M. *J. Mater. Chem. C* **2014,** *2* (43), 9167-9181.
216. Wang, D.; Yan, Q.; Zhong, F.; Li, Y.; Fu, M.; Meng, L.; Huang, Y.; Li, L. *Langmuir* **2018,** *34* (43), 13006-13013.
217. Escarcega-Bobadilla, M. V.; Zelada-Guillen, G. A.; Pyrlin, S. V.; Wegrzyn, M.; Ramos, M. M. D.; Gimenez, E.; Stewart, A.; Maier, G.; Kleij, A. W. *Nat. Commun.* **2013,** *4*, 2648.
218. Zhao, J.; Liu, B.; Feng, Z.; Jin, D.; Dang, W.; Yang, X.; Zhou, G.; Wu, Z.; Wong, W.-Y. *Polym. Chem.* **2017,** *8* (41), 6368-6377.
219. Wezenberg, S. J.; Escudero-Adan, E. C.; Benet-Buchholz, J.; Kleij, A. W. *Inorg. Chem.* **2008,** *47* (8), 2925-2927.
220. Vagin, S. I.; Reichardt, R.; Klaus, S.; Rieger, B. *J. Am. Chem. Soc.* **2010,** *132* (41), 14367-14369.
221. Ren, Y.; Shi, Y.; Chen, J.; Yang, S.; Qi, C.; Jiang, H. *RSC Adv.* **2013,** *3* (7), 2167-2170.
222. Anselmo, D.; Salassa, G.; Escudero-Adan, E. C.; Martin, E.; Kleij, A. W. *Dalton Trans.* **2013,** *42* (22), 7962-7970.
223. Fleischer, E. B.; Shachter, A. M. *Inorg. Chem.* **1991,** *30* (19), 3763-9.
224. Zhou, C.-Q.; Liao, T.-C.; Li, Z.-Q.; Gonzalez-Garcia, J.; Reynolds, M.; Zou, M.; Vilar, R. *Chem. - Eur. J.* **2017,** *23* (19), 4713-4722.
225. Ariffin, E. Y.; Tan, L. L.; Karim, N. H. A.; Heng, L. Y. *Sensors* **2018,** *18* (4), 1173/1-1173/16.
226. Sheldrick, G. M. *Acta Crystallogr., Sect. C: Struct. Chem.* **2015,** *71* (1), 3-8.
227. Spek, A. L. *Acta Crystallogr., Sect. C: Struct. Chem.* **2015,** *71* (1), 9-18.
228. Gandolfi, C.; Miyashita, N.; Kurth, D. G.; Martinho, P. N.; Morgan, G. G.; Albrecht, M. *Dalton Trans.* **2010,** *39* (19), 4508-4516.
229. Sanz, M.; Cuenca, T.; Galakhov, M.; Grassi, A.; Bott, R. K.; Hughes, D. L.; Lancaster, S. J.; Bochmann, M. J. O. **2004,** *23* (22), 5324-5331.
230. Nielson, A. J.; Telfer, S. G.; Waters, J. M. *Polyhedron* **2012,** *33* (1), 97-106.
231. Durr, C. B.; Williams, C. K. *Inorg. Chem.* **2018,** *57* (22), 14240-14248.
232. Bhattacharjee, C. R.; Das, G.; Mondal, P.; Rao, N. V. S. *Polyhedron* **2010,** *29* (16), 3089-3096.
233. Traill, P. R.; Young, C. G. *J. Magn. Reson.* **1990,** *90* (3), 551-6.
234. Berger, S.; Bock, W.; Frenking, G.; Jonas, V.; Mueller, F. *J. Am. Chem. Soc.* **1995,** *117* (13), 3820-9.
235. Nielson, A. J.; Telfer, S. G.; Waters, J. M. *Polyhedron* **2012,** *33* (1), 97-106.
236. Chakraborty, S.; Bhattacharjee, C. R.; Mondal, P.; Prasad, S. K.; Rao, D. S. S. *Dalton Trans.* **2015,** *44* (16), 7477-7488.
237. Zhang, W.; Zhang, S.; Zhang, Z.; Yang, H.; Zhang, A.; Hao, X.; Wang, J.; Zhang, C.; Pu, J. *J. Phys. Chem. B* **2017,** *121* (31), 7519-7525.

APPENDIX A

Characterization of the ligands and the complexes

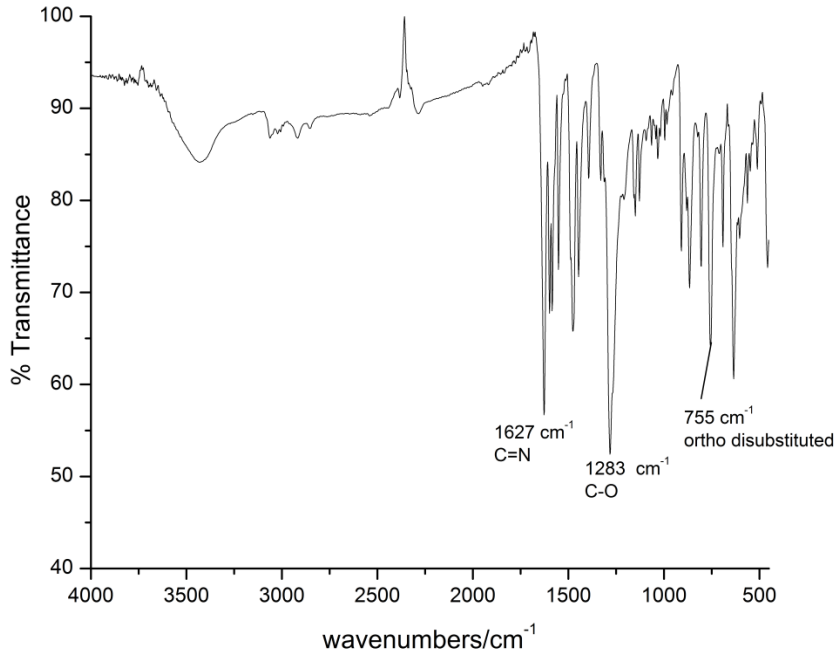

Figure A1. An FTIR spectrum of [Ti(salen)$(OPh)_2$] in KBr disc

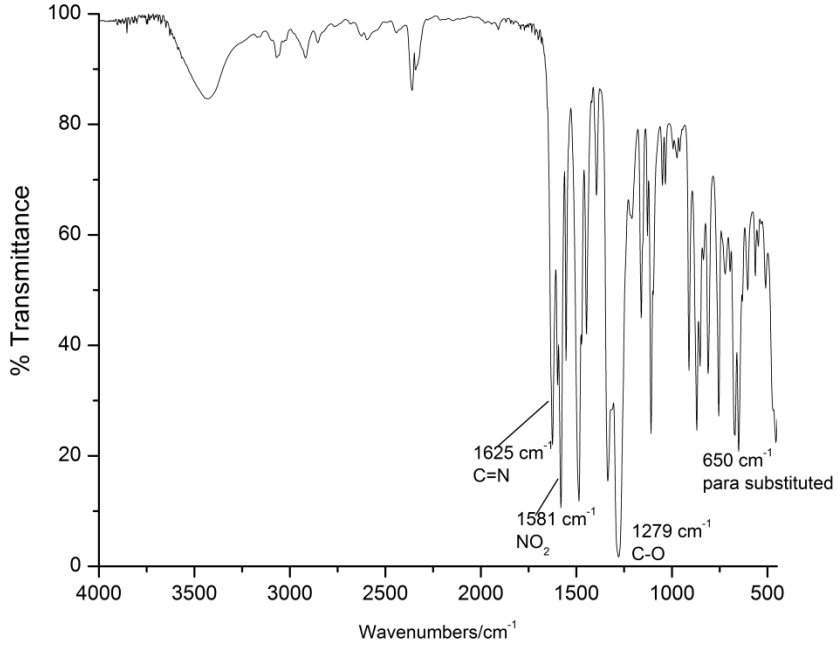

Figure A2. An FTIR spectrum of [Ti(salen)(OPh- *para*-$NO_2)_2$] in KBr disc.

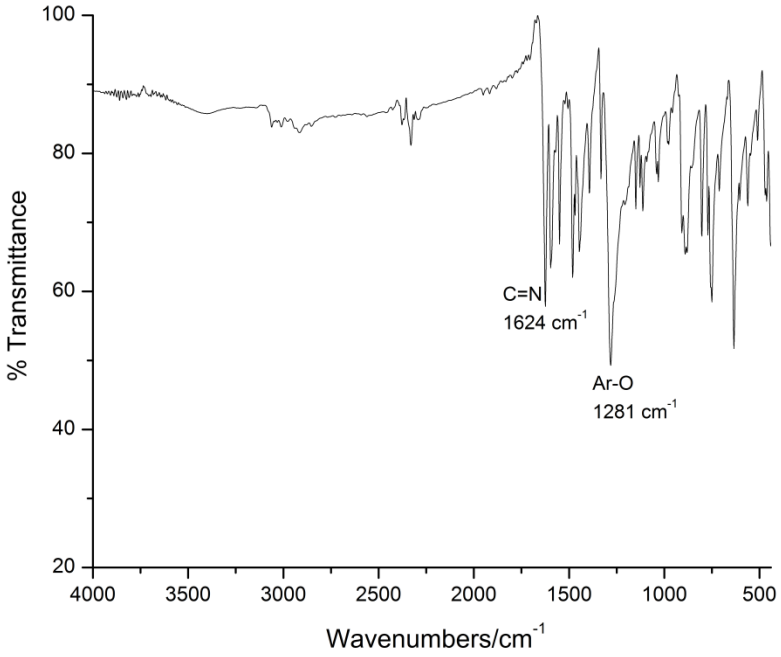

Figure A3. An FTIR spectrum of [Ti(salen)(OPh-ortho$CH_3)_2$] in KBr disc.

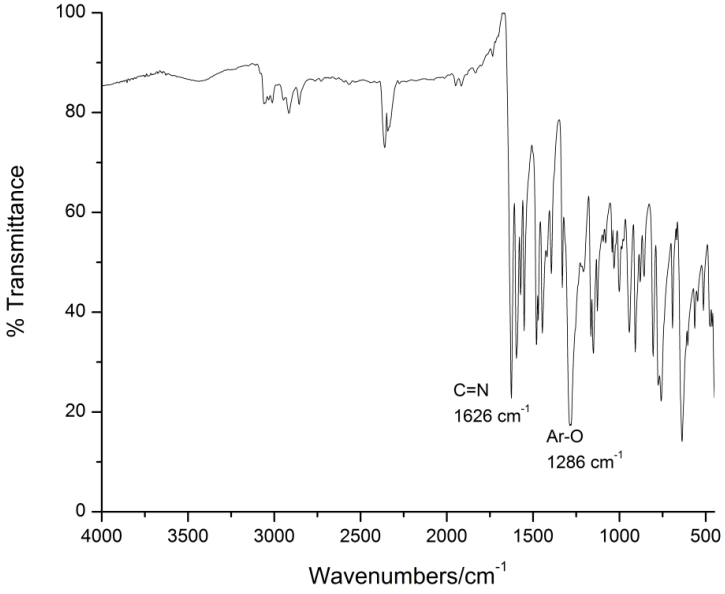

Figure A4. An FTIR spectrum of [Ti(salen)(OPh-meta-$CH_3)_2$] in KBr disc.

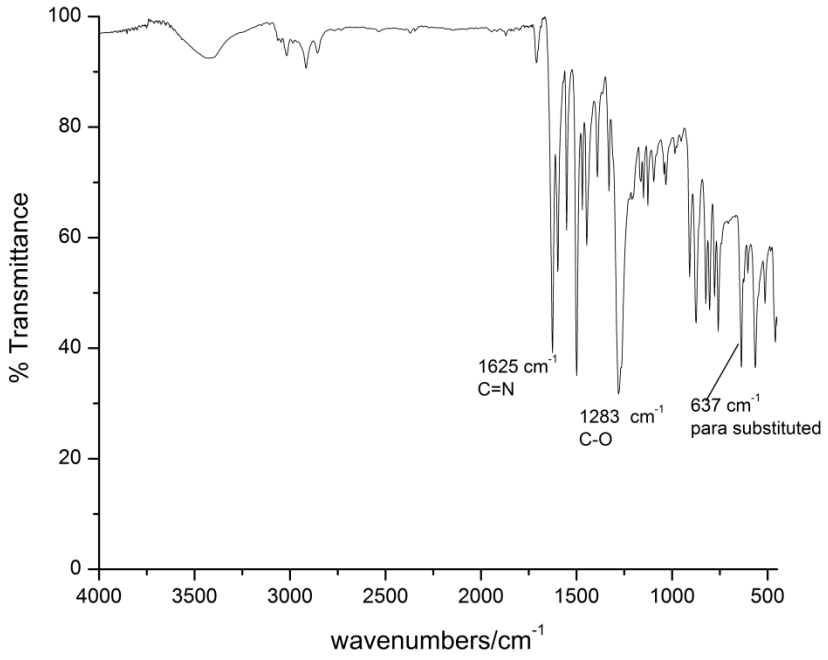

Figure A5. An FTIR spectrum of [Ti(salen)(OPh-para-CH_3)$_2$] in KBr disc.

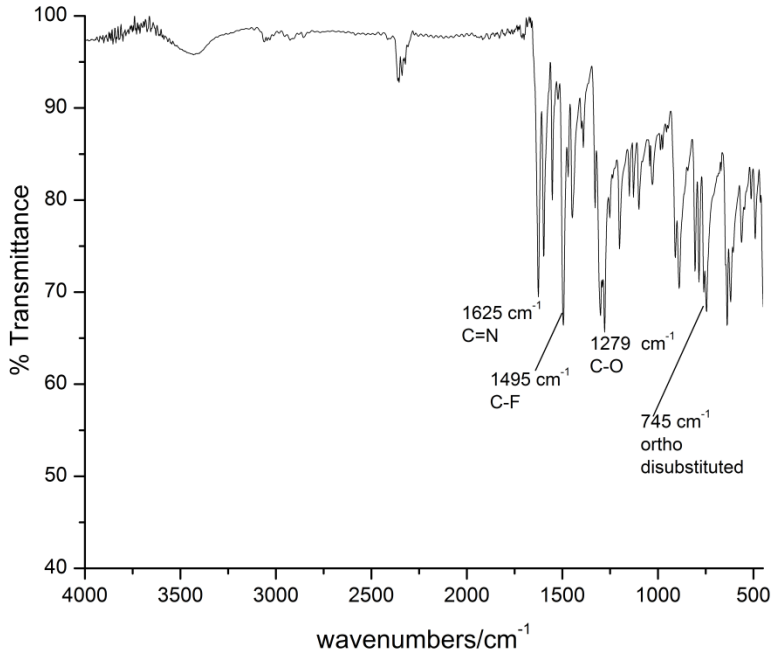

Figure A6. An FTIR spectrum of [Ti(salen)(OPh-ortho-F)$_2$] in KBr disc.

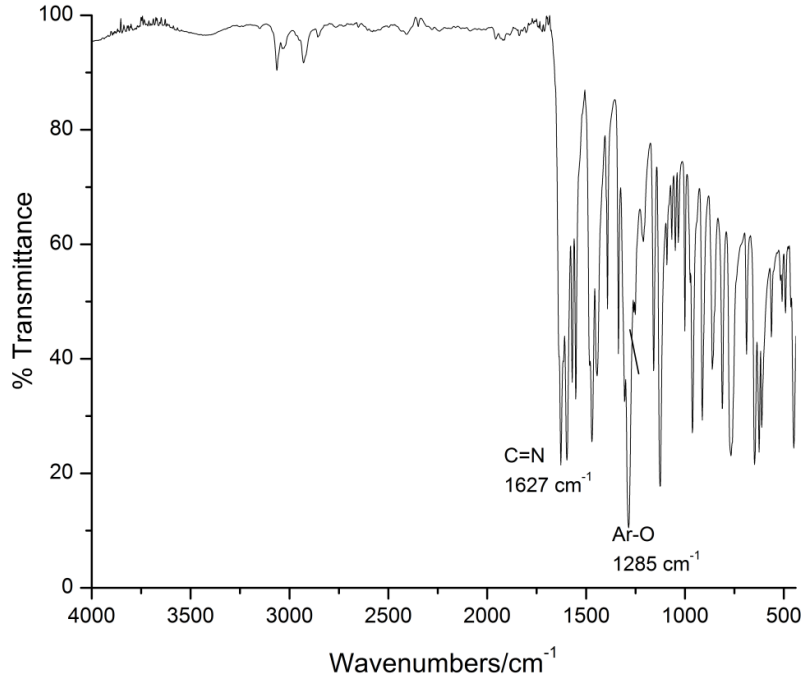

Figure A7. An FTIR spectrum of [Ti(salen)(OPh-meta-F)$_2$] in KBr disc.

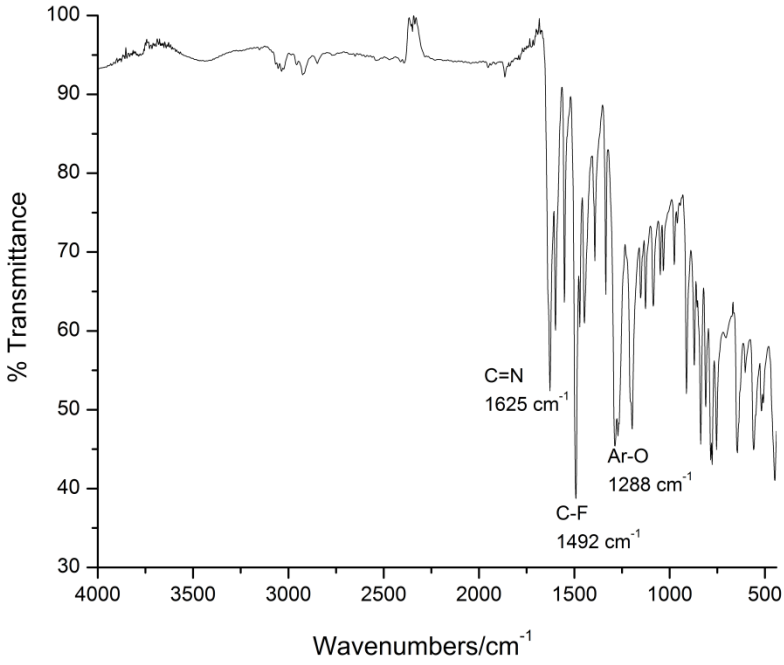

Figure A8. An FTIR spectrum of [Ti(salen)(OPh-para-F)$_2$] in KBr disc

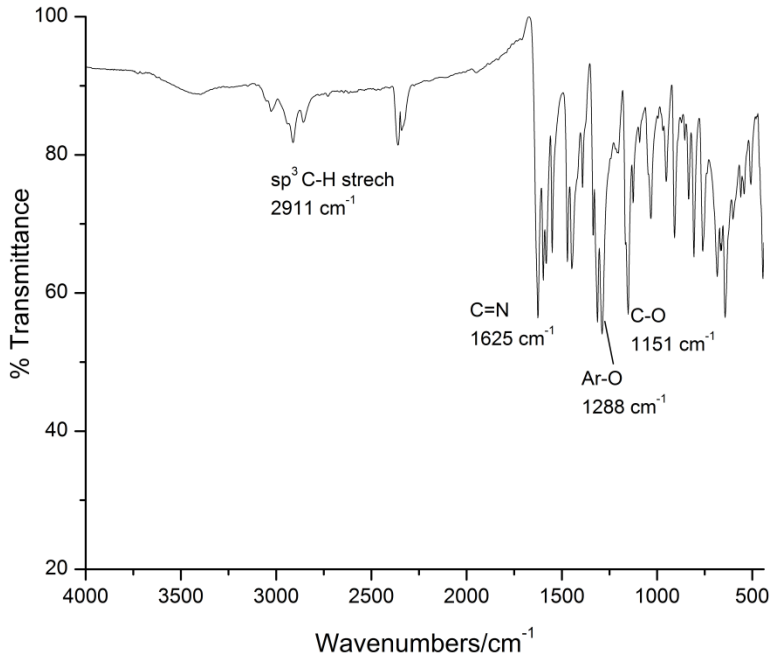

Figure A9. An FTIR spectrum of [Ti(salen)(3,5-dimethylphenolate)$_2$] in KBr disc.

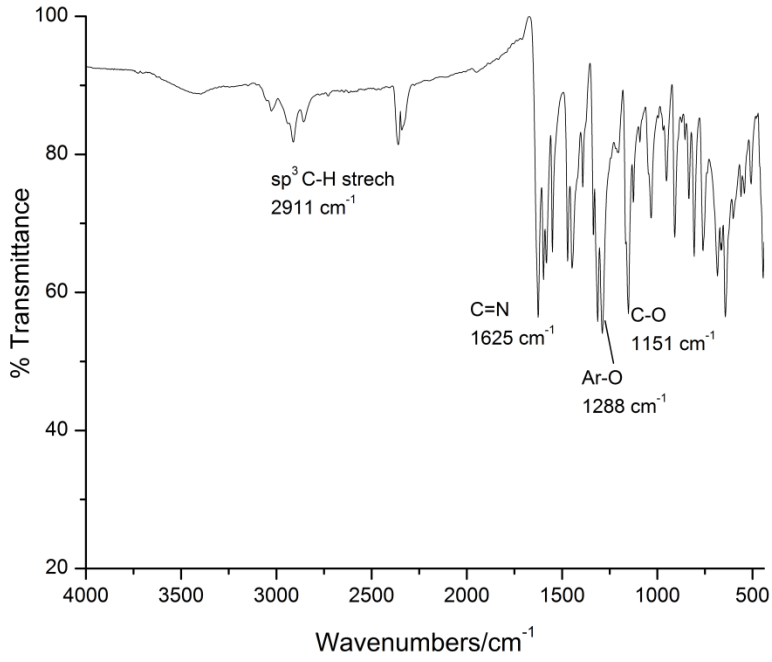

Figure A10. An FTIR spectrum of Ti(salen)(3,5-bis(trifluoromethyl)phenolate)$_2$]

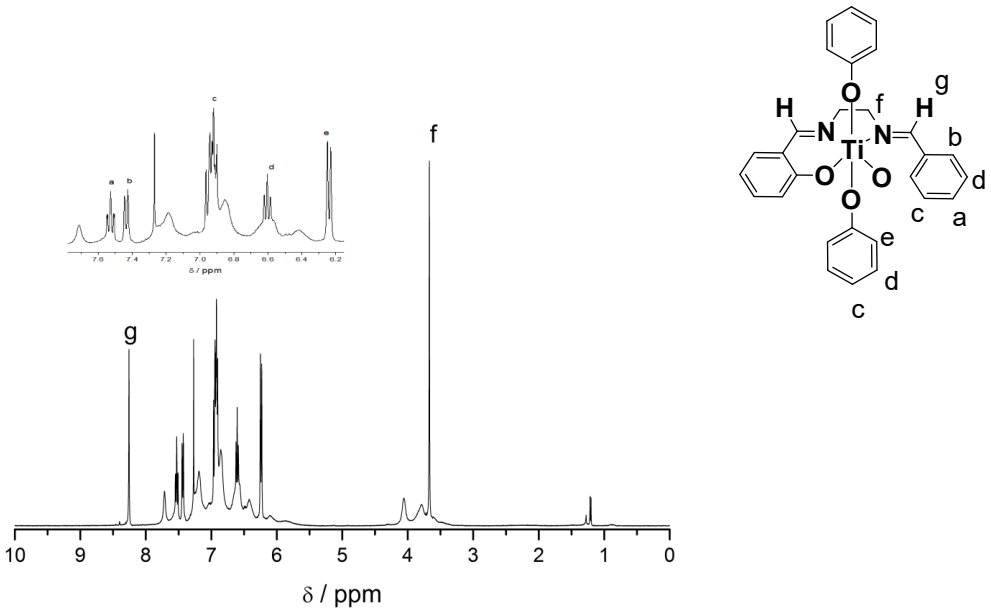

Figure A11. ^{1}H NMR Spectrum of [Ti(salen)$(OPh)_2$] in $CDCl_3$.

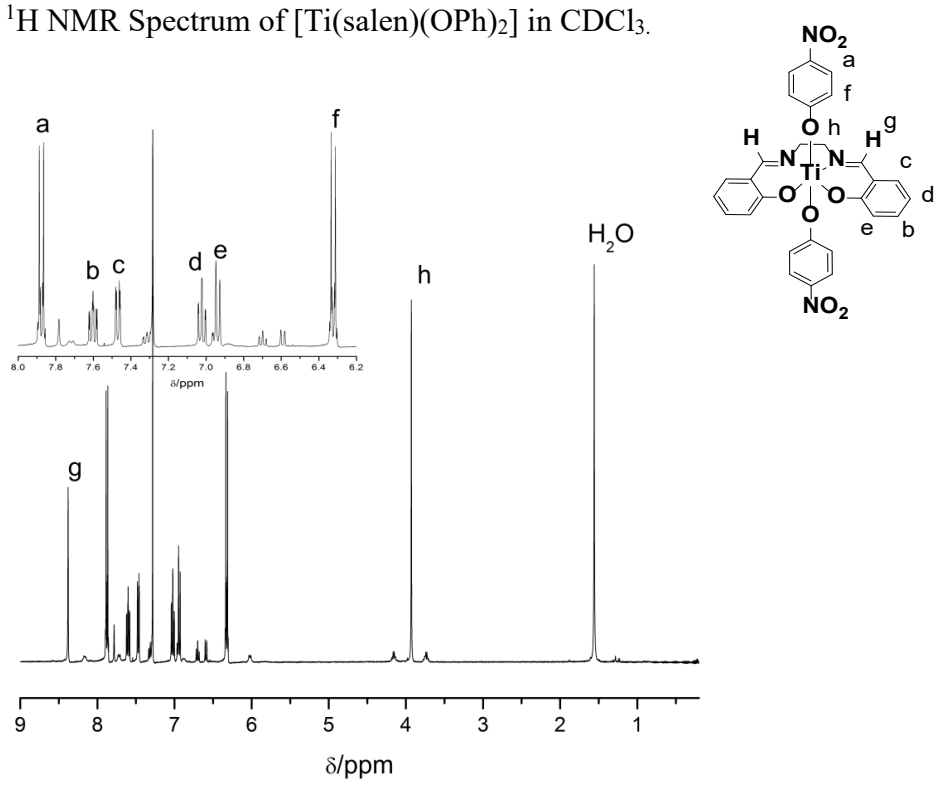

Figure A12. ^{1}H NMR spectrum of [Ti(salen)$(OPh\text{-}NO_2)_2$] in $CDCl_3$

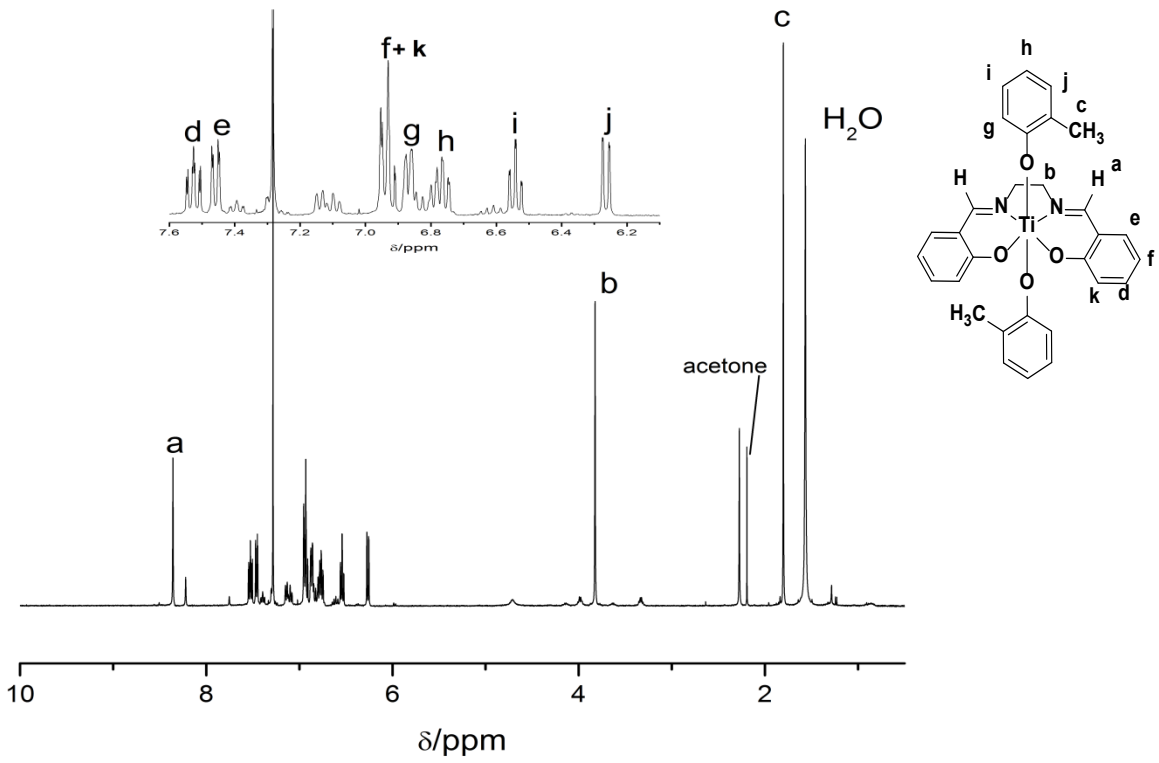

Figure A13. ^{1}H NMR spectrum of [Ti(salen)(OPh-*ortho*-CH_3)$_2$] in $CDCl_3$

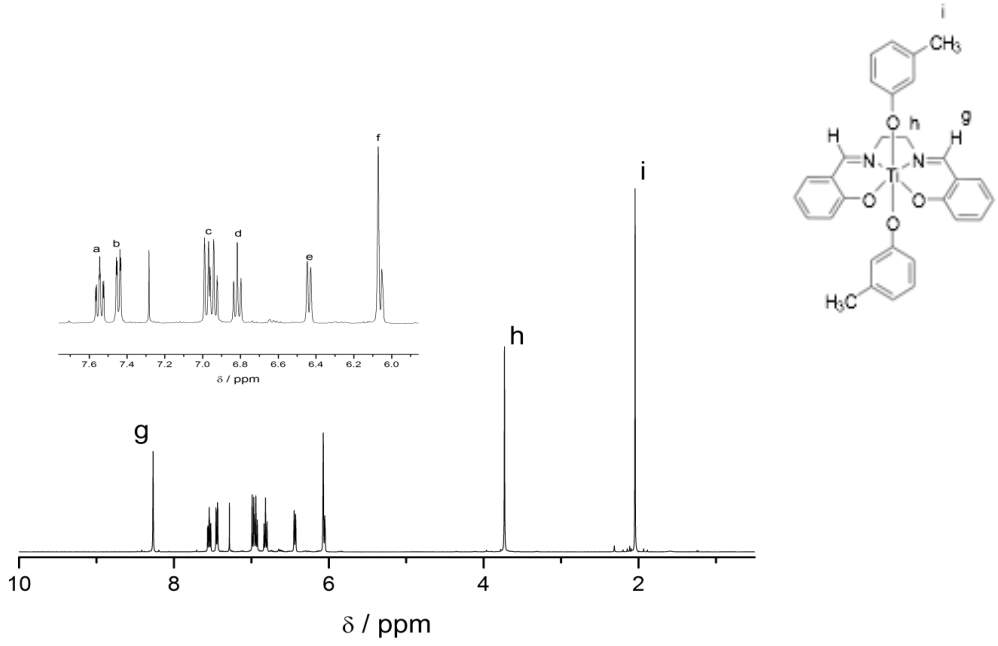

Figure A14. ^{1}H NMR spectrum of [Ti(salen)(OPh-*meta*-CH_3)$_2$] in $CDCl_3$

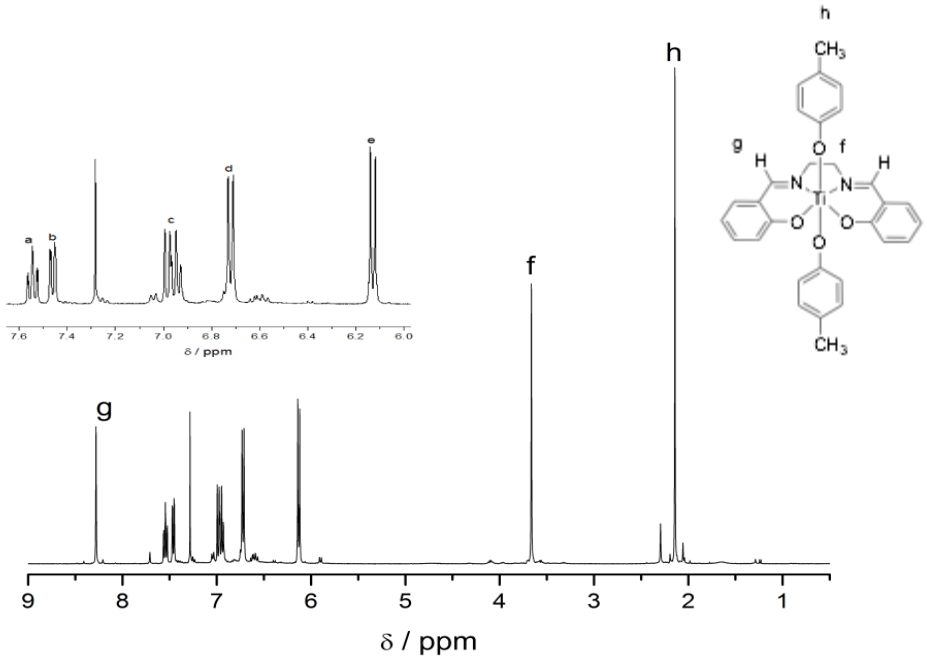

Figure A15. ^{1}H NMR spectrum of [Ti(salen)(OPh-*para*-CH_3)$_2$] in $CDCl_3$.

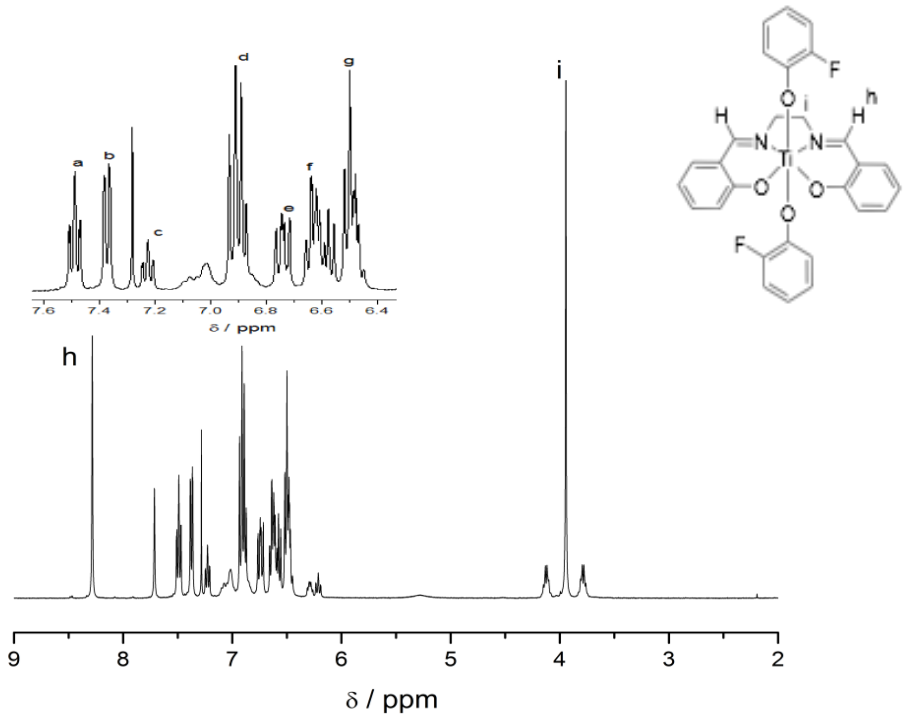

Figure A16. ^{1}H NMR spectrum of [Ti(salen)(OPh-*ortho*-F)$_2$] in $CDCl_3$

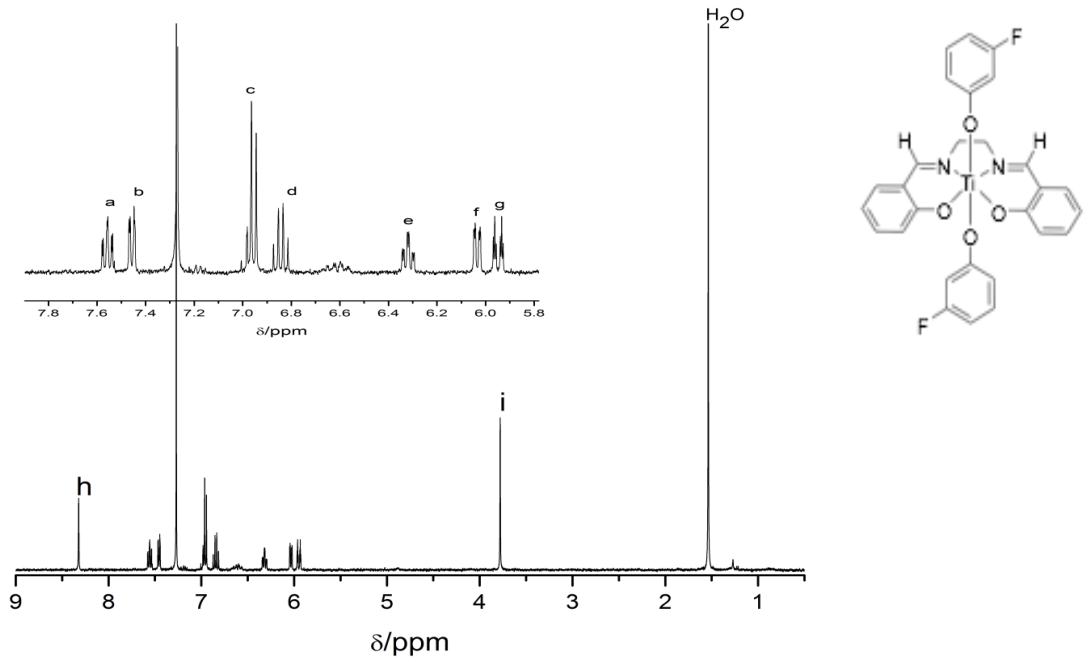

Figure A17. ^{1}H NMR spectrum of [Ti(salen)(OPh-*meta*-F)$_2$] in $CDCl_3$

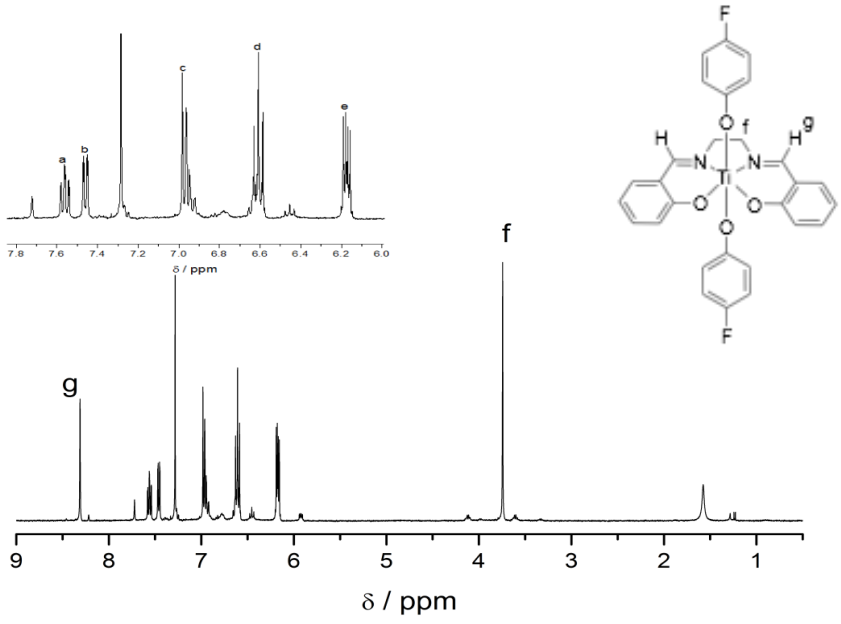

Figure A18. ^{1}H NMR spectrum of [Ti(salen)(OPh-*para*-F)$_2$] in $CDCl_3$.

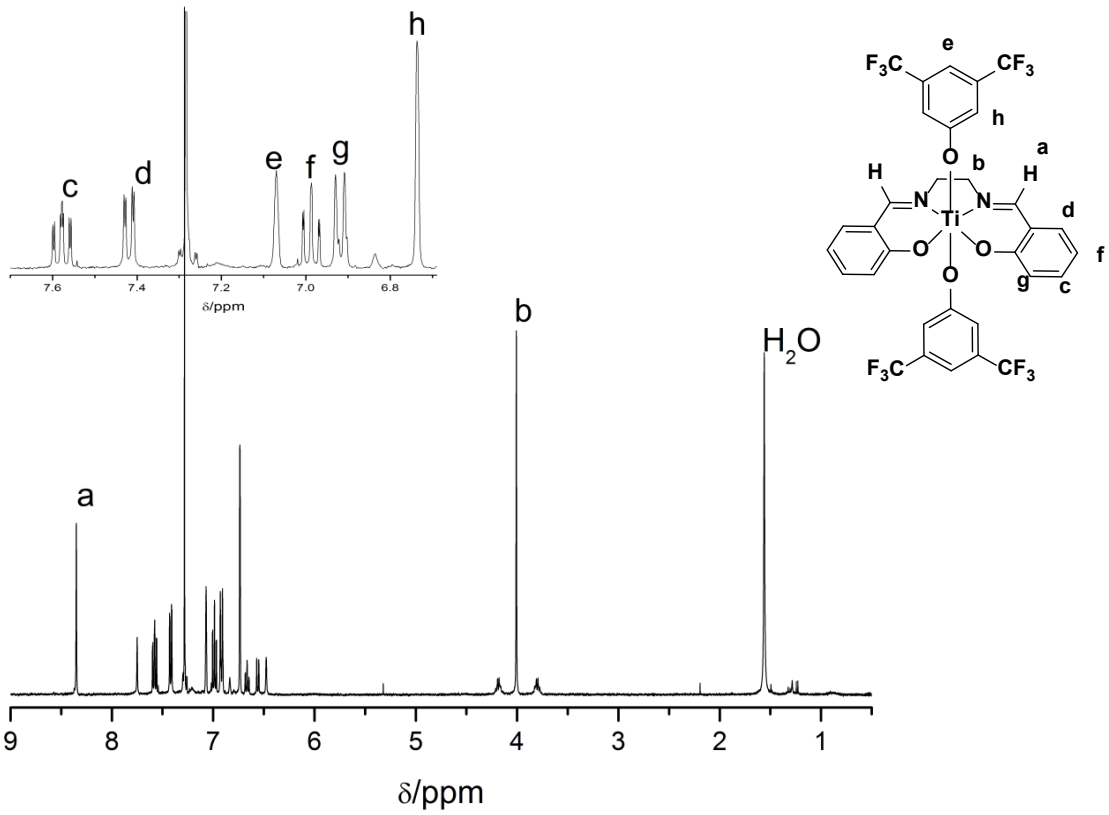

Figure A19. ^{1}H NMR spectrum of [Ti(salen)(3,5-bistrifluoromethylphenolate)$_2$] in $CDCl_3$.

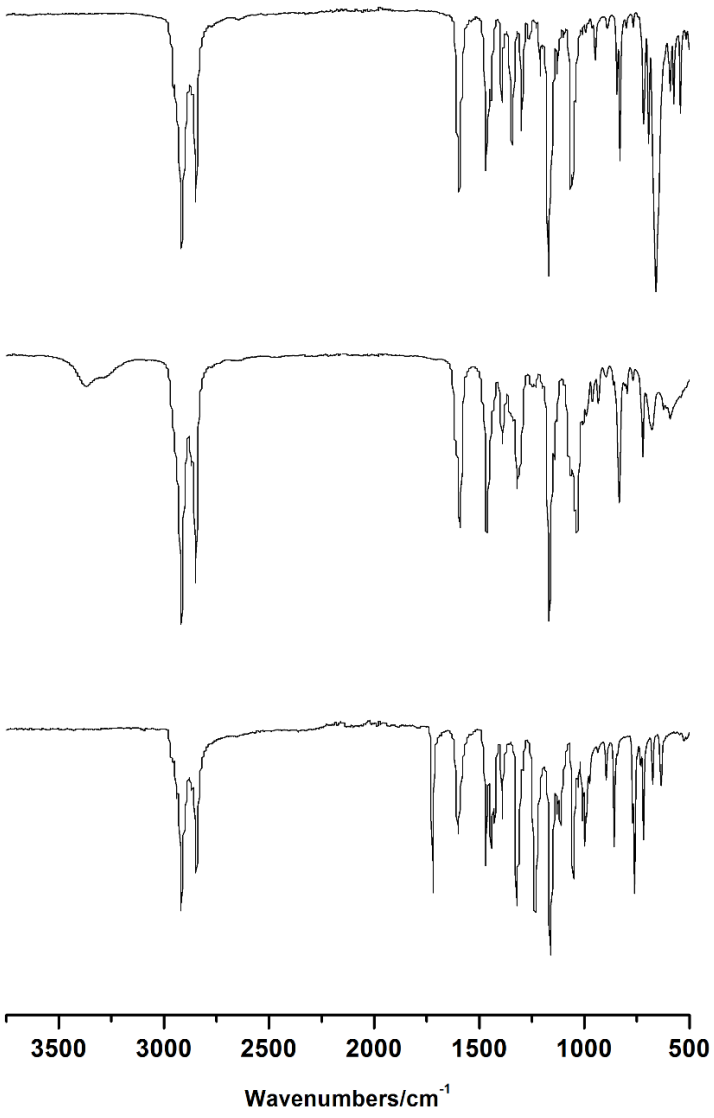

Figure A20. FTIR spectra of precursor ligands. 3,5-bis(dodecyloxy)benzylbromide *(top)* ,3.5-bis(dodecyloxy)phenylmethanol *(middle)*, and methyl-3,5-bis(dodecyloxy)benzoate *(bottom)*.

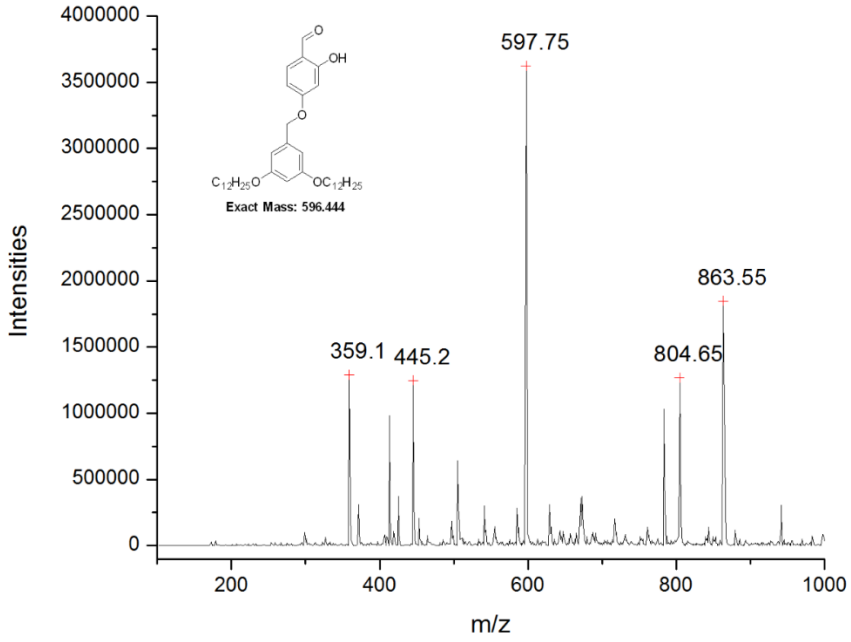

Figure A21. ESI-MS of the C_{12}-2,4-sal using MeOH as solvent in positive ion mode.

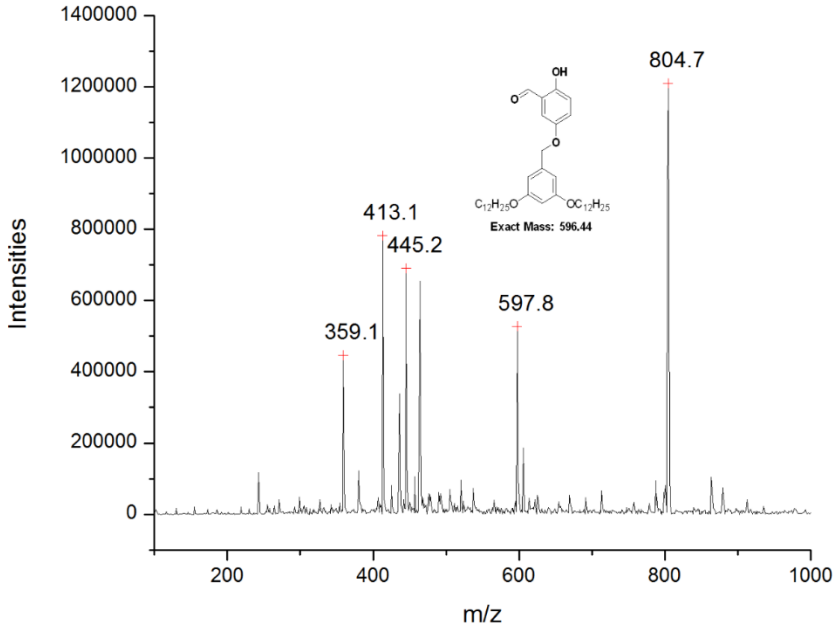

Figure A22. ESI-MS of the C_{12}-2,5-sal using MeOH as solvent in positive ion mode.

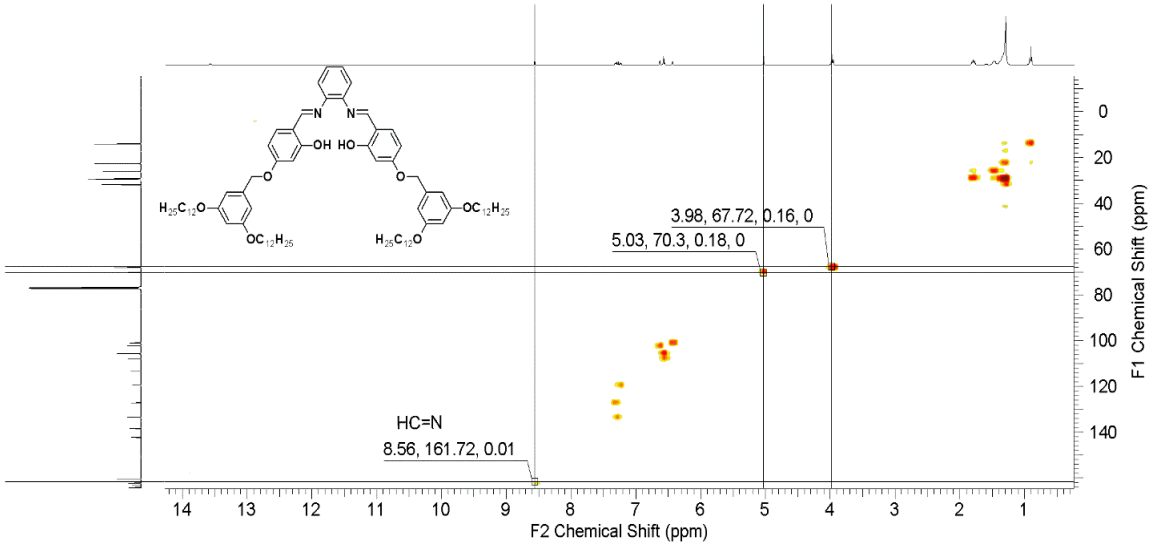

Figure A23. 2-D NMR spectra of C_{12}-2,4-salphen ligand

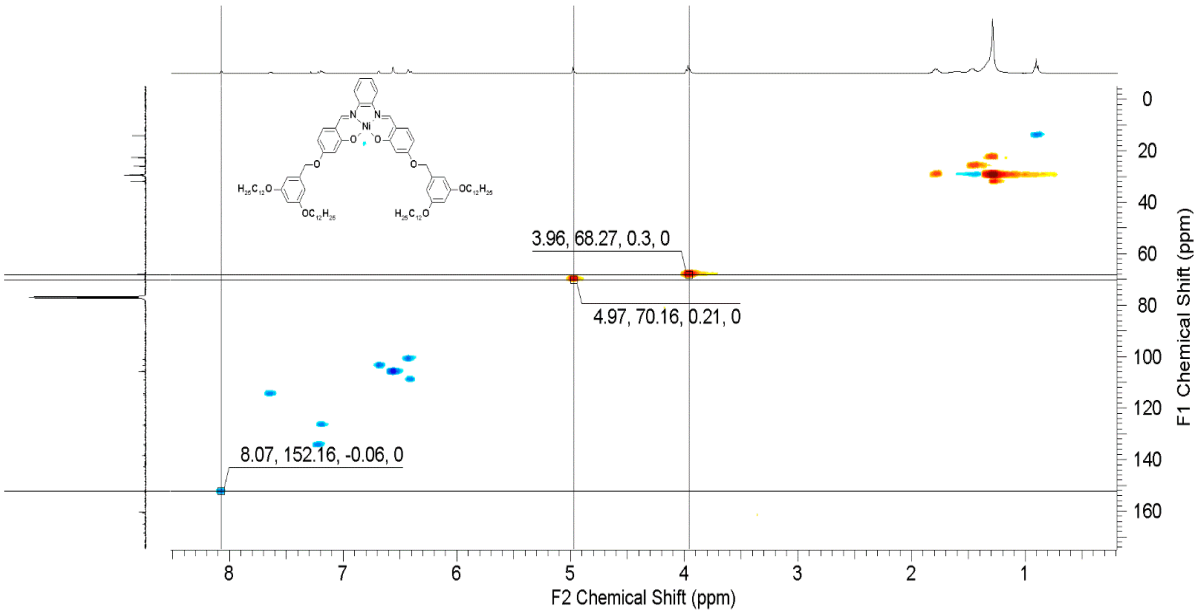

Figure A24. 2-D NMR spectra of complex **14.**

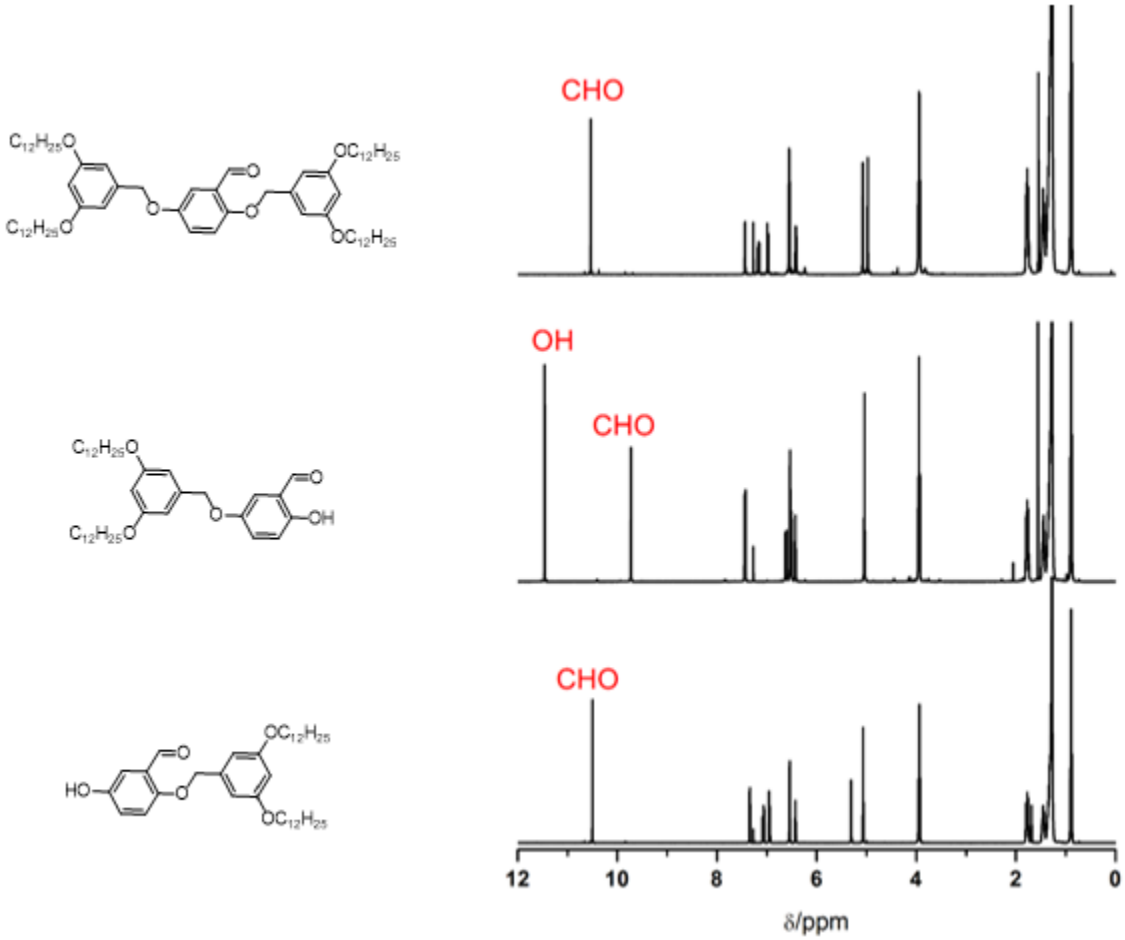

Figure A25. ^{1}H NMR spectra of various side product from during the reaction of bis(alkoxy)benzylbromide and 2,5-dihydroxybenzaldehyde.

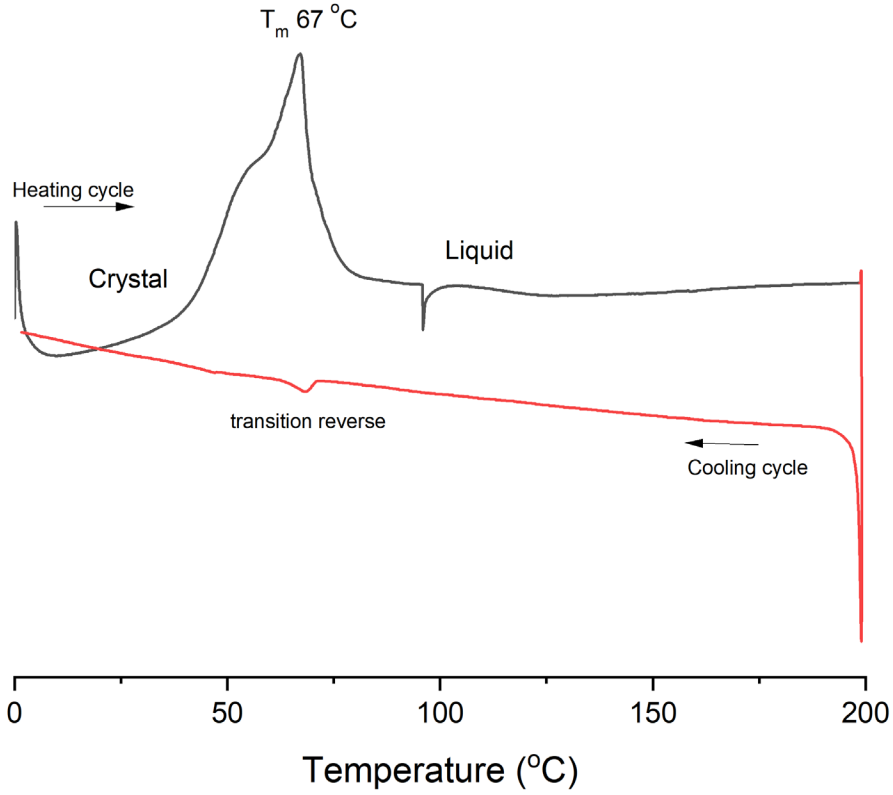

Figure A25. DSC thermogram of the complex **13**.

APPENDIX B

Permission for the figure 28

License Number	4942110343622
License date	Nov 04, 2020
Licensed Content Publisher	Elsevier
Licensed Content Publication	Journal of Organometallic Chemistry
Licensed Content Title	Liquid crystal behaviour of ionic allylpalladium complexes containing 2-pyrazolylpyridine as bidentate N,N′-ligand
Licensed Content Author	M.C. Torralba,M. Cano,J.A. Campo,J.V. Heras,E. Pinilla,M.R. Torres
Licensed Content Date	Feb 1, 2006
Licensed Content Volume	691
Licensed Content Issue	4
Licensed Content Pages	14
Type of Use	reuse in a thesis/dissertation
Portion	figures/tables/illustrations
Number of figures/tables/illustrations	1
Format	both print and electronic
Are you the author of this Elsevier article?	No
Will you be translating?	No
Title	SYNTHESIS, CHARACTERIZATION, SPECTROSCOPIC, AND MESOMORPHIC STUDIES OF NEW SCHIFF BASE LIGANDS AND TITANIUM, COBALT, NICKEL AND COPPER METAL CENTERS
Institution name	Old Dominion University
Expected presentation date	Nov 2020
Portions	Figure 6
Requestor Location	Raj k Gurung 1049w, 49th st. Apt#424 NORFOLK, VA 23508 United States Attn: Raj k Gurung
Publisher Tax ID	98-0397604
Total	**0.00 USD**

Royal Society of Chemistry - License Terms and Conditions

This is a License Agreement between Raj Kumar Gurung ("You") and Royal Society of Chemistry ("Publisher") provided by Copyright Clearance Center ("CCC"). The license consists of your order details, the terms and conditions provided by Royal Society of Chemistry, and the CCC terms and conditions.

All payments must be made in full to CCC.

Order Date	04-Nov-2020	**Type of Use**	Republish in a thesis/dissertation
Order license ID	1075224-1	**Publisher**	ROYAL SOCIETY OF CHEMISTRY
ISSN	1477-9234	**Portion**	Image/photo/illustration

LICENSED CONTENT

Publication Title	Dalton transactions	**Country**	United Kingdom of Great Britain and Northern Ireland
Author/Editor	Royal Society of Chemistry (Great Britain)	**Rightsholder**	Royal Society of Chemistry
Date	01/01/2003	**Publication Type**	e-Journal
Language	English		

REQUEST DETAILS

Portion Type	Image/photo/illustration	**Distribution**	Worldwide
Number of images / photos / illustrations	1	**Translation**	Original language of publication
Format (select all that apply)	Print, Electronic	**Copies for the disabled?**	No
Who will republish the content?	Academic institution	**Minor editing privileges?**	No
Duration of Use	Life of current edition	**Incidental promotional use?**	No
Lifetime Unit Quantity	Up to 499	**Currency**	USD
Rights Requested	Main product		

NEW WORK DETAILS

Title	SYNTHESIS, CHARACTERIZATION, SPECTROSCOPIC, AND MESOMORPHIC STUDIES OF NEW SCHIFF BASE LIGANDS AND TITANIUM, COBALT, NICKEL AND COPPER METAL CENTERS	**Institution name**	Old Dominion University
		Expected presentation date	2020-11-11
Instructor name	Alvin Holder		

ADDITIONAL DETAILS

Order reference number	N/A	**The requesting person / organization to appear on the license**	Raj Kumar Gurung

Permission for the figure 30

License Number	4942100315725
License date	Nov 04, 2020
Licensed Content Publisher	John Wiley and Sons
Licensed Content Publication	Angewandte Chemie International Edition
Licensed Content Title	Discotic Liquid Crystals: From Tailor-Made Synthesis to Plastic Electronics
Licensed Content Author	Martin Tosoni, Alina Schreivogel, Sven Sauer, et al
Licensed Content Date	Jun 15, 2007
Licensed Content Volume	46
Licensed Content Issue	26
Licensed Content Pages	56
Type of Use	Dissertation/Thesis
Requestor type	University/Academic
Format	Print and electronic
Portion	Figure/table
Number of figures/tables	2
Will you be translating?	No
Title	SYNTHESIS, CHARACTERIZATION, SPECTROSCOPIC, AND MESOMORPHIC STUDIES OF NEW SCHIFF BASE LIGANDS AND TITANIUM, COBALT, NICKEL AND COPPER METAL CENTERS
Institution name	Old Dominion University
Expected presentation date	Nov 2020
Portions	Figure 5 and Figure 6
Requestor Location	Raj k Gurung 1049w, 49th st. Apt#424 NORFOLK, VA 23508 United States Attn: Raj k Gurung
Publisher Tax ID	EU826007151
Total	**0.00 USD**

VITA

Raj Kumar Gurung
Department of Chemistry and Biochemistry
Old Dominion University
Norfolk, VA, 23529

Education
December 2020……Ph.D. Chemistry, Old Dominion University, Norfolk, VA
May 2009……M.Sc. Chemistry, Tribhuvan University, Kathmandu, Nepal
May 2007……B.Sc. Chemistry, Tribhuvan University, Kathmandu, Nepal

List of Publications:

1. **Gurung Raj. K**.; McMillen, Collin. D.; Jarrett William. L.; Holder Alvin. A."Synthesis, Characterization, NMR spectroscopic, and X-ray Crystallographic Studies of new Titanium(IV) Schiff Base Salen Complexes: Formation of intriguing titanium(IV) species" Inorganica Chimica Acta (2020), 505, 119496.

2. Lawrence, Mark A. W.; McMillen, Colin D.;**Gurung, Raj K.**; Celestine, Michael J.; Arca, Jessa F.; Holder, Alvin A. J. Chem. Crystallogr. 2015, 45(8), 427-433

3. Hurtado, M.; Sankpal, U. T.; Maram, R.; Patel, R.; Basha, R.; Chhabra, J.; Brown, D. T.; **Gurung, R. K.**; Holder, A. A.; Simecka, J.; Basha, R. Invest. New Drugs 2019, 37 (1), 27-34

4. Hurtado, M.; Sankpal, U. T.;Kaba A.; Mahammad S.; Chhabra, J.; Brown, D. T.; **Gurung, R. K.**; Holder, A. A.; Simecka, J.; Basha, R. Cellular Physiology and Biochemistry 2018, 51, 1894-1904

5. Hurtado, M.; Prokai L.;Sankpal, U. T.; Levesque B.;Maram R.; Chhabra, J.; Brown, D. T.; **Gurung, R. K.**; Holder, A. A.; Vishwanath J.K.; Basha, R. Process Biochemistry Accepted 22 October 2019

6. Stephen J. Beebe; Michael J. Celestine; Jimmie L. Bullock; Shayna Sandhaus; Jessa Faye Arca; Donald M. Cropek; Tekettay A. Ludvig;Sydney, R. Foster; Jasmine S. Clark; Floyd A. Beckford; Criszcele M. Tano; Elizabeth A. Tonsel-White; **Raj K. Gurung** ; Courtney E. Stankavich; Yuk-Ching Tse-Dinh; William L. Jarrett; and Alvin A. Holder; J. Ionorg. Biochem. Accepted

7. **Book Chapter**: Book title: Ruthenium Complexess: Photochemical and Biomedical Applications. Editors: Alvin A. Holder, Wesley Browne, Lothar Lilge, Mark A.W. Lawrence, and Jimmie L. Bullock. Book chapter: "Ruthenium-containing complexes with cobalt and hydrogenases for hydrogen production" by Michael J. Celestine, **Raj K. Gurung**, and Alvin A. Holder. Publishers: Wiley-VCH Verlag GmbH Co. KGaA, 2015